

**QUANTUM LOOP CURRENT IN MOLECULAR
AND NANOSCALE JUNCTION DEVICES:
THEORETICAL AND COMPUTATIONAL
PERSPECTIVES**

A Thesis Submitted

To
Sikkim University



**In Partial Fulfillment of the Requirement for the
Degree of Doctor of Philosophy in Physics**

By

Umesh Dhakal

Department of Physics
School of Physical Sciences

July 2022

CERTIFICATE

This is to certify that the Ph.D. thesis entitled "**Quantum Loop Current in Molecular and Nanoscale Junction Devices: Theoretical and Computational Perspectives**", submitted to Sikkim University in partial fulfillment of the requirement for the degree of Doctor of Philosophy in Physics, represents the work carried out by **Mr. Umesh Dhakal** in the Department of Physics, Sikkim University, Gangtok, Sikkim. The results are original and have not been submitted anywhere else for any other degree. It is recommended this Ph.D. thesis be placed before the Examiners for evaluation.

Head of the Department
(Dr. Ajay Tripathi)
Department of Physics
School of Physical Sciences
Sikkim University
Gangtok- 737102

Place: Gangtok, Sikkim, India

Date:

CERTIFICATE

This is to certify that the work presented in the dissertation "**Quantum Loop Current in Molecular and Nanoscale Junction Devices: Theoretical and Computational Perspectives**", being submitted by **Mr. Umesh Dhakal** for the award of Ph.D. in Physics was carried out by him under my supervision.

Dr. Dhurba Rai

Ph.D. Supervisor

Department of Physics

School of Physical Sciences

Sikkim University

Place: Gangtok, Sikkim, India

Date:

Declaration

I, **Umesh Dhakal**, declare that this thesis titled "**Quantum Loop Current in Molecular and Nanoscale Junction Devices: Theoretical and Computational Perspectives**" submitted by me for the award of **Doctor of Philosophy** in Physics at **Sikkim University** is my original work. It is further declared that the present thesis does not contain materials previously published. I do confirm that

- The content of this thesis is based on the work which I have performed myself while in candidature for a Ph.D. degree at this University.
- This thesis has not been submitted for any degree to any other University or institution.
- The content of this thesis has been subjected to anti-plagiarism software (**URKUND**) and was found satisfactory.

(Umesh Dhakal)

Roll No.: 14PDPY05

Regn. No.:14/Ph.D/PHY/05

Date:

Recommended that the thesis be placed before the Examiners for evaluation

(Dr. Dhurba Rai)

Ph.D. Supervisor

Date:

In loving memory of my Father

Lt. Shyam Kumar Dhakal

Dedicated to my

*Mother Jamuna Dhakal, Sister Sunita Dhakal,
Brother Basu Dhakal, Bhauju Divya Chhetri and
Nani Vaibhav Dhakal . . .*

Acknowledgements

This thesis is the result of a number of challenging but rewarding experiences that have come together to make this compilation. My entire tenure as a research scholar was filled with bitterness, difficulty and frustration, but so did encouragement, faith, and a bond of trust leading to the successful completion of the research assignment. After years of perseverance, I finally realised that teamwork is what matters most. Those who encouraged my interest and helped me grow as a researcher deserve special mention. It is a pleasure to express my gratitude to them.

I owe a debt of gratitude to my supervisor, Dr. Dhurba Rai, Assistant Professor in the Department of Physics at Sikkim University, for allowing me to explore the majority of the research topics covered in this thesis. I've learned a lot from him, especially about how to deal with difficulties and problems in the quickest and most efficient way. Without his diligence and prompt assistance, it would have been challenging to successfully complete this thesis.

My sincere thanks to each faculty member of the department for their kind instruction, counsel, and cooperation during my time as a research scholar. My profound gratitude is extended to all of my friends, brothers, sisters, and labmates who never hesitate to lend me support in those stressful situations.

I am thankful to my best friend, Yam Prasad Rai, who has been a constant companion since our undergraduate days. He is an entertainer who gave suggestions and words of encouragement that proved helpful in those trying times.

In addition, I would like to thank the University Grants Commission (UGC), Govt. of India, for its financial support throughout my research work.

It is hard to express how appreciative and respectful I am of my parents, whose unconditional care, support and numerous sacrifices have served as a never-ending source of motivation to push myself a little further, especially during the end of this arduous journey. Even though they had no idea what I was doing, they nevertheless showed true trust and hope, which made it easier for me to finish this work.

My dear father (Baba), who passed away while I was working on this thesis, was a special inspiration and motivator who never wavered in his belief in my capacity to excel academically, despite the challenges I faced. Your blessings, best wishes, and belief in me have allowed me to embark on this trip even though you vanished into thin air. I adore you, Baba!

I will always be grateful to my younger sister Dr. Sunita Dhakal for her support in those difficult times. She is a champion who offered unceasing mental, emotional, and sympathetic support. A special mention should also be made of my nephew Vaibhav Dhakal, my sister-in-law Divya Chhetri, and my elder brother Basu Dhakal, who all made substantial contributions in their unique ways to the accomplishment of this adventure.

Lastly, I acknowledge how little I was able to accomplish throughout my research, but I believe that my efforts, as presented in this thesis, will help enhancing our understanding of the fascinating subject of Molecular Electronics.

Umesh Dhakal

July 2022

Preface

This thesis deals with quantum loop current in molecular and nanoscale junction devices. The thesis is arranged into five chapters that collectively comprise the systematic study of the subject undertaken in this work. Each chapter begins with an abstract that provides the outline of the work and includes background information on the subject studied. Motivation leading to each work, as presented in Chapters 2 through 4, is described in the section, “Scope of the Work”, followed by a discussion on the model and computational techniques employed in each work. The noteworthy findings of the study are presented in the “Results and Discussion” section. A summary and concluding remarks are included at the end of each of these chapters, followed by a list of relevant references from the past and present. Other related studies and results that are not included in the published papers are also presented. The last chapter offers a succinct assessment of the work covered in the thesis along with suggestions for further research on a few chosen topics.

Chapter 1 gives a brief review of the necessary background materials for the work carried out in this thesis starting with a preamble to the molecular electronics with a focus on single-molecule junction devices. The theoretical formulation of electron transport through a molecular junction based on Landauer’s approach is presented. The description of the transmission function within Landauer’s formulation and the non-equilibrium Green’s function (NEGF)-based expression of current under the steady-state condition are presented. Various factors affecting the electron transport through the molecular junctions are discussed. The chapter concludes with an overview of molecular thermoelectricity, which also serves as a background for Chapter 4.

Chapter 2 focuses on the role of electrode-molecule coupling strengths on the magnetic field-based control of electron transport properties of molecular ring structures. This is studied in the model graphene nano-sheet junctions simulated by the hexagonal polycyclic aromatic hydrocarbons (PAHs) connected to the metal electrodes. The possibility of magnetic field-based current control in the suitably constructed graphene nano-sheet junctions is considered.

Chapter 3 discusses quantum loop current in an open ring system along with a method for calculating loop current (referred to herein as circular current) without determining the local currents. At the certain bias voltage range, the circular current at low coupling far exceeds the net current through the ring. The circular current-induced force is examined and the reliability issues concerning the circular current in a molecular ring junction are explored.

Chapter 4 opens with a systematic investigation of thermoelectric properties of molecules in presence of a magnetic field. A benzene ring and C_{60} fullerene are considered for the purpose. The possibility of modulation of thermoelectric power by an applied magnetic field is explored.

Chapter 5 briefly summarizes the main conclusions of the work carried out in this thesis. The future direction of research in this area is discussed. A list of future works on a few selected topics is given, along with an outline and explanation.

The thesis concludes with the index of the thesis that fills the last pages.

List of Publications

(A) Referred Journals:

- Umesh Dhakal and Dhurba Rai, "Circular current and induced force in a molecular ring junction", *J. Phys.: Condens. Matter* **31**, 125302 (2019).
doi.org/10.1088/1361-648X/aafd09
- Umesh Dhakal and Dhurba Rai, "Magnetic field control of current through model graphene nanosheets", *Phys. Lett. A* **383**, 2193 (2019).
doi.org/10.1016/j.physleta.2019.04.018

(B) In Preparation:

- Umesh Dhakal, Yam P. Rai, and Dhurba Rai, "Magnetic field effects on thermoelectric properties of ring structure molecular junctions".

(C) Other work of author (Submitted):

- Yam P. Rai, Umesh Dhakal, and Dhurba Rai, "Magnetic field control of exciton through the stacked PAM junction".

Presentations in National/ International Conferences/Workshops

- **Poster Presentation** on the topic “Effective control of current by magnetic field in model graphene nanosheets junction: A theoretical approach” at International Conference on Nanotechnology : Ideas, Innovation and Initiatives - 2017, in IIT Roorkee, Dec 06th – 08th, Uttarakhand, India.
- **Oral Presentation** on the topic “Effective control of current by magnetic field in model graphene nanosheets junction : A theoretical approach” at National Conference on Trends in Science and Technology 27th -28th Feb, 2018, in Salesian College, Siliguri, W.B, India.
- **Participated** Refresher Course on Basic Physics and Topology organized by Deptt. of Physics Sikkim University, Gangtok, Jan 29, 2018 to Feb 09, 2018, India.

Contents

Declaration	iii
Acknowledgements	v
Preface	vii
Presentations in National/ International Conferences/Workshops	x
List of Figures	xiii
1 Introduction: The Background	1
1.1 Preamble	2
1.2 Single-Molecule Junctions	5
1.2.1 Experimental methods	6
1.2.2 Theoretical methods	8
1.3 Fundamentals of Electron Transport Through MJs	14
1.3.1 Metal-Molecule coupling	15
1.3.2 Anchoring groups	17
1.3.3 Interface geometry	18
1.3.4 Electron-phonon interaction	20
1.4 Quantum Loop Current	23
1.5 Current-Induced Force	25
1.6 Molecular Thermoelectricity	26
1.7 Thermoelectric power	27
1.8 Figure of merit	29
1.9 Thesis Outline	30
References	32
2 Magnetic Field Influence On Electronic Transport In Ring Structures	41
2.1 Background	42
2.2 Scope of the Work	45
2.3 Computational Framework	46
2.3.1 Model graphene nanosheets and the Hamiltonian	48
2.3.2 Inclusion of Coulomb interaction	51
2.3.3 Steady-state current through the junction	53
2.4 Numerical Results and Discussion	55

Contents

2.4.1	Magnetic field effect on transmission probability	56
2.4.2	Effect of contact coupling	59
2.4.3	Current-voltage characteristics	62
2.5	Summary and Concluding Remarks	69
	References	71
3	Circular Current-Induced Force In Molecular Junctions	78
3.1	Background	79
3.2	Scope of the Work	81
3.3	Computational Framework	82
3.4	Model and Formulation	83
3.4.1	Local current in the molecular bridge	83
3.4.2	Circular current in a ring junction	85
3.4.3	An alternative formulation of the circular current	87
3.4.4	Circular current-induced force	89
3.5	Numerical Results and Discussion	90
3.5.1	Circular current	90
3.5.2	Current-induced force	92
3.6	Summary and Concluding Remarks	98
	References	100
4	Thermoelectric Properties of Molecular Junctions in Externally Applied Magnetic Field	105
4.1	Background	106
4.2	Scope of the Work	109
4.3	Model and Theoretical Framework	110
4.3.1	Tight-binding Hamiltonian	110
4.3.2	Thermopower and figure of merit	112
4.4	Numerical Results and Discussion	114
4.4.1	Seebeck coefficient	115
4.4.2	Figure of merit	119
4.4.3	Field effect on the transport properties of C_{60}	122
4.4.4	Magnetic field effect on thermopower	126
4.5	Summary and Concluding Remarks	129
	References	130
5	Future Prospects	136
	References	142
	Index	143

List of Figures

1.1	An illustration of a SMJ in a “metal-molecule-metal” configuration.	4
1.2	Schematic representation of (a) scanning tunneling microscopy based break junction (STMBJ) and (b) mechanically controllable break junction (MCBJ). Figure adapted from Ref. [26]	7
1.3	Schematic representation of mesoscopic tunnel junction or barrier, consisting of contact leads (L, R) and the central scattering region. Length of the arrows represent the amplitude of the incident electron wave from the left, transmitted to the right and reflection back to the left side. The junction is maintained at a bias voltage V that sets current I through the junction.	9
1.4	Schematic of broadening of frontier energy level ϵ_{LUMO} of the bridging molecule in a MJ. The broadening line width is Γ . The bias voltage V modulates the electron energy states in the metal contact leads (L, R) over the filled states under the Fermi energy level E_F .	16
1.5	Schematic of a MJ wherein a molecule M binds to the metal contacts L, R (e.g., Au) through the anchor groups, X=-SH, -NH ₂ etc.	18
1.6	Representative three different adsorption configurations. Current is maximum for bridge configuration and least for on-top configuration.[59]	19
1.7	Schematic of transport properties of a MJ for elastic ($eV < h\nu$) and inelastic ($eV > h\nu$) transport. Figure adapted from Ref. [63]	22
1.8	Representative internal current distribution (arb. unit) showing loop current in a C_{60} molecular bridge at a given finite bias voltage. Figure adapted from Ref. [76]	24

List of Figures

1.9 Sign of Seebeck coefficient. (a) Negative for electron dominated current conduction through energy levels above E_F , (b) Positive for hole dominated current conduction through energy levels below E_F . $f(E)$ is the Fermi distribution of electrons in the metal contacts. 29

2.1 Schematic illustration of the hexagonal PAHs as increasingly large sheets of graphene with symmetric (para- p) and asymmetric (m -meta and o -ortho) connections of the contact leads as specifically labelled for a benzene ring. Graphene nanosheet fragments, (b)-(d) have zigzag edges and correspond to the coronene series of benzenoid systems, viz., coronene (C_{24}), circum-coronene (C_{54}) and dicircum-coronene (C_{96}), whereas (e)-(g) have armchair edges; C_{42} , C_{114} , and C_{222} , respectively. 49

2.2 Effects of the magnetic field on the transmission probability $T(E)$ around the LUMO energy of graphene nanosheets with asymmetric (meta-) connection of metal leads for (a) benzene (C_6), the coronene series of PAHs, viz., (b) coronene (C_{24}), (c) circum-coronene (C_{54}) and (d) dicircum-coronene (C_{96}), while (e)-(g), correspond to C_{42} , C_{114} , and C_{222} , respectively. The two transmission peaks at zero fields evolve into a single peak, increasing to its maximum value, $T(E) = 1$, beyond which the peak splits into two. Quantitatively equivalent results are obtained for contact lead at the ortho position. The highest field applied in each case indicates a field beyond which the current stays essentially constant. 57

2.3 (a) Current (in arb. units) through a meta-connected C_{222} graphene corresponding to electron transport within a small energy window ΔE around the LUMO energy of its isolated counterpart at various magnetic field values are indicated. A small shoulder at zero field illustrates the consequence of the split degeneracy brought on by the asymmetric connection of the metal leads. (b) Current through para connected C_{222} , while the inset depicts corresponding transmission probability around the LUMO energy. 58

List of Figures

2.4 (a) Plot of magnetic field B_0 (a measure of the field required for effective control of current) as a function of the number of carbon atoms in the meta-connected model graphene nanosheets for coupling strength $\Gamma=5$ meV (solid line), 0.1 eV (dashed line) and 1 eV (dashed-dotted line). B_0 value for C_6 and C_{24} for $\Gamma = 1$ eV are 2.48 kT and 380 T, respectively. (b) Plot of B_0 as a function of Γ for C_6 (solid line) and C_{222} (dashed-dotted line) with slopes ~ 2.5 T/meV and 5 mT/meV, respectively. 60

2.5 Transmission profile for C_{42} and C_{222} , for B and Γ in the range (0-5 T) and (1-10 meV), respectively. These profiles correspond to the transmission through the respective LUMO energies of the isolated configurations. The locus of transmission maxima $T(E) = 1$ is represented by the dotted line along the peaks, and the corresponding fields are B_0 values. 61

2.6 (a) I-V characteristics of a meta-connected C_{222} for fields, 0 T (solid line) and 3 T (dashed-dotted line) at 10 K with $\Gamma=1$ eV. (b) Respective I-V curves at the same scale are plotted in the presence of Coulomb interaction ($V_C=6$ eV) for comparison. Inset exhibits NDR at around 0.7 V. (c) Plot showing current as a function of applied magnetic field (B) for Coulomb interaction, $V_C=0$ (solid line), 3 eV (dashed line) and 6 eV (dashed-dotted line), at bias voltage $V=1.2$ V. Inset displays dI/dB as a function of B for respective interactions. 63

2.7 (a) I-V characteristics of a meta-connected benzene ring for the fields, 0 T (solid line) and 5 T (dashed-dotted line), at 10 K, $\Gamma=5$ meV. (b) Respective I-V curves in the presence of Coulomb interaction ($V_C=100$ meV). 65

List of Figures

2.8	Transmission probability as a function of electron energy (corresponding to the arrows in the I-V characteristic, Fig. 2.5 (b)) for a meta-connected benzene ring at bias voltages; 2.25, 2.50, 2.80, 3.50 V, showing the evolution of transmission peaks in the respective energy windows $E_F \pm eV/2$ ($E_F = 0$) for the fields, zero (solid line) and 5T (dashed line), $\Gamma=5$ meV. The upper edge of the energy window is represented by the dashed vertical line in each picture; in the bottom panel (3.50 V), it is located at 1.75 eV. No transmission peaks are located in the energy windows except the ones shown above.	66
3.1	Schematic showing current distribution in a two-terminal junction with a benzene ring coupled to an external bias circuit through sites (a, b) . Current configuration shown in the ring corresponds to $V > 2.6$ V, wherein current I_1 in the upper arm is in opposite direction to the total current I .	86
3.2	Bias-induced circular current I_c in a benzene ring junction computed using Eqs. 3.5 and 3.9 for an asymmetric (meta-) connection of the metal lead. They overlap as depicted and are identically similar. Inset shows the bond current ($I_k, k = 1, 2$) in the upper and lower segments of the benzene ring.	91
3.3	Plot of average current-induced force (F_{ave}) on a carbon atom in an asymmetrically (meta-) linked benzene ring as a function of transport current (I) through the molecular ring junction. $I - V$ curve of the junction, exhibiting a ledge at $2V$ is due to the split of otherwise degenerate energy levels of the benzene ring owing to the asymmetric connection of the metal leads, is presented in the inset.	93

List of Figures

3.4	Circular current-induced force on a carbon atom is depicted as a function of circular current in a meta-connected benzene ring for three different coupling strengths (a) $\Gamma = 0.05$ eV, (b) 0.50 eV, and (c) 1.50 eV for $\gamma = 10$. The downward and upward arrows represent force corresponding to an increase in bias voltage in the range $(0 - 2V)$ and $(2 - 4V)$ respectively. Inset depicts the variation of circular current with the bias voltage at respective coupling strengths. The current magnification ratio (I_c/I) achieving its maximum value $\sim 118, 15,$ and 6 at the resonant bias of $2V$ is also presented.	96
4.1	Schematic depiction of the (a) benzene and (b) fullerene molecular junction studied in this work. Transport of the electrons between the left and right leads ($K = L, R$) appears due to the difference $\Delta\mathcal{T}$ between the leads' temperatures, \mathcal{T}_L and \mathcal{T}_R . The hot left lead and cold right lead are kept at temperatures $\mathcal{T}_L = \mathcal{T} + \Delta\mathcal{T}/2$ and $\mathcal{T}_H = \mathcal{T} - \Delta\mathcal{T}/2$, respectively.	115
4.2	Variation of (a) transmission probability $T(E)$, (b) logarithmic transmission $\text{Log}T(E)$ and (c) Seebeck coefficient S , as a function of energy for a para-connected benzene ring junction. The vertical dotted line represents the position of Fermi energy at ~ 0.5 eV above the HOMO energy level, as estimated from the experimental zero-bias conductance value, $G \sim 0.012G_0$ with a positive thermopower, $S > 0$. [22, 23]	117
4.3	Same as in Fig. 4.2 for a C_{60} junction connected symmetrically to the contact leads. The Fermi level that is positioned at ~ 0.02 eV below the LUMO is estimated from the experimental zero-bias conductance value, $G \sim 0.12G_0$ with a negative thermopower, $S < 0$. [24, 25]	118
4.4	Thermoelectric properties of a symmetrically connected benzene ring junction: (a) Electrical conductance, (b) thermopower, (c) thermal conductance, and (d) figure of merit, as a function of incident energy E , calculated for metal-molecule coupling strength $\Gamma=0.1$ eV and temperature $T=300$ K.	119

List of Figures

4.5	(a) Electrical conductance, (b) thermopower, (c) thermal conductance, and (d) ZT as a function of energy E , for a symmetrically connected C_{60} fullerene, calculated for metal-molecule coupling strength $\Gamma=0.1$ eV and temperature $T=300$ K.	120
4.6	Evolution of transmission probability as a function of electron energy around the LUMO state of a C_{60} fullerene molecule connected asymmetrically to the metal electrodes at zero temperature for the metal-molecule coupling strength, $\Gamma = 0.01$ eV.	123
4.7	(a) C_{60} fullerene junction. (b) Field influence on the I-V characteristics of an asymmetrically-connected C_{60} for $\Gamma = 0.01$ eV at zero temperature and field is applied along the C_3 symmetric axis. Essentially indistinguishable I-V characteristics are obtained for the field applied along the C_2 axis (not shown).	124
4.8	(a) Same as in Fig. 4.7, however, with an impurity atom placed at the center (red color). (b) I-V characteristics in presence of impurity energy level placed just below the LUMO. The inset shows a current around 0.4V bias voltage corresponding to current conduction through the impurity energy level.	125
4.9	Magnetic field effects on the thermopower or Seebeck coefficient S around the LUMO energy of the symmetrically connected fullerene molecular junction for four different values of the magnetic field, $B = 0, 25 T, 50 T,$ and $100 T$	127

Chapter1

Introduction: The Background

Abstract

This chapter provides an outline of the most popular and trending topics concerning the work undertaken in this thesis. Background materials and relevant literature are presented, as well as the strategy of the work, with details covered in the individual chapters.

1.1 Preamble

Miniaturization of electronic device components down to the molecular size has been one of the top priorities in the field of nanotechnology since the proposal of molecular rectifiers in 1974 [1] leading to the unprecedented advent of the “Molecular Electronics”, [2, 3] the origins of which can be traced to late 1950s. [4–6] The concept of using a wide range of single molecules, molecular aggregates, or nano-size assemblages of molecules as device components with specialised capabilities is at the heart of molecular electronics. On both the theoretical and experimental fronts, significant progress has been made, culminating in the development of a new class of approaches and methodologies that have the potential to revolutionize physics and engineering at the molecular scale. [6] In particular, a number of physical phenomena that are often not accessible in ordinary silicon-based materials have been found in molecules that are appropriate for device applications. [7] Also, because the size of the molecules allows for the various quantum effects to manifest, molecular electronics are progressively being acknowledged as a viable alternative to some challenges encountered in traditional semiconductor-based electronic devices. For instance, solving the heating effect, restricted functionality, and fabrication expense are all significant challenges in semiconductor-based devices. Molecules, on the other hand, use the quantum effect of electrons, hence their electrical transport properties differ from those of semiconductor devices. This allows the molecules to have more control over electron transport, allowing

them to be used as potential wires, diodes, transistors, switches, and memory devices in molecular circuits.[8, 9] Small volume, integration compatibility, efficient operation, and power economy are all possible advantages of molecular devices over their silicon counterparts.[10]

The rapid development of experimental techniques in recent years down to the nanoscale level and in-depth theoretical research has made substantial discoveries in molecular electronics. In terms of technology, the once-difficult challenge of creating a single-molecule electronic device is now becoming a reality and becoming increasingly simple.[11] The building blocks of the molecular electronics, viz., the molecular junctions (MJs), which are made by sandwiching single-molecule between electrodes, have shown to be an excellent platform for investigating quantum transport at the molecular level. Fig. 1.1 depicts a single-molecule junction (SMJ) as a fundamental component in single-molecule electronic devices. Studies on MJs have contributed significantly to the understanding of the fundamental transport mechanisms in molecules and demonstrated a variety of intriguing electron transport phenomena, including rectification, transistor effects, interference effects, switching operation, negative differential resistance, optoelectronic phenomena, spintronics, and thermoelectricity.[12–14]

In molecular electronics, tuning quantum interference in the coherent

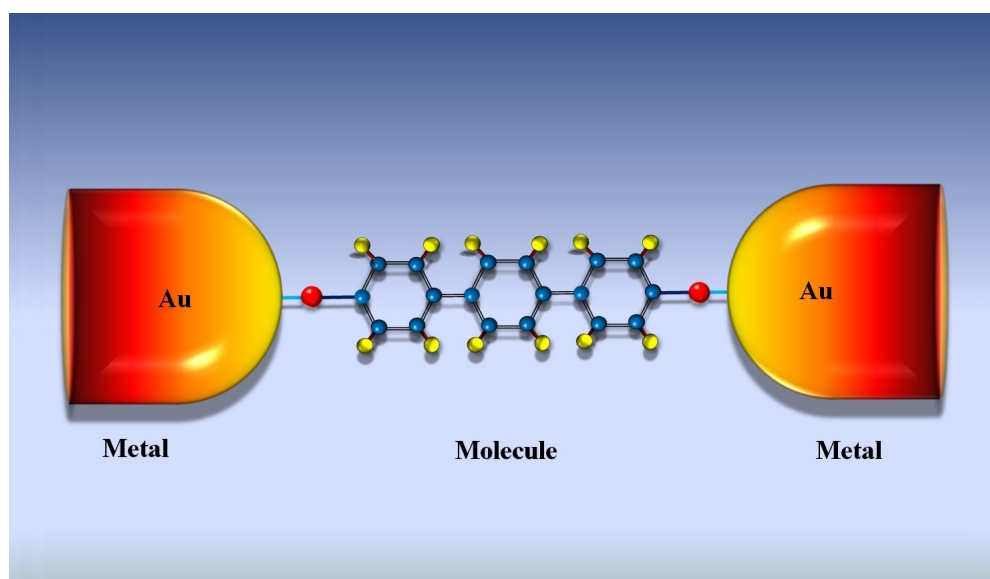


FIGURE 1.1: An illustration of a SMJ in a “metal-molecule-metal” configuration.

transport of electrons through molecular ring junctions could prove to be an effective approach for current control. Under certain conditions, an externally applied magnetic field can vary the energy levels of ring structure molecules, allowing control of the electron transmission function, which accounts for electron transport through the molecules.[15, 16] The formation of circular currents and the associated effects are important features of electron transport through ring structures.[17] Electronic device components composed of ring molecules have reliability challenges due to the accompanying circular current-induced force. These are the themes of interest that have been considered in this thesis.

The study of heat-to-electrical energy conversion at a molecular level in the light of quantum interference phenomena that can be tuned for improved thermoelectric properties is also possible using ring structure MJs. Given the wide diversity of ring molecules and customizable features and functionalities, the

study of thermoelectricity in molecules could provide an alternate avenue for fulfilling future energy needs with effective thermoelectric power conversion and the design of energy-efficient molecular devices. In the design and operation of energy-efficient molecular devices, the ability to manage heat transfer, dissipation, and conversion into electricity are crucial. This is where the ring structure junctions may outperform other configurations. Identifying the mechanism for modulating the thermoelectric power of MJs is the first critical step in moving beyond the bimetallic thermoelectric devices. This is one of the topics addressed in this work. In what follows, we briefly outline the trending topics that are essential and serve as the basic foundation of the research conducted in this thesis.

1.2 Single-Molecule Junctions

The field of single-molecule electronics grew out of a 1974 proposal that molecules could have rectifying capabilities.[1] Despite the promise of smaller, more efficient, and cost-effective electronic devices, the practical realization took nearly two decades from the initial claim when the first single-molecule transport measurements were reported in 1997.[18] This triggered a race to develop the best experimental techniques for fabricating single-molecule devices and investigating the different phenomena that occur in the setup. Thus, the MJs can be considered a powerful tool to explore the physical processes taking place at the molecular level.[19, 20] Perhaps, the enormous advantages foreseen in the molecule-based “bottom-up” approach may have prompted the experimentalists to keep pushing

the field forward.[14, 21–23] On the other hand, from the very beginning the theoretical tools to examine the microscopic complexities of what happens at the molecular level, and most importantly, their comparative performance over one another made consistent development. We here briefly review the experimental and theoretical methods widely used in the study of electronic transport characteristics of the MJs.

1.2.1 Experimental methods

Experimenting on various properties concerning the electron transport phenomena at the molecular level is both fascinating and difficult. Among several methods, the break junction technique has emerged as one of the most reliable experimental methods for creating the SMJ and has proven to be particularly useful in the measurement of the conductance of individual molecules.[24] The two most common types of break junctions are (a) scanning tunneling microscope-based break junctions (STMBJs) and (b) mechanically controllable break junctions (MCBJs).[25, 26] A sketch of these techniques is presented in Fig. 1.2. The STMBJs work by repeatedly forming and rupturing the STM tip contact with the substrate, which is commonly gold tip-gold substrate, in the presence of target molecules. The breaking of contact between the metal tip and metal substrate enables the formation of MJs in a “metal-molecule-metal” configuration, cf. Fig. 1.1. Current is measured and studied as a function of tip distance from the substrate until a single-molecule connection is established. In contrast, in the MCBJs, a

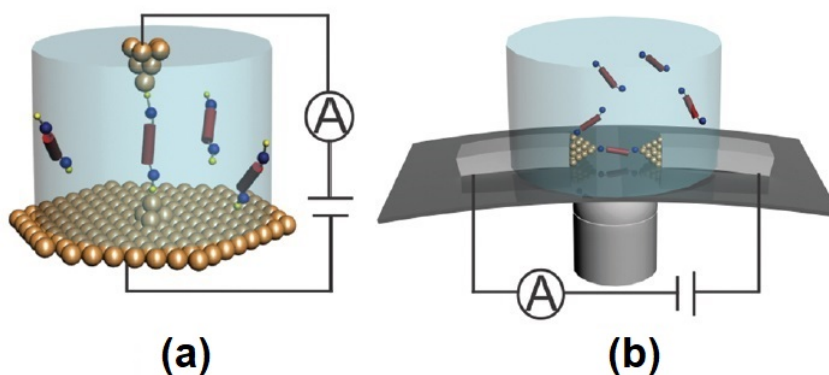


FIGURE 1.2: Schematic representation of (a) scanning tunneling microscopy based break junction (STMBJ) and (b) mechanically controllable break junction (MCBJ). Figure adapted from Ref. [26]

notched metal wire is bonded to a substrate and a mechanical actuator is used for bending the substrate in a solution containing target molecules. While the solvent evaporates, the metal wire containing target molecules adsorbed on its surface bends and eventually breaks, leaving a metal-metal gap filled with target molecules. Current readings are taken until the wire breaks up forming a metal-molecule-metal bridge. This is repeated until the characteristics of a SMJ are achieved confirming the presence of a single molecule between the two metal contacts. While both approaches can be used to create SMJs, the MCBJ technique has a few advantages over the STMBJ. The MCBJ, for example, is insensitive to vibrational noise. Its flexibility over the STMBJ adds an extra feature by allowing it to integrate with multiple spectroscopic techniques, like UV-Vis and Raman, to extract structural information while simultaneously measuring transport properties. Due to mechanical stability, the MCBJ setup enables the study of the current-voltage characteristics in the course of stretching and elongation of the sample molecules. The other methods for fabricating a molecular scale gap

for a SMJ include the lithographic and electromigration techniques.[27, 28] Junction characterizations through transport measurements establish the presence of a single molecule between the metal contacts.

1.2.2 Theoretical methods

The formulation of theoretical descriptions and simulations of electron transport through MJs that reproduce experimentally observed phenomena is a difficult task because it necessitates methods that can describe the electronic structure and dynamics of molecules taking into account the correlation effects associated with the electron-electron and electron-phonon many-body interactions. Nonetheless, from the start of ideas of molecular devices, theoretical approaches have evolved gradually and significantly, allowing the study of the fundamental mechanisms of electron transport through the MJs.[29–31]

The basic description of electron transport through MJs evolved from the Landauer formulation of scattering of the non-interacting electrons at the mesoscopic tunnel junction or barrier. A schematic representation of the scattering mechanism is shown in Fig. 1.3. The left and right contact regions/leads are the reflectionless electron reservoirs that inject electrons into the central mesoscopic system according to the Fermi distributions of the leads at the respective chemical potentials $\mu_{S/D}$. In the absence of electron-electron interactions and inelastic scattering, electron transport through a mesoscopic junction can be described in terms of transmission probability function $T(E)$ that each electron at energy E scatters

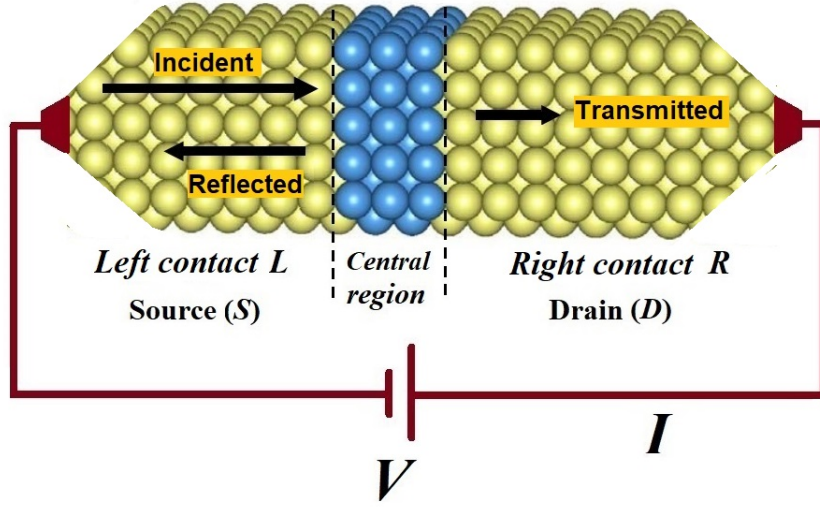


FIGURE 1.3: Schematic representation of mesoscopic tunnel junction or barrier, consisting of contact leads (L, R) and the central scattering region. Length of the arrows represent the amplitude of the incident electron wave from the left, transmitted to the right and reflection back to the left side. The junction is maintained at a bias voltage V that sets current I through the junction.

through the junction maintained at a bias voltage V . If an electron entering from left is transmitted through the central region to the right side with an energy equal to the Fermi energy E_F of the contact lead, the electric conductance that defines the zero bias response corresponding to one electron conduction channel is [32, 33]

$$G = \left. \frac{dI}{dV} \right|_{V=0} = \frac{2e^2}{h} T(E_F). \quad (1.1)$$

Within the non-interacting picture of electron transport, the electron conduction at zero external bias is only due to the difference in Fermi distribution functions of the contact leads. Note that the factor of “2” in the above relation carries the significance of the electron spin degeneracy. Thus, for one fully open channel, i.e., for $T(E_F) = 1$, the conductance is $G_0 = 2e^2/h = 77.48 \mu S$, which is the quantum of electrical conductance. Consider that an electron is injected from the left in the

mode k (conduction channel) and emerges out of the scattering region in the mode k' with transmission amplitude $t_{kk'}$. Each of such electron contributes $2e^2/h|t_{kk'}|^2$ to the conductance. Therefore, the total conductance is

$$G = \frac{2e^2}{h} \sum_{k,k'} |t_{kk'}|^2, \quad (1.2)$$

where the summation extends over all input and output modes (kk'). The finite bias response at zero temperature is obtained by integrating the transmission probability function over all electron energies between the chemical potential energy $\mu_{L/R} = E_F \pm V/2$ of the contact leads, i.e.,

$$I = \frac{2e^2}{h} \int_{\mu_L}^{\mu_R} T(E) dE. \quad (1.3)$$

It must be mentioned here that a symmetric potential drop of $V/2$ at the left/right interfaces has been found to reproduce better experimental I-V characteristics.[34] At finite temperature, the Fermi distributions ($f_L(E), f_R(E)$) of the electrons in the contact leads must be taken into account in evaluating the net transport of electrons. Also, in the case of inelastic scattering events involving energy exchange, the electrons outside the conduction window ($\mu_R - \mu_L$) may contribute to the total electron transport. Thus, a more general expression of the current reads[33]

$$I = \frac{2e^2}{h} \int_{-\infty}^{+\infty} T(E) (f_L(E) - f_R(E)) dE. \quad (1.4)$$

Central to the current calculation is the determination of transmission probability $T(E)$ for which one may use the scattering theory which, however, cannot capture the intricate details of electron-electron interactions and many-body effects, though decoherence phenomena (thermal dephasing) can be studied within the phenomenological model-based density matrix formulation.[35] Also, the bulk properties of the contact lead affecting the electron transport through the bridging molecule cannot be described. Alternative to this in determining $T(E)$ is a widely used method of the Green's function technique that allows, in principle, the inclusion of various interactions.[33] The basic structure of the Hamiltonian in the transport problem is

$$\hat{H} = \hat{H}_M + \hat{H}_K + \hat{H}_{KM}, \quad K = L, R \quad (1.5)$$

where \hat{H}_M is the Hamiltonian of the molecule, \hat{H}_K is the Hamiltonian representing the bulk contact leads ($K = L, R$) and \hat{H}_{KM} is the coupling Hamiltonian. The only problem is the Hamiltonian matrices for the contact leads which are infinite-dimensional. In Green's function formulation, the influence of the contact leads is accounted for through the self-energies $\Sigma_{K=L,R}$ that enter in the retarded Green's function of the molecule. Due to the finite contact region of the contact leads, whereby only the localized atomic orbitals near the contact region significantly overlap with the molecular orbitals for the electron transport, the self-energy matrices are considered finite-dimensional and the numerical calculation is possible. All information on the transport properties of the molecule will be contained in

the retarded Green's function matrix G^r of the molecule

$$G^r(E) = [EI - H_M - \Sigma(E)]^{-1}, \quad (1.6)$$

where I is the identity matrix and $\Sigma(E) = \Sigma_L(E) + \Sigma_R(E)$ is the total self-energy.

All the matrices are expressed within the finite-dimensional Hilbert space of the molecule. The transmission function is then evaluated as

$$T(E) = Tr[\Gamma^L G^r \Gamma^R G^a], \quad (1.7)$$

where the trace is taken in the basis set of the molecule. $G^a = G^\dagger$ is the advanced Green's matrix and $\Gamma^{L,R} = i[\Sigma_{L,R} - \Sigma_{L,R}^\dagger]$ are the broadening function matrices of the leads, i.e., the coupling matrices. The influence of the bulk contact leads enter implicitly through the self-energies, $\Sigma_{L,R}$. It must be mentioned here that a MJ connected across a bias voltage V that sets current I to flow through the molecule is a non-equilibrium system. An appropriate description requires the non-equilibrium Green's function (NEGF) method which, however, results in the same expression for the transmission function $T(E)$, i.e., Eq. 1.7 for the non-interacting electrons as considered in the Landauer's approach.[33] It is to be noted that the Landauer picture of electron transport through elastic scattering breaks down when the interactions are present.

The inclusion of interactions in the Hamiltonian of the central region in the MJ set is crucial in reproducing the experimental results of the transport

problems. This is usually done using the NEGF formalism, also referred to as the Keldysh formalism.[36, 37] Central to the NEGF formalism is the Keldysh equation that defines the lesser Green's function as

$$G^<(E) = G^r(E)\Sigma^<(E)G^a(E), \quad (1.8)$$

where $\Sigma^< = \Sigma_L^< + \Sigma_R^<$ is the total lesser self-energy of the contact leads. The lesser self-energies $\Sigma_{L,R}^<$ of the leads are related to the broadening functions $\Gamma^{L,R}$ as $\Sigma_{L,R}^< = if_{L,R}\Gamma^{L,R}(E)$, where $f_{L,R}$ is the Fermi distribution of electrons in the contact leads (L, R). Within the NEGF formalism, the current under the steady-state situation can be calculated using the Meir-Wingreen formula,[38]

$$I = \frac{e}{\pi\hbar} \int_{-\infty}^{+\infty} \frac{i}{2} \text{Tr} [(f_L\Gamma^L - f_R\Gamma^R)(G^r - G^a) + (\Gamma^L - \Gamma^R)G^<] dE. \quad (1.9)$$

For the scope of this thesis, we heavily rely on the NEGF method and its wide range of applicability providing insight into the physics of transport across the MJs. The only concern with the NEGF method is that it is based on the perturbation theory, which renders it an approximate method. Any assumption and simplification thereof or the inclusion of interaction in the molecule will be discussed in the respective chapters.

Another important theoretical description that merits special mention is

the quantum master equations (QMEs), which are extensively used in the investigation of the electron transport dynamics in the MJs.[39–41] Though numerically exact, the QMEs are restricted to weak contact coupling to the bridging molecule and cannot capture the effects resulting from the broadening feature of the molecular energy levels associated with the contact couplings. Predictive and self-consistent calculations of the transport properties of the molecules usually involve *ab initio* treatments.[42–44] Such calculation schemes are gaining more popularity that combines the non-equilibrium Green’s function technique with the density-functional-based tight-binding simulation approach.[45–47] Computational packages are now available for the calculation of the transport properties of molecular-scale devices.

In what follows, we provide a brief outline of the most important physical mechanisms concerning electron transport through the MJs and factors influencing electron transport.

1.3 Fundamentals of Electron Transport Through MJs

In the MJs, several fundamental physical mechanisms govern the electron transport through the bridging molecules.[21] Understanding them is a prerequisite as well as a challenging task for an effective, reliable and robust design that benefits the architecture for molecular electronic applications.

1.3.1 Metal-Molecule coupling

Metal-molecule interface plays a decisive role in the electron transport through the bridging molecules. Depending on the strength of metal-molecule bonding with a range of binding energies corresponding to bonding strengths that vary from weak physisorption to strong chemisorption, the discrete frontier molecular orbitals get hybridised to varying degrees when they are coupled to continuum states of the metal. This gives rise to the broadening of the molecular energy levels leading to a smeared resonance for alignment between the frontier energy levels of the molecule with the energy states of the metal contacts. In practice, the level alignment of the molecular energy levels is done with the application of a gate voltage that makes them enter the conduction window, $\mu_{L/R} = E_F \pm V/2$. The level resonance can be directly linked to the energy barrier and efficiency for electrons crossing the interface. In fact, the peaks in the transmission function $T(E)$ correspond to the electron transport through the level resonance states. Also, the position of the highest occupied molecular orbital (HOMO) or the lowest unoccupied molecular orbital (LUMO) energies relative to Fermi level E_F is central in determining the zero-bias conductance of the junction.

Since the level alignment, broadening and electron transport are inter-related, an accurate description of level broadening is important in determining the electron transport, the stronger the coupling, the larger the level broadening leading to an enhanced transport. The quantitative measure of the metal-molecule

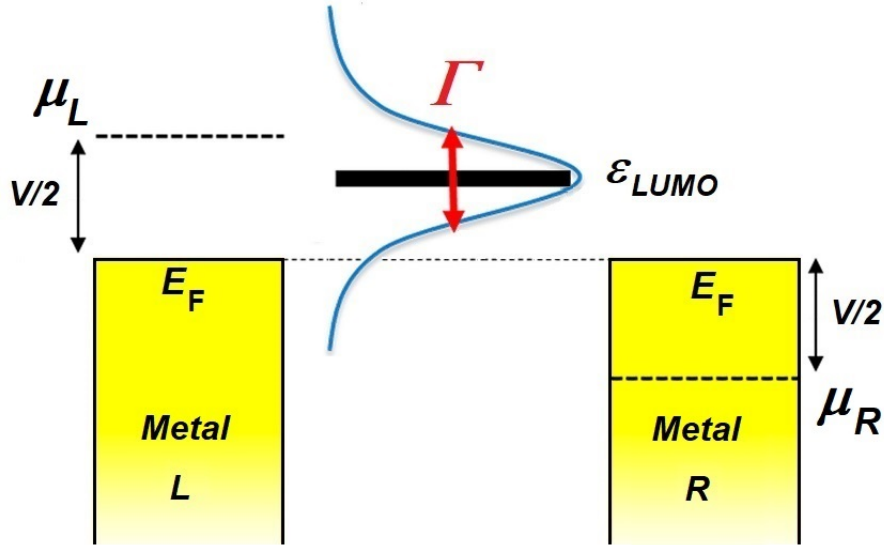


FIGURE 1.4: Schematic of broadening of frontier energy level ϵ_{LUMO} of the bridging molecule in a MJ. The broadening line width is Γ . The bias voltage V modulates the electron energy states in the metal contact leads (L, R) over the filled states under the Fermi energy level E_F .

coupling is the resulting broadening of the molecular energy levels with the line-shape taking up a Lorentzian form as exemplified in Fig. 1.4. The level broadening is described by a broadening function, i.e., line width Γ , which can also be related to the time taken for an electron placed in that energy level to escape into the contact lead. It must be noted, however, that the broadening effect as described by a Lorentzian profile is true only if the embedding self-energies $\Sigma_{L,R}$ quantifying the coupling of the molecular orbital to the continuum states of the metal leads are purely imaginary, i.e., $\Sigma_{L,R} = -i/2\Gamma_{L,R}$. In general, the self-energy includes a real part that corresponds to a shift in the energy of the discrete molecular energy states, while the imaginary part is associated with the resonance broadening. Also, the level broadening could be different for different energy levels, however, in the study where conduction through individual energy levels is less relevant, one

usually uses the so-called “wide band limit”, for which the broadening is energy-independent. In a practical situation, the contact coupling could be asymmetric, i.e., $\Gamma_L \neq \Gamma_R$, which could lead to distinct transport properties, such as rectification that can be inferred from asymmetric I-V characteristics.[48, 49] Usually, the contact coupling of the order of a few tens of meV or less is considered a weak coupling.[50]

1.3.2 Anchoring groups

A critical issue that invites special attention is the formation of a reliable electronic coupling and robust mechanical contact between the bridging molecule and the metal leads. Therefore, it is crucial to understand how the anchoring group affects the electron transport through the MJs, and possibly the thermoelectric properties.[51] A suitable anchoring group should have a strong binding and efficient electrical contact between the molecule and the metal contacts, thereby lowering the energy barrier for sufficient electron transport for device applications. However, it is known that each anchoring group has shortcomings and limitations over others.[52, 53] Among various anchoring groups,[54] the most widely studied and commonly used anchoring groups are thiol and amine groups, cf Fig. 1.5. In fact, thiol ($-\text{SH}$) is studied and used extensively to establish contact between the molecule and the metal contacts (usually gold) due to the strong affinity of sulfur with metals. Although the thiol-gold (S-Au) interaction is known for covalent bonding this, however, exhibits variations and fluctuations that affect the

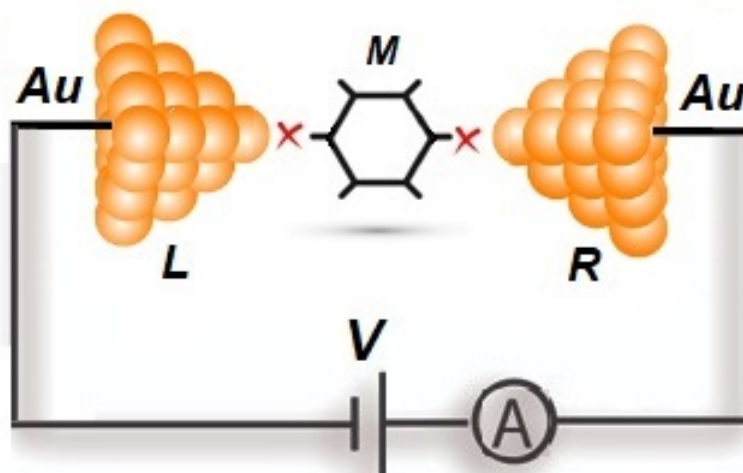


FIGURE 1.5: Schematic of a MJ wherein a molecule M binds to the metal contacts L, R (e.g., Au) through the anchor groups, $X=-SH, -NH_2$ etc.

transport characteristics of the bridging molecules. Also, the thiol group need not necessarily be chemisorbed to gold contacts. Instead, it may be physisorbed retaining the hydrogen atom intact.[55] The amine ($-NH_2$) group is also been subjected to various tests. The binding of amine to gold contacts is known to be a weak covalent bond but exhibits stable and more well-defined transport properties than the thiol-anchored molecules do, thereby providing a potential platform in the fabrication of the molecular electronic components.[53, 56]

1.3.3 Interface geometry

The geometry of metal contacts at the metal-molecule interface is crucial in deciding the stability of the MJ devices, which is also important in controlling electron transport through molecular devices. The rational design of metal lead into atomic-scale planar contact provides greater stability while the atomic-scale sharp

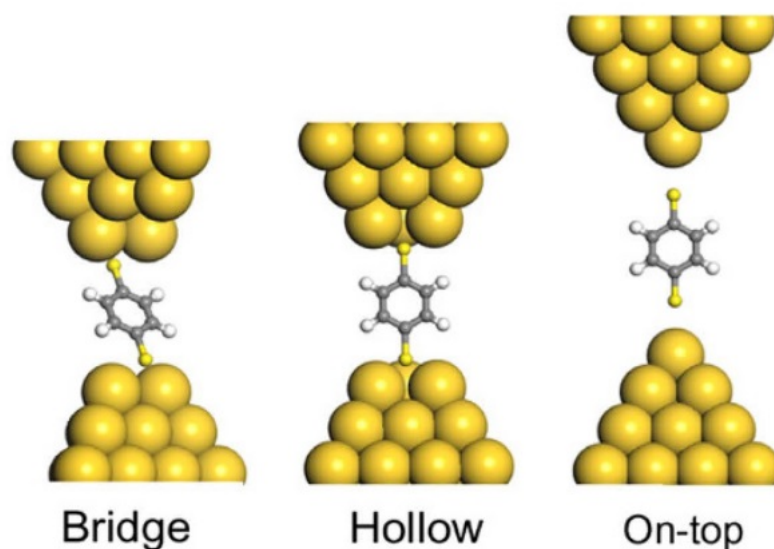


FIGURE 1.6: Representative three different adsorption configurations. Current is maximum for bridge configuration and least for on-top configuration.[59]

contact leads to higher electron transport due to enhanced coupling between the molecule and point contact lead.[57] Also, the adsorption configurations of the molecules on the metal surface greatly affect electron transport. For instance, the adsorbed molecule lying almost parallel to the metal surface, such as Au(111), or perpendicular to the surface, for example, can potentially impact the electron transport across the interface.[58] Fig. 1.6 depicts the three different adsorption configurations of benzene dithiol on gold contacts. Calculations show the current is maximum for the bridge configuration and least for the on-top configuration.[59] Of interest to us is the metal-molecule coupling geometry, which could be either a symmetric connection to the metal leads or an asymmetric configuration. It was observed that when a ring structure molecule is connected symmetrically to metal contact, the conductance is larger than when the connection is asymmetric.[17, 60]

This is more easily exemplified in the case of a benzene ring with metal leads connected in the para position for symmetric configuration and in the meta position for asymmetric configuration.[15] Particularly in a molecule possessing degenerate energy levels, the asymmetric connection of the metal contacts lifts the degeneracy, opening up the energy gap between them, while the symmetric connection does not affect the degeneracy of the energy levels. The degenerate energy levels of the molecule conduct more when brought into resonance compared to the split energy levels. This makes the symmetric connection have a greater conductance than the asymmetric connection. This can also be understood in terms of quantum interference of electron waves in the molecule. In a symmetric connection, the electron waves interfere constructively resulting in enhanced conduction, while in the asymmetric connection, the electron waves interfere destructively leading to reduced conduction. This interpretation, however, cannot be easily applicable in the multi-ring structure junctions. It is both the metal-molecule coupling geometry and quantum interference that play inter-related roles in determining electron transport in ring structure MJs.

1.3.4 Electron-phonon interaction

Understanding and controlling energy loss mechanisms during electron transport through MJs is fundamental for the development of molecule-based devices. Interaction of electrons with the molecular vibrational motion during electron transport through molecules leading to inelastic scattering between electrons and phonons

is known to be an important source of energy dissipation.[61] Due to the narrow gap between the metal contacts, most of the electron flows through the molecule ballistically (i.e., electrons' mean free path is larger than the gap, $l \gg L$) without any energy loss (the so-called elastic transport), however, only a small fraction of transport electrons undergo inelastic scattering processes. It is this small fraction of inelastically scattered electrons that lead to relevant events that show up in the inelastic electron tunnelling spectroscopy (IETS) and induce local heating effects.[62] Inelastic processes play an important role in the loss of coherence or dephasing of the tunneling electrons. Viewed from the perspective of molecular energy levels, the electrons are transported through the energy levels of a vibrationally excited molecule in a variety of vibrational modes leading to characteristic conductance different from elastic transport. In fact, excitations of specific vibrational modes by injecting electrons from the contact leads show up sharp features in the differential conductance as illustrated in Fig. 1.7. When the applied voltage V exceeds characteristic vibrational energy of the molecule, it causes an inelastic event that an electron passing through the molecule deposits energy corresponding to a single quantum of vibration ($h\nu$) leading to an increase in the rate at which electron flows. This behavior would lead to changes in the slope of the current I , changes in the values of the conductance ($G = dI/dV$), and peaks ($G = d^2I/dV^2$) in the IETS spectrum. The peaks correspond to inelastic behavior associated with the excitation of a vibrational mode of the bridging molecule in the MJs. The vibrational excitations caused by the conducting electrons can

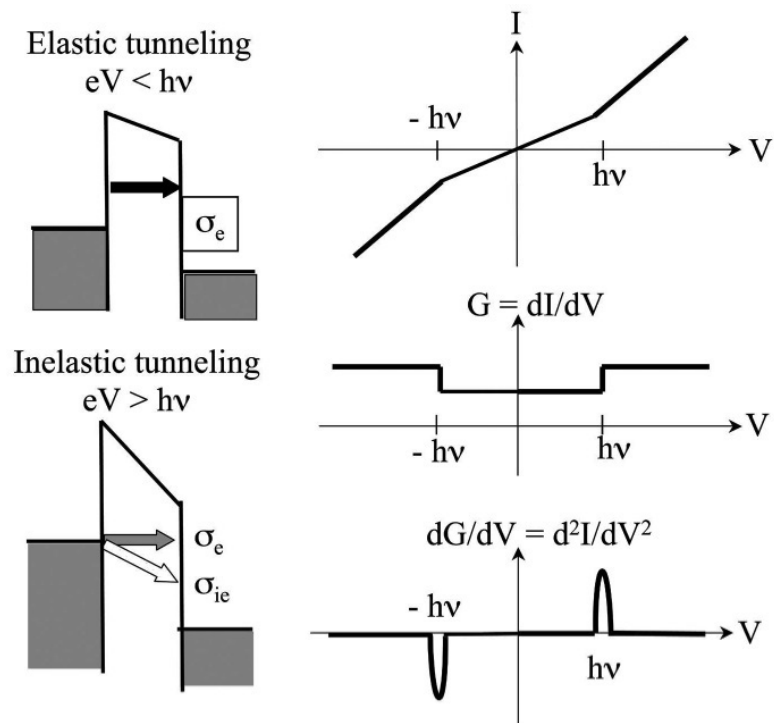


FIGURE 1.7: Schematic of transport properties of a MJ for elastic ($eV < h\nu$) and inelastic ($eV > h\nu$) transport. Figure adapted from Ref. [63]

change molecular configurations, thereby affecting the functionality and performance of the molecule-based devices. The extreme case could be that the local heating effects may lead to the ultimate breakdown of the junction. It is therefore desired to remove heat generated by electronic energy dissipation which depends on the ability of the molecule to relax vibrational quanta into the contact leads. Significant progress has been made in heat management at the molecular scale level.[64, 65]

1.4 Quantum Loop Current

Theoretical studies of the electron transport properties of a mesoscopic quantum ring coupled to metal contacts have been ongoing for quite some time.[66–69] Transmission resonances associated with ring energy level degeneracy corresponding to the opposite angular momenta $\pm m$ of electrons in the symmetrically connected rings account for enhanced electron transmission over the asymmetric counterpart in which degeneracy is lifted. In the quantum interference picture, this is attributed to the constructive interference of electron waves in the symmetrically connected rings.[70] Also, the possibility of magnetic field control of electron transport through such a ring under a weak coupling situation has been investigated.[71–73] In the same spirit, the peculiarity of asymmetric geometry connection of the molecular rings to the contact leads, which allows electron transmission to be modulated by an externally applied magnetic field has attracted enormous interest in comparison to its symmetric version.[15–17]

Characteristic of an asymmetrically connected quantum loop (mesoscopic or molecular ring) is the circulating current in the loop with magnitude and direction dependent on the injected electron energy i.e., on the bias voltage.[17, 74] Under certain bias voltage, such loop or circulating current (hereafter, circular current) far exceeds the total current through the molecule. Such a current magnification is typical in a molecular bridge consisting of molecular rings.[75, 76] A schematic of quantum loop current in a C_{60} molecular bridge is shown in Fig.

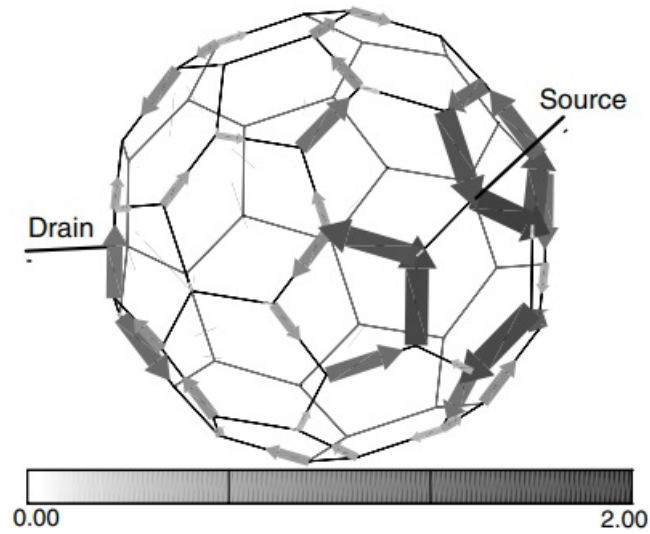


FIGURE 1.8: Representative internal current distribution (arb. unit) showing loop current in a C_{60} molecular bridge at a given finite bias voltage. Figure adapted from Ref. [76]

1.8. Concerning the work presented in this thesis, certain aspects like the circular current, asymmetric connection and magnetic field effect are of prime importance. The very definition of circular current as a component of current that acts as a sole source of induced magnetic flux in the ring is discussed in Ref. [17] and the circular current is evaluated in terms of bond currents. However, the bond currents are experimentally not accessible and thus it is imperative to look for an alternative method to determine the circular current in the ring. This is carried out in the line with the definition of persistent current in the superconducting ring. This is presented in a later chapter. Also, the circular current-induced force is investigated. We now briefly present the notion of current-induced force.

1.5 Current-Induced Force

The future of molecular electronics depends critically on the reliability and reproducibility of the device characteristics. The local heating effect in the MJ, as discussed in the preceding section, poses a significant challenge to the reliability issue.[62, 77] In addition, the current magnifying effect seen in the ring structure junctions may exaggerate the situation to the point where the MJ ceases to work due to current-induced force leading to atomic rearrangements, or even mechanical failure. The current-induced forces are roughly proportional to the magnitude of the current.[77, 78]

The Hellmann-Feynman forces that have been generalised for the transport problems are usually used in the calculation of current-induced forces.[79] They are evaluated as the gradients of total energy with respect to the movement of atomic nuclei. The current-induced forces arise, fundamentally, through the momentum transfer from the transport electrons to the atomic nuclei.[80, 81] Physically, even in the limit of elastic electron transport, for example, zero or negligibly small electron-vibration coupling, the atomic nuclei configuration in the molecule determines the effective potential the transport electrons feel, which determines the characteristic current-voltage relationship of the bridging molecule. The ability the transport electrons exert a net force on individual atomic nuclei cannot be ignored.[62] Concerning reliability, a molecular ring device designed without due

attention to the circular-current induced force would be indeed questionable in future. This is the focus of the study presented in this thesis.

1.6 Molecular Thermoelectricity

One of the major concerns in the MJ devices is the power dissipation in the form of heat, which may cause a thermal runaway of molecular devices and thus heat management is indispensable. This is the major reason why molecular thermoelectricity in particular has seen an upsurge in interest in recent years, though the discovery of thermoelectricity in bimetallic junctions is two centuries old. The study of molecular thermoelectricity focuses on the conversion of waste heat into usable electrical power (Seebeck effect), which is feasible provided molecules with high thermoelectric efficiency could be identified. The reverse process in which a passage of electric current develops temperature difference (Peltier effect) can be viewed as heat transport at the expense of electric power. Both of these processes are potentially important in the energy filtering properties of molecules, for example, in the heat management in molecular devices. Traditional or more recent thermoelectric junction devices are predominantly made up of metal alloys or inorganic materials.^[82] Although their efficiency significantly improved in the last few decades, it is highly desirable to design and study thermoelectric junction devices at a molecular scale in the hope of resolving heating effects in the MJ. Understanding how atomically precise structural modifications in molecules might alter the thermopower of molecular devices is extremely important. The development of

next-generation energy-efficient molecular devices may benefit significantly from the study of molecular thermoelectricity.[83–85]

Our concern in this thesis is the study of the magnetic field effect on the thermoelectric power (also known as Seebeck coefficient, S) and thermoelectric figure of merit (ZT) of single-molecule thermoelectric junction device. We now briefly review the thermoelectric power and figure of merit that quantify the effectiveness of a MJ as a thermoelectric device.

1.7 Thermoelectric power

The induced thermoelectric voltage in the Seebeck effect will be quantified in terms of thermopower (i.e., Seebeck coefficient, S) as a measure of the magnitude of an induced voltage due to temperature difference across that material. It is the difference between the Fermi distribution of electrons at higher and lower temperatures that induce the thermoelectric voltage.

For the calculation of thermoelectric properties like thermopower or Seebeck coefficient, the Landauer formalism is commonly used. Within this formalism, the thermoelectric power of MJs can be expressed in terms of electron transmission function $T(E)$. For a voltage difference ΔV caused by temperature difference $\Delta\mathcal{T}$, the Seebeck coefficient is

$$S = -\frac{\Delta V}{\Delta\mathcal{T}} = -\frac{\pi^2 k_B^2 \mathcal{T}}{3e} \frac{1}{T(E_F)} \frac{\partial T(E_F)}{\partial E}, \quad (1.10)$$

where $\mathcal{T} = \mathcal{T}_L + \mathcal{T}_R$ is the average temperature of the contact leads (L, R). It must be mentioned that this expression is valid only for non-interacting electrons as the Landauer formalism does not capture interactions and inelastic processes. Thus, in calculating the Seebeck coefficient within Landauer's approach, one simply needs to evaluate the transmission function $T(E)$ at the Fermi energy of the contact leads. It is worth noting that the sign of the Seebeck coefficient depends on the slope of the transmission function at the Fermi energy, E_F . In the MJs, the Fermi energy level of the contact leads normally lies in the HOMO-LUMO gap. For if E_F lie above E_{LUMO} or below E_{HOMO} , the molecule would gain or lose an electron respectively. In situations where E_F lie close to E_{LUMO} , the slope of the transmission function is positive and thus $S < 0$. Sign reversal takes place when E_F is close to E_{HOMO} . In the former case, the current conduction is electron dominated, through the LUMOs, while in the latter case, it is hole dominated, through the HOMOs. One may also consider S to represent the electric potential of the cold contact lead w.r.t hot lead. For instance, if electrons transfer from hot to cold lead, the cold lead becomes negative w.r.t the hot lead and S is negative. On the other hand, if holes transfer in the same direction, the cold contact lead would be positive w.r.t the hot lead, in which case, S is positive. This is exemplified in Fig. 1.9. For the MJs consisting of a wide range of molecules attached to the gold contacts, the value of S is measured to range from ~ -50 to $+50 \mu V K^{-1}$.^[86] The dependence of S on the molecular length has been extensively studied. In most of the cases, the dependence is found to be linear. Possible tuning of S through the environmental conditions is been studied.^[87] Most importantly, the electrostatic

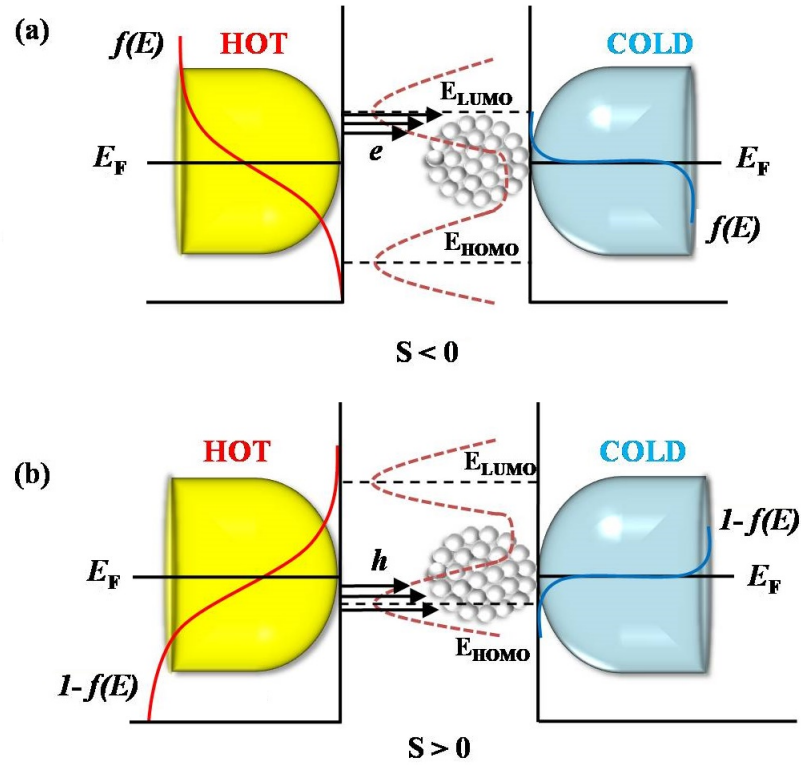


FIGURE 1.9: Sign of Seebeck coefficient. (a) Negative for electron dominated current conduction through energy levels above E_F , (b) Positive for hole dominated current conduction through energy levels below E_F . $f(E)$ is the Fermi distribution of electrons in the metal contacts.

control of thermoelectric properties of SMJs is quite promising.[88] Also recently, it has been demonstrated that the quantum interference effects can be exploited to modulate the thermopower of the SMJs.[89–92]

1.8 Figure of merit

The performance of MJs as thermoelectric devices for the conversion of heat into electricity is characterized by a dimensionless quantity called the figure of merit, $ZT = GS^2\mathcal{T}/k$. An efficient thermoelectric device corresponds to values $ZT > 1$.

In the expression, G is the electrical conductance of the junction and $k = k_{el} + k_{ph}$ is the thermal conductance due to electrons and phonons. It is evident that the thermoelectric materials for which k is small, while G and S are large, would be required for an efficient energy conversion, for which organic materials are suitable due to low thermal conductivity (k_{ph}), however, their electrical conductivity (k_{el}) is much lower than that of the inorganic materials. This leads the ZT of inorganic materials to be larger than that of organic materials.[93] A major hurdle in the determination of ZT of MJs is the experimental measurement of k_{ph} , which is very challenging due to extremely small heat flow across the MJs. Very recent measurements show k_{ph} of the order of a few tens of pW/K.[65, 94]

Due to difficulty in the measurement of k_{ph} , the value of ZT for SMJ is not yet determined experimentally. Several theoretical studies have shown that ZT for SMJs is still far less than unity,[95, 96] however, predictions on the feasibility to increase the ZT value [97, 98] have attracted much attention in the study of the ZT value of the SMJs in recent years.

1.9 Thesis Outline

The purpose of this thesis is to study the electron transport through the ring structure molecular junctions and investigate the possible magnetic field control of current through such junctions. The study also includes the reliability issues of the ring junctions as a result of a potential current-induced force associated with the

induced circular current in the ring. The thermoelectric properties of molecular junctions are also examined for any potential effects of the externally applied magnetic fields. Each chapter begins with an abstract of the work presented in that chapter, followed by background information that effectively acts as a literature review of the work in question. Relevant theory and model calculations are presented, and the conclusions are provided at the end.

In chapter 2, we investigate the possibility of magnetic field control current through ring structure junctions, which we consider as the hexagonal polycyclic aromatic hydrocarbons (PAHs) attached to the metal contacts. These PAHs can be considered to simulate the nano-sized graphene sheets. In order to investigate the effect of the current-induced force in a ring junction, we study the current distribution in the ring and identify the bias-induced circular current in the ring from the magnetic response of the ring to an external magnetic flux in the zero-flux limit. The reliability issues associated with circular current-induced force are discussed. These are presented in Chapter 3. In Chapter 4, we present the influence of external magnetic field on the thermoelectric properties, viz., Seebeck coefficient and figure of merit of a C_{60} -based single-molecule junction. Finally, Chapter 5 summarises the key findings of the work presented in the thesis and discusses possible directions for future work.

References

- [1] A. Aviram and M. A. Ratner, *Chem Phys Lett.* **29**, 277 (1974).
- [2] M. A. Ratner, *Nat. Nanotechnol.* **8**, 378 (2013).
- [3] J. P. Bergfield and M. A. Ratner, *Phys. Status Solidi B* **250**, 2249 (2013).
- [4] H. Choi and C. C. M. Mody, *Soc. Stud. Sci.* **39**, 11 (2009).
- [5] S. M. -González and P. J. Low, *Aust. J. Chem.* **69**, 244 (2015).
- [6] E. Scheer and J. C. Cuevas, *Molecular Electronics: An Introduction to Theory and Experiment*, (World Scientific Series in Nanoscience and Nanotechnology, 2017, Vol 15, 2nd Ed.).
- [7] N. A. Zimbovskaya, *Transport Properties of Molecular Junctions*, (Springer New York, NY, 2013).
- [8] M. R. Stan, P. D. Franzon, S. C. Goldstein, J. C. Lach, and M. M. Ziegler, *Proc. IEEE* **91**, 1940 (2003).
- [9] S. V. Aradhya and L. Venkataraman, *Nat. Nanotechnol.* **8**, 399 (2013).
- [10] P. T. Mathew and F. Fang, *Engineering* **4**, 760 (2018).
- [11] C. W. Fullera, P. S. Padayattia , H. Abderrahima et al. *Proc. Natl. Acad. Sci.* **119**, 1 (2022).
- [12] N. J. Tao, *Nat. Nanotechnol.* **1**, 173 (2006).

References

- [13] J. Del Nero, F. M. de Souza, and R. B. Capaz, *Comput. Theor. Nanosci.* **4**, 1 (2010).
- [14] F. Evers, R. Korytar, S. Tewari, and J. M. van Ruitenbeek, *Rev. Mod. Phys.* **92**, 035001 (2020).
- [15] D. Rai, Oded Hod and A. Nitzan, *J. Phys. Chem. Lett.* **2**, 2118 (2011).
- [16] D. Rai, Oded Hod and A. Nitzan, *Phys. Rev. B* **85**, 155440 (2012).
- [17] D. Rai, O. Hod, and A. Nitzan, *J. Phys. Chem. C* **114**, 20583 (2010).
- [18] M. A. Reed, C. Zhou, C. J. Muller, T. P. Burgin, and J. M. Tour, *Science* **278**, 252 (1997).
- [19] Y. Zang, E. -D. Fung, T. Fu, S. Ray, M. C. Garner, A. Bores, M. L. Steigerwald, S. Patil, G. Solomon, and L. Venkataraman, *Nano Lett.* **21**, 673 (2021).
- [20] Z. Li, L. Mejia, J. Marrs, H. Jeong, J. Hihath, and I. Franco, *J. Phys. Chem. C* **125**, 3406 (2021).
- [21] H. Song, M. A. Reed, and T. Lee, *Adv. Mater.* **23**, 583 (2011).
- [22] R. J. Nichols and S. J. Higgins, *Annu. Rev. Anal. Chem.* **8**, 389 (2015).
- [23] H. Chen and J. F. Stoddart, *Nat. Rev. Mater.* **6**, 804 (2021).
- [24] K. Wang and B. Xu, *Top Curr Chem (Z)* **375**, 17 (2017).

- [25] L. Sun, Y. A. D. -Fernanded, T. A. Gschneidtner, F. Westerlund, S. L. -Avila, and K. M. -Poulsen, *Chem. Soc. Rev.* **43**, 7378 (2014).
- [26] V. Kaliginedi, A. V. Rudnev, P. M. -Garcia, M. Baghernejad, C. Huang, W. Hong, and T. Wandlowski, *Phys. Chem. Chem. Phys.* **16**, 23529 (2014).
- [27] H. S. J. van der Zant, E. A. Osorio, M. Poot, and K. O'Neill, *Phys. Stat. Sol. (b)* **243**, 3408 (2006).
- [28] A. Gee, A. H. Jaafar, and N. T. Kemp, *Nanotechnology* **31**, 155203.
- [29] *The Oxford Handbook of Nanoscience and Technology*, (Edited by A. V. Narlikar and Y. Y. Fu, Oxford University Press, Vol. I, 2010).
- [30] M. Thoss and F. Evers, *J. Chem. Phys.* **148**, 030901 (2018).
- [31] L. -L. Nian, L. Ma, and J. -T. Lu in *Nanogap Electrodes, Ch. 2*, (Edited by T. Li, WILEY-VCH, Boschstr, 2021).
- [32] S. Datta, *Electronic Transport in Mesoscopic Systems*, (Cambridge University Press, 1995).
- [33] M. Di Ventra, *Electrical Transport in Nanoscale Systems*, (Cambridge University Press, 2008).
- [34] S. Datta, W. Tian, S. Hong, and R. Reifenberger, *Phys. Rev. Lett.* **79**, 2530 (1997).
- [35] V. B. -Moshe, D. Rai, S. S. Skourtis, and A. Nitzan, *J. Chem. Phys.* **133**, 054105 (2010).

- [36] H. Haug and A. P. Jauho, *Quantum Kinetics in Transport and Optics of Semiconductors*, (Springer Solid-State Sciences, 1996).
- [37] L. A. Banyai, *Lectures on the Non-Equilibrium Theory of Condensed Matter*, (World Scientific, 2nd. Ed., 2020).
- [38] Y. Meir and N. S. Wingreen, *Phys. Rev. Lett.* **68**, 2512 (1992).
- [39] U. Harbola, M. Esposito, and S. Mukamel, *Phys. Rev. B* **74**, 235309 (2006).
- [40] M. Esposito and M. Galperin, *J. Phys. Chem. C* **114**, 20362 (2010).
- [41] A. Erpenbeck, L. Gozendofer, C. Schinabeck, and M. Thoss, *Eur. Phys. J.: Spec. Top.* **227**, 1981 (2019).
- [42] T. N. Todorov, *J. Phys.: Condens. Matter* **14**, 3049 (2002).
- [43] M. Brandbyge, J. -L. Mozos, P. Ordejón, J. Taylor, and K. Stokbro, *Phys. Rev. B* **65**, 165401 (2002).
- [44] S. -H. Ke, W. Yang, S. Curtarolo, and H. U. Baranger, *Nano Lett.* **9**, 1011 (2009).
- [45] M. Brandbyge, J. -L. Mozosm, P. Ordejon, J. Taylor, and K. Stokbro, *Phys. Rev. B* **65**, 165401 (2002).
- [46] A. Di Carlo, A. Pecchia, L. Latessa, Th. Frauenheim, and G. Seifert, in *Introducing Molecular Electronics*, (Edited by G. Cuniberi, K. Richter, and G. Fagas, Springer, 2005).

- [47] B. Hourahine, B. Ardi, V. Blum, et al. *J. Chem. Phys.* **152**, 124101 (2020).
- [48] G. Zhang, M. A. Ratner, and M. G. Reuter, *J. Phys. Chem. C* **119**, 6254 (2015).
- [49] X. Song, X. Yu, and W. Hu, *J. Phys. Chem. C* **124**, 24408 (2020).
- [50] R. Frisenda and H. S. J. van der Zant, *Phys. Rev. Lett.* **117**, 126804 (2016).
- [51] S. R. Akbarabdi and M. M. Asl, *Front. Phys.* **9**, 727325 (2021).
- [52] F. Chen, X. Li, J. Hihath, Z. Huang, and N. Tao, *J. Am. Chem. Soc.* **128**, 15874 (2006).
- [53] R. Frisenda, S. Tarkuc, E. Galan, M. L. Perrin, R. Eelkema, F. C. Grozema, and H. S. J. van der Zant, *Beilstein J Nanotechnol.* **6**, 1558 (2015).
- [54] E. Leary, A. La Rosa, M. Teresa. Gonzalez, G. R. -Bollinger, N. Agrait, and N. Martin, *Chem. Soc. Rev.* **44**, 920 (2015).
- [55] M. S. Inkpen, Z. -F. Liu, H. Li, L. M. Campos, J. B. Neaton, and L. Venkataraman, *Nat. Chem.* **11**, 351 (2019).
- [56] I. S. Kristensen, D. J. Mowbray, K. S. Thygesen, and K. W. Jacobsen, *J. Phys.: Condens. Matter* **20**, 374101 (2008).
- [57] Z. Zhao, R. Liu, D. Mayer, M. Coppola, L. Sun, Y. Kim, C. Wang, L. Ni, X. Chen, M. Wang, Z. Li, T. Lee, and D. Xiang, *Small* **14**, 1703815 (2018).
- [58] R. B. Pontes, F. D. Novaes, A. Fazzio, and A. J. R. da Silva, *J. Am. Chem. Soc.* **128**, 8996 (2006).

- [59] Y. Komoto, S. Fujji, H. Nakamura, T. Tada, T. Nishino, and M. Kiguchi, *Sci. Rep.* **6**, 26606 (2016).
- [60] M. Gantenbein, L. Wang, A. A. Al-jobory, A. K. Ismael, C. J. Lambert, W. Hong, and M. R. Bryce, *Sci. Rep.* **7**, 1794 (2017).
- [61] G. Foti and H. Vazquez, *J. Phys. Chem. Lett.* **9**, 2791 (2018).
- [62] Z. Huang, B. Xu, Y. Chen, M. Di Ventra, and N. Tao, *Nano Lett.* **6**, 1240 (2006).
- [63] C. Joachim and M. A. Ratner, *Proc. Natl. Acad. Sci.* **102**, 8801 (2005).
- [64] Y. Wang and Z. Xu, *Nat. Commun.* **5**, 4297 (2014).
- [65] N. Mosso, H. Sadeghi, A. Gemma, S. Sangtarash, U. Drechsler, C. Lambert, and B. Gotsmann, *Nano Lett.* **19**, 7614 (2019).
- [66] J. Yi, G. Cuniberti, and M. Porto, *Eur. Phys. J. B* **33**, 221 (2003).
- [67] E. R. Hedin, R. M. Cosby, Y. S. Joe, and A. M. Satanin, *J. Appl. Phys.* **97**, 063712 (2005).
- [68] J. Bruning, L. A. Chernozatonskii, V. V. Demidov, and V. A. Geyler, *Russ. J. Math. Phys.* **14**, 417 (2007).
- [69] B. M. Baltateanu, *Acta Phys. Pol. A* **120**, 1047 (2011).
- [70] J. L. Speyer, I. V. Ovchinnikov, D. Neuhauser, and D. Baugh, *J. Chem. Phys.* **123**, 124704 (2005).

References

- [71] O. Hod, R. Baer, and E. Rabani, *J. Phys. Chem. B* **108**, 14807 (2004).
- [72] O. Hod, E. Rabani, and R. Baer, *Acc. Chem. Res.* **39**, 109 (2006).
- [73] O. Hod, R. Baer, and E. Rabani, *J. Phys.: Condens. Matter* **20**, 383201 (2008).
- [74] A. M. Jayannavar, P. S. Deo, and T. P. Pareek, *Physica B* **212**, 261 (1995).
- [75] S. Nakanishi and M. Tsukada, *Jpn. J. Appl. Phys.* **37**, 3805 (1998).
- [76] S. Nakanishi and M. Tsukada, *Phys. Rev. Lett.* **87**, 126801 (2001).
- [77] Z. Yang, M. Chshiev, M. Zwolak, Y. -C Chen, and M. Di Ventra, *Phys. Rev. B* **71**, 041402(R) (2005).
- [78] M. Di Ventra, S. T. Pantelides, and N. D. Lang, *Phys. Rev. Lett.* **88**, 046801 (2002)
- [79] M. Di Ventra and S. T. Pantelides, *Phys. Rev. B* **61**, 16207 (2000).
- [80] T. N. Todorov, D. Dundas, J. -T. Lu, M. Brandbyge, and P. Hedegard, *Eur. J. Phys.* **35**, 065004 (2014).
- [81] T. N. Todorov, D. Dundas, A. T. Paxton, and A. P. Horsfield, *Beilstein J. Nanotechnol.* **2**, 727 (2011).
- [82] R. Mulla and C. W. Dunnill, *Carbon Trends* **4**, 100077 (2021).
- [83] Y. Dubi and M. Di Ventra, *Rev. Mod. Phys.* **83**, 131 (2011).

References

- [84] D. Wang, L. Liu, X. Gao, C. -an Di, and D. Zhu, *CCS Chem.* **3**, 2212 (2021).
- [85] S. Park, S. Kang, and H. J. Yoon, *Nano Lett.* **22**, 3953 (2022).
- [86] L. R. -Garcia, C. Evangelini, G. R. -Bollinger, and N. Agrait, *Chem. Soc. Rec.* **45**, 4285 (2016).
- [87] N. A. Zimbovskaya, *J. Phys.: Condens. Matter* **26**, 275303 (2014).
- [88] Y. Kim, W. Jeong, K. Kim, W. Lee, and P. Reddy, *Nat. Nanotechnol.* **9**, 881 (2014).
- [89] D. Nozaki, S. M. Avdoshenko, H. Sevincli, and G. Cuniberti, *J. Appl. Phys.* **116**, 074308 (2014).
- [90] H. Sadeghi, *J. Phys. Chem. C* **123**, 12556 (2019).
- [91] R. Almughathawi, S. Hou, Q. Wu, Z. Liu, W. Hong, and C. Lambert, *ACS Sens.* **6**, 470 (2021).
- [92] H. Chen, Y. Chen, H. Zhang, W. Cao, C. Fang, Y. Zhou, Z. Xiao, J. Shi, W. Chen, J. Liu, and W. Hong, *Chin. Chem. Lett.* **33**, 523 (2022).
- [93] Y. -J. Zeng, D. Wu, X. -H. Cao, W. -X. Zhou, L. -M. Tang, and K. -Q. Chen, *Adv. Funct. Mater.* 1903873 (2019).
- [94] L. Cui, S. Hur, Z. A. Akbar, J. C. Klockner, W. Jeong, F. Pauly, S. -Y. Jang, P. Reddy, and E. Meyhofer, *Nature* **572**, 628 (2019).

-
- [95] M. Burkle, T. J. Hellmuth, F. Pauly, and Y. Asai, *Phys. Rev. B* **91**, 165419 (2015).
- [96] C. A. Perroni, D. Ninno, and V. Cataudella, *J. Phys.: Condens. Matter* **28**, 373001 (2016).
- [97] C. M. Finch, V. M. G. -Suarez, and C. J. Lambert, *Phys. Rev. B* **79**, 033405 (2009).
- [98] A. Torres, R. B. Pontes, A. J. R. da Silva, and A. Fezzio, *Phys. Chem. Chem. Phys.* **17**, 5386 (2015).

Chapter2

Magnetic Field Influence On Electronic Transport In Ring Structures[†]

Abstract

Within the framework of the tight-binding approximation, the magnetic field control of current across the model graphene nanosheet junction is investigated. The bridging graphene nanosheets' otherwise degenerate energy levels are split by the geometrically asymmetric connection of the contact leads, creating energy-resolved transmission peaks, which the applied magnetic field modulates for a transmission maximum. It is observed that whereas the contact coupling has a substantial impact on controlling the current in smaller structures, its influence is significantly diminished in bigger structures. Also, the model calculations with inter-site Coulomb interactions are found to sustain sensitivity to the magnetic field.

[†]Work presented in this chapter is based on the research article:
Magnetic field control of current through model graphene nanosheets.
Umesh Dhakal and Dhurba Rai, *Phys. Lett. A* **383**, 2193 (2019).

2.1 Background

One of the most significant advances in the recent molecular and nano-scale research is the manipulation of the conduction characteristics of the single-molecular junctions (SMJs), which often comes with a great surprise.[1] As discussed in the preceding chapter, the basic component that characterizes SMJ-based devices is the molecule bridging the contact leads (electrodes). Recently, the intensified studies of the electronic transport properties of the SMJs have attracted much attention as they are expected to soon serve as the basic building blocks of previously envisioned molecular-scale electronics devices.[2-4] Despite enormous success in designing microscopic devices using molecules with a bottom-up approach to avoid the problems that would otherwise encounter in the top-down approach as in the conventional silicon devices, a number of challenges still persist. Moreover, there are no systematic characterization techniques for enhancing their viability and performance. It is where the theoretical and computational studies play a crucial role in laying a foundation for the prediction of the necessary and desired features appropriate for the device applications, hence offering guiding principles for the realization, improvement, and integration of the molecular devices. As a result, the combined efforts of experimental, theoretical, and computational investigations have resulted in the development of novel and innovative techniques for the fabrication of the SMJs with desired features.[5, 6]

Among others,[7–12] the most widely used method for modulating current conduction through the SMJs involves applying gate voltage in the bridging molecule so as to align the molecular energy levels with respect to the Fermi energy E_F of the metal contacts for efficient conduction,[13, 14] or by means of applying magnetic field leading to the interference-based controlled conduction.[15–19] The gate voltage shifts the molecular energy levels into/out of the energy window ($E_F \pm |e|V/2$), where V is the bias voltage. Since only those energy levels in the energy window contribute to the current, and their number can be altered by the gate voltage, effective control of the current conduction can be achieved. In contrast, the applied magnetic field $\vec{B} = \vec{\nabla} \times \vec{A}$ induces an additional phase $\exp\left(\frac{ie|}{\hbar} \int \vec{A} \cdot d\vec{l}\right)$ in the electron waves thereby affecting their interference in the molecular ring structures, where \vec{A} is magnetic vector potential corresponding to the externally applied magnetic field \vec{B} , and $\Phi_0 = h/|e|$ is the flux quantum. By varying the magnetic flux Φ enclosed between the electrons' paths, the relative phase $\Delta\phi = \frac{|e|}{\hbar} \oint \vec{A} \cdot d\vec{l} = 2\pi \frac{\Phi}{\Phi_0}$ of the interfering electron waves can be tuned for effective current control. Furthermore, it has been demonstrated that the magnetic field may provide three-terminal ring devices with exceptional controllability, allowing the current conduction to be shifted from one output terminal to the other when the direction of the magnetic field is reversed.[19] However, tuning electron wave interference at the molecular-size ring structures requires an unrealistically high magnetic field for the flux through the ring of the order of flux quantum.[19, 20] Thus, for a given field, increasing the number of ring structures increases the magnetic flux through the bridging molecules.[20, 21]

Despite the challenges, extensive research has been done over the years on the idea of using relatively small magnetic fields to influence the current conduction through the molecular ring junctions.[22, 23]. However, this is challenging since certain conditions must be satisfied. The lead-molecule coupling must be weak, and the energy levels of the bridging molecule must be degenerate in order to induce energy split that can be modulated by the external magnetic field. Additionally, the bridging molecule needs to be connected to the electrodes asymmetrically. For the transmission peaks that can be modulated by the applied magnetic fields, temperature must be small for relatively small decoherence, i.e., thermal dephasing. Of all, the most crucial requirement is the possession of the degenerate energy levels within the accessible energy range, which is often the case with ring structures.[24] The asymmetrically connected contact leads split the energy levels for the well-resolved energy transmission peaks at low coupling, which the applied field narrows down by moving them closer to each other.[25, 26] This results in an enhanced transmission that reaches its maximum ($T \sim 1$) at the energy level crossing or at the minimum energy gap in case of avoided crossing when such circumstances arise.

A significant quantity of interest directly related to the current conduction properties is the negative differential resistance (NDR), characterized by a decrease in current with an increase in bias voltage. This has gained widespread interest both theoretically and experimentally due to its potential applications in fast switching, sensors, logic and memory devices.[27, 28] Any NDR modulation

with an applied magnetic field would provide an additional feature in the device applications. In this work, such possibilities have been investigated.

2.2 Scope of the Work

In this chapter, we shall explore the magnetic field control of current through the model graphene nano-sheet junction within the tight-binding framework. The model graphene nano-sheets are simulated by the hexagonal polycyclic aromatic hydrocarbons (PAHs) having zigzag and armchair edges. The PAHs having zigzag edges includes the coronene series viz., coronene ($C_{24}H_{12}$), circum-coronene ($C_{54}H_{18}$) and dicircum-coronene ($C_{96}H_{24}$) while those having armchair edges include ($C_{42}H_{18}$), ($C_{114}H_{30}$) and ($C_{222}H_{42}$). These PAHs can also be considered a bottom-up approach for the realisation of nano-sized graphene sheets.[21, 29, 30]

The study of magnetic field effects on molecules offers a good opportunity to single out molecules in terms of their adaptability to a wide range of magnetic field strengths, the extent of modulation of their energy levels, and their ability to integrate into the device architecture. Studying how the contact coupling and applied magnetic field affect the energy levels and transmission spectra in ever-larger graphene nanosheet fragments is both necessary and significant. It is expected that for larger graphene nanosheets, the current control can be achieved at relatively small magnetic field strengths due to increased magnetic flux through the graphene

sheet. Additionally, it is intriguing to look into how the inter-site Coulomb interactions affect the magnetic field sensitivity of the current conduction. This is because when a molecule is weakly coupled to the metal leads, the electrons will spend a sufficient amount of time inside the molecular bridge before leaving it. As a result, it is anticipated that the Coulomb interaction between the electrons may have a striking impact on the electron transport and, consequently, on the current-voltage characteristics. For instance, the Coulomb interaction is found to inhibit the current through a benzene ring that is weakly connected to the metal leads.[31] Here, we analyse the inter-site Coulomb repulsion between the electrons and investigate the impact of the magnetic field on the I-V characteristics. We also consider the possibility of using graphene nanosheets as magnetic sensors, which would give the graphene-based molecular junction devices additional functionality.

2.3 Computational Framework

We now present the computational details of the works presented in this chapter. We employed the tight-binding method in conjunction with the non-equilibrium Green's function (NEGF) technique to calculate the steady-state electron transport properties through the molecular junction.[32, 33] The NEGF method is the most widely used method due to its versatility and numerical stability, in contrast to alternative methods based on the Redfield master equations (RME) [34–37] and transfer matrix approaches.[38] Despite its mathematical complexity, the

NEGF method for computing quantum transport properties has a number of advantages over competing approaches. For instance, because the level of complexity in the NEGF scales as N^2 against N^6 in the RME, where N is the dimension of Hilbert space, the NEGF approach is capable of treating large-sized structures effectively. Additionally, it may be expanded to encompass a multi-body quantum system, enabling the inclusion of electron-electron interactions [39] and electron-phonon interactions [40] in a unified and organised framework. We have considered the hexagonal PAHs to simulate the increasingly large fragments of graphene nanosheets having both the zigzag edges which include, coronene ($C_{24}H_{12}$), circumcoronene ($C_{54}H_{18}$), and dicircum-coronene ($C_{96}H_{24}$) and the graphene nanosheet with the armchair edges which includes ($C_{42}H_{18}$), ($C_{114}H_{30}$), and ($C_{222}H_{42}$).

Throughout the chapter, we have considered the magnetic field in the range of (0-5 T) and the lead-molecule coupling Γ in the range of (0.005 - 1 eV). We use low temperature ($T=10$ K) and choose Γ for a given system in such a way that the energy split (ΔE) resulting from the asymmetric connection of the contact leads to the bridging molecule is larger than the thermal energy ($k_B T$), i.e., $\Delta E > k_B T$. Unless otherwise stated, we have assumed that the inter-site Coulomb repulsion $V_{\langle i,j \rangle}$ between the nearest-neighbor carbon atoms is uniform i.e., $V_c = 6$ eV, which is less than the on-site Coulomb repulsion, $U \sim (10 - 11$ eV).[41]

2.3.1 Model graphene nanosheets and the Hamiltonian

The model graphene nanosheets that we use for the study of the effects of magnetic field on the electron transport through such structures are shown in Fig. 2.1. The bridging molecular structures are described by the tight-binding Hamiltonians with the on-site energy ϵ_i and the nearest-neighbor hopping integral $t_{\langle ij \rangle}$. The bridging molecules, i.e., PAHs are coupled to the metal electrodes, source (S) and drain (D), which are considered as the free electron reservoirs, each at its thermal equilibrium with chemical potential, μ_L and μ_R respectively. As shown in Fig. 2.1, the bridging molecule can be connected through the atomic sites, ($1, p/m/o$), thus making the connection either symmetric (p -para) or asymmetric (m -meta or o -ortho). However, it must be noted that in all the cases, metal leads are at relative positions $1/2$, $1/3$, and $1/6$ of the outer peripheral ring but the contact leads can be moved along the zigzag edges, (b)-(d) and along the armchair edges, (e)-(g), while still maintaining the relative position between the contact leads and the molecules. The strength of the coupling between the molecule and the metal leads ($K = L, R$) is characterized by the broadening function Γ^K , which in our case is considered to be equal on both contact sites, i.e., $\Gamma^L = \Gamma^R = \Gamma$, and are considered independent of the incident electron energy E , the so-called wide-band approximation. An increase of Γ enhances the electronic coupling between the continuum states in the metal leads and the molecular energy levels that result in the broadening of the molecular energy levels. The coupling Γ can be related to the rate Γ/\hbar at which an electron escapes from the molecule into the contact leads.

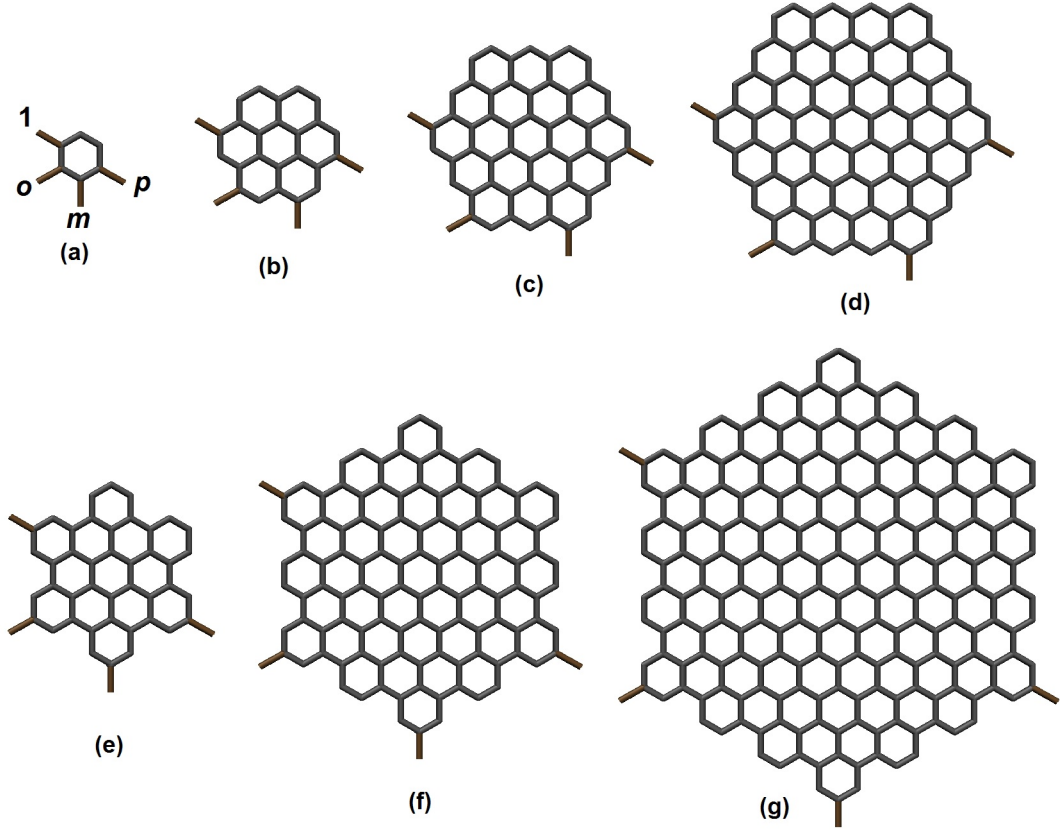


FIGURE 2.1: Schematic illustration of the hexagonal PAHs as increasingly large sheets of graphene with symmetric (para- p) and asymmetric (m -meta and o -ortho) connections of the contact leads as specifically labelled for a benzene ring. Graphene nanosheet fragments, (b)-(d) have zigzag edges and correspond to the coronene series of benzenoid systems, viz., coronene (C_{24}), circum-coronene (C_{54}) and dicircum-coronene (C_{96}), whereas (e)-(g) have armchair edges; C_{42} , C_{114} , and C_{222} , respectively.

We apply a uniform magnetic field ($\vec{B} = \vec{\nabla} \times \vec{A}$) perpendicular to the molecular plane. The applied magnetic field changes the nearest-neighbor hopping integral t_{ij}^0 up to a phase factor, i.e., $t_{ij} \rightarrow t_{ij} \exp(i2\pi\delta\phi_B/\phi_0)$, where $\delta\phi_B = \int_{\vec{r}_i}^{\vec{r}_j} \vec{A} \cdot d\vec{l}$ is the magnetic flux through the triangle spanned by the position vectors (\vec{r}_i, \vec{r}_j) of the nearest-neighboring sites $\langle i, j \rangle$ and $\phi_0 = h/|e|$ is the flux quantum. This method of introducing a magnetic field in the calculations through a phase factor in the hopping integral is known as Peierls substitution [42, 43] and is a widely used approximation in tight-binding calculations. Within the London approximation,

this phase factor also follows from the resonance or hopping integral between the two atomic sites with magnetic field-dependent atomic orbitals.[22, 44] The field-dependent atomic orbitals which are also called London atomic orbitals or gauge-including atomic orbitals (GIAOs) were first introduced to ensure the gauge invariance of the results.

To this end, we introduce the interaction-free Hamiltonian of the molecular junction under consideration, which is the sum of the Hamiltonian of the metal leads, that of the bridging molecule and that describing the electron tunneling between the molecule and the metal leads, i.e.,

$$\hat{H}_0 = \hat{H}_K + \hat{H}_M + \hat{H}_{KM}, \quad (2.1)$$

where \hat{H}_K describe the contact leads K ($K = L, R$) that are considered the free-electron reservoirs, \hat{H}_M describes the molecule M , while \hat{H}_{KM} describes the coupling between the molecule and the contact leads. As discussed in Chapter 1, their explicit expressions are as follows

$$\hat{H}_K = \sum_{k \in K} \epsilon_k \hat{c}_k^\dagger \hat{c}_k; K = L, R, \quad (2.2)$$

$$\hat{H}_M = \sum_{i \in M} \epsilon_i \hat{d}_i^\dagger \hat{d}_i - \sum_{\langle ij \rangle \in M} (t_{ij} \hat{d}_i^\dagger \hat{d}_j + H.c.), \quad (2.3)$$

$$\hat{H}_{KM} = \sum_{k \in K} (v_{ik} \hat{d}_i^\dagger \hat{c}_k + H.c.), i \in M. \quad (2.4)$$

Here $\hat{d}_i^\dagger(\hat{d}_i)$ and $\hat{c}_k^\dagger(\hat{c}_k)$ denotes the creation (annihilation) operator for an electron at site i in the molecule and at site k in the lead, respectively. The coupling matrix elements, $v_{ik} = \delta_{i,1}v_{Lk}$ for ($k \in L$) and $\delta_{i,n}v_{Rk}$ for ($k \in R$), describe the electron tunneling between the contact leads and the molecule through the sites $(1, n) = (1, p/m/o)$ in the molecule. Here p, m, o denotes the para, meta and ortho position of the right metal contact (output lead) at the site n w.r.t the left metal contact (input lead) attached at site 1. They are related to the broadening function as $\Gamma_{i,j \in M}^K = 2\pi \sum_{k \in K} v_{ik}^* v_{jk} \rho(E)$, where $\rho(E)$ is the density of states in the metal contacts, which within the wide-band approximation is independent of energy as is the case considered in this work. We now consider the inclusion of the Coulomb interaction in the calculations.

2.3.2 Inclusion of Coulomb interaction

We consider an extended version of the tight-binding model, viz., the t-V model for investigating the effect of inter-site Coulomb interaction on the magnetic field control of current through the graphene nanosheet considered in the present work.[45, 46] The Hamiltonian is given by

$$\hat{H} = \hat{H}_0 + \sum_{\langle i,j \rangle \in M} V_{ij} \hat{n}_i \hat{n}_j, \quad (2.5)$$

where V_{ij} is the inter-site Coulomb repulsion between the electrons occupying the nearest-neighboring sites $\langle i, j \rangle$ in the molecule and $\hat{n}_i = \hat{c}_i^\dagger \hat{c}_i$ is the on-site occupation number operator. Unlike the Hubbard model, the t-V model is simpler due to the absence of spin degrees of freedom, since there can be at most one electron per site and no on-site Coulomb interaction, U .

The effect of inter-site Coulomb repulsion V_{ij} can be described by a single-particle Hamiltonian in the form Eq. (2.1), however, with renormalised on-site energies and hopping integrals,[47–49]

$$\epsilon_i \rightarrow \tilde{\epsilon}_i = \epsilon_i + \sum_j V_{ij} \langle \hat{n}_j \rangle, \quad (2.6)$$

$$t_{ij} \rightarrow \tilde{t}_{ij} = t_{ij} + V_{ij} \langle \hat{c}_j^\dagger \hat{c}_i \rangle. \quad (2.7)$$

Note that the effect of inclusion of the Coulomb interaction is the renormalization of the on-site energy and hopping integral, which respectively depends on the site-occupation $\langle \hat{n}_j \rangle$ and the bond-charge $\langle \hat{c}_j^\dagger \hat{c}_i \rangle$. We like to stress here that since the introduction of the inter-site Coulomb interaction leads to subsequent renormalization of the on-site energy and hopping integral, the electrons in the molecular bridge are essentially non-interacting and the molecular junction device is described by the same single-particle Hamiltonian Eq. (2.1), however, with the effective on-site energy and hopping integral expressed in Eq. (2.6) and Eq. (2.7).

2.3.3 Steady-state current through the junction

We use the non-equilibrium Green's function (NEGF) formalism to study electron transport through the molecular junctions under consideration. As discussed in Chapter 1, the NEFG calculations begin with the construction of the retarded Green's function, which is defined as $(E - H)^{-1}$, where H , in principle, is an infinite-dimensional Hamiltonian representing the molecular junction consisting of the metal electrodes that have infinite-dimensional degrees of freedom. However, it is not possible to invert an infinite dimensional matrix but the problem is usually overcome by incorporating the effects of the metal electrodes on the bridging molecule through the self-energy corrections in molecular Hamiltonian. This greatly simplifies the problem to the effect the effective Hamiltonian to work with is now reduced to a finite-dimensional matrix in the Hilbert space spanned by the molecular basis set. Thus, the retarded Green's function is

$$G^r(E) = [E - H_M - \Sigma_L - \Sigma_R]^{-1}, \quad (2.8)$$

where Σ_L and Σ_R are the self-energies that essentially describe the coupling of the molecule to the leads ($K = L, R$). They are related to the broadening function as $\Gamma_K = i [\Sigma_K - \Sigma_K^\dagger]$. The lesser Green's function $G^<(E)$ that contains information relating to the density of occupied states in the molecule can be expressed through

the Keldysh equation as,

$$G^<(E) = G^r(E)\Sigma^<(E)G^a(E), \quad (2.9)$$

where $G^a(E)$, the so-called advanced Green's function, is the Hermitian conjugate of the matrix Eq. (2.8), i.e., $G^a(E) = [G^r(E)]^\dagger$ and $\Sigma^<(E) = \Sigma_L^<(E) + \Sigma_R^<(E)$ is the total lesser self-energy. The lesser self-energy of the metal lead K is expressed as $\Sigma_K^< = if_K(E)\Gamma^K(E)$, where $f_K = 1/[1 + \exp((E - \mu_K)/k_B T)]$ is the Fermi-distribution function for the occupancy of the energy states in the metal lead K at temperature T and chemical potential μ_K . The average on-site occupation number $\langle \hat{n}_j \rangle = \langle \hat{c}_j^\dagger \hat{c}_j \rangle$ and the bond charge $\langle \hat{c}_j^\dagger \hat{c}_i \rangle$ in Eqs. 2.6 and 2.7 are calculated self-consistently from the lesser Green's function as

$$\langle \hat{c}_j^\dagger \hat{c}_i \rangle = \frac{\hbar}{i} G_{ij}^<(\tau = 0) = \frac{1}{2\pi i} \int G_{ij}^<(E) dE. \quad (2.10)$$

To calculate the steady-state current, we use the Meir-Wingreen formula,[50]

$$I = \frac{e}{\pi\hbar} \int \frac{i}{2} \text{Tr} [(f_L \Gamma^L - f_R \Gamma^R) (G^r - G^a) + (\Gamma^L - \Gamma^R) G^<] dE. \quad (2.11)$$

Throughout the calculations, we have assumed that the applied bias voltage V falls symmetrical on both metal-molecule interfaces, so that $\mu_L = E_F + eV/2$ and $\mu_R = E_F - eV/2$, while the potential remains constant in the bridging molecule.

2.4 Numerical Results and Discussion

We now present the characteristic response of the model graphene nanosheets when subjected to an externally applied uniform magnetic field in terms of modification in the electron transmission spectra and the I-V characteristics. For all the models considered here, viz., benzene (C_6H_6), coronene ($C_{24}H_{12}$), circum-coronene ($C_{54}H_{18}$) and dicircum-coronene ($C_{96}H_{24}$), $C_{42}H_{18}$, $C_{114}H_{30}$, and $C_{222}H_{42}$, the tight-binding parameters, viz., on-site energy, nearest-neighbor hopping integral, C-C bond length and angle are considered uniform and set to $\epsilon = -1.7$ eV, $t_{\langle i,j \rangle} = 2.7$ eV, 1.40\AA and 120° , respectively. While the actual value of on-site energy for a carbon atom estimated from the experimental ionization potentials of various hydrocarbons is -6.5 eV,[51] this value would be influenced by the local electrostatic potential in the junction, and for definiteness, we set this to -1.7 eV so that the frontier molecular orbitals are positioned within the accessible energy range. However, the actual value of bond length and bond angle may vary slightly,[52] but we assume no variation in the energy parameters. We have considered the coupling strength Γ in the range (5 meV - 1 eV) [53–57] and the inter-site Coulomb repulsion V_{ij} between the nearest-neighbor sites to be uniform, $V_C=6$ eV,[41] which is relatively smaller than the on-site Coulomb repulsion, ($U \sim 10 - 11$ eV), for sp^2 hybridized carbon atom.[41, 58–61] For all the structures under consideration, the temperature of the junction is set at 10 K and both the transmission probability and current are calculated for Fermi energy E_F fixed at zero in the energy scale.

2.4.1 Magnetic field effect on transmission probability

The magnetic field is applied along the negative z -axis and perpendicular to the plane of graphene nanosheets oriented to lie on the xy -plane. Field effects on the transmission probability $T(E)$ around the lowest unoccupied molecular orbital (LUMO) energy levels for an asymmetric (meta-) connection of the metal leads are shown in Fig. 2.2. It is evident that the effect is generic which involves the evolution of two zero-field transmission peaks, corresponding to the coupling-induced splitting of the otherwise degenerate energy levels, into one as the externally applied magnetic field narrows down the gap between them. This results in an enhanced transmission peak, which then grows to a maximum $T(E) \sim 1$ at the position of the LUMO energy level for the respective field values, $B_0=12.8$ T for benzene, (7.3, 8.5, 4.5 T) for ($C_{24}H_{12}, C_{54}H_{18}, C_{96}H_{24}$) and (4.7, 8.4, 4.8 T) for ($C_{42}H_{18}, C_{114}H_{30}, C_{222}H_{42}$). Beyond this, as seen in Fig. 2.2, the single resonant transmission peak splits into two while the area under the curve essentially remains the same. It is important to note that, although not shown here for brevity, similar features were also seen in the transmission probability for contact leads in the ortho position. In accordance with Onsager symmetry, we have also seen that the transmission probability $T(E)$ is unaffected by the change in field direction, i.e., $T(E, \vec{B}) = T(E, -\vec{B})$. Since the area under the transmission probability curve directly correlates to the current through the molecular junction, the current increases with an increase in magnetic field strength until the peak at above field values split into two well-separated peaks, beyond which the current remains

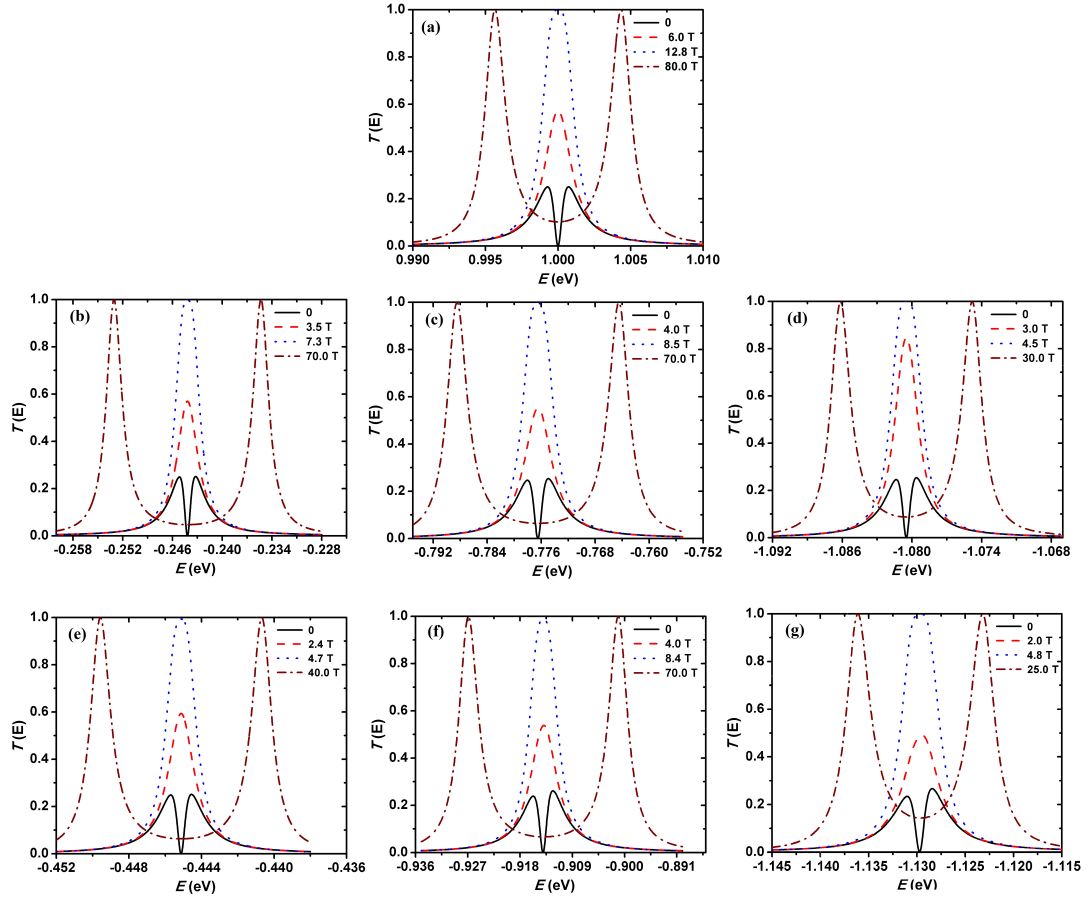


FIGURE 2.2: Effects of the magnetic field on the transmission probability $T(E)$ around the LUMO energy of graphene nanosheets with asymmetric (meta-) connection of metal leads for (a) benzene (C_6), the coronene series of PAHs, viz., (b) coronene (C_{24}), (c) circum-coronene (C_{54}) and (d) dicircum-coronene (C_{96}), while (e)-(g), correspond to C_{42} , C_{114} , and C_{222} , respectively. The two transmission peaks at zero fields evolve into a single peak, increasing to its maximum value, $T(E) = 1$, beyond which the peak splits into two. Quantitatively equivalent results are obtained for contact lead at the ortho position. The highest field applied in each case indicates a field beyond which the current stays essentially constant.

essentially constant. This is shown in Fig. 2.3 (a) for C_{222} leading to effective control of current by the applied magnetic field, while the I-V characteristics are shown later in the next section in connection with the effect of Coulomb interaction and the NDR effect. Note that a small shoulder at zero field is due to split degeneracy resulting from the asymmetric geometrical connection (i.e., ortho- or

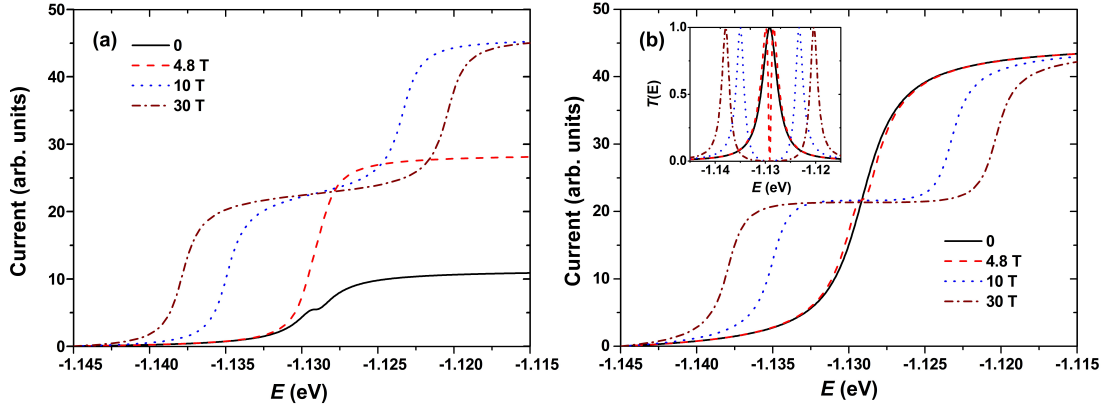


FIGURE 2.3: (a) Current (in arb. units) through a meta-connected C_{222} graphene corresponding to electron transport within a small energy window ΔE around the LUMO energy of its isolated counterpart at various magnetic field values are indicated. A small shoulder at zero field illustrates the consequence of the split degeneracy brought on by the asymmetric connection of the metal leads. (b) Current through para connected C_{222} , while the inset depicts corresponding transmission probability around the LUMO energy.

meta-) of the metal leads, while the emergence of the second step-like feature at higher fields, as shown in the figure for $B = 10$ and 30 T, is due to the entry of new energy levels into the energy window by the applied magnetic field. In contrast, though not illustrated, the degenerate energy levels for the contact leads in the para position are unaffected, resulting in just one transmission peak ($T(E) \sim 1$) around the LUMO energy of the isolated configuration. On the application of an external magnetic field, this transmission peak splits into two well-resolved peaks while the area under the curve remains unchanged. Thus, the symmetrically connected molecular junction does not exhibit magnetic field-controlled features other than the step-like structure that results from the entry of new energy levels into the energy window at higher magnetic field values as shown in Fig. 2.3 (b) for C_{222} .

2.4.2 Effect of contact coupling

To study the effect of the lead-molecule coupling strength on the magnetic field control of current through the model graphene nanosheets under consideration, we plot in Fig. 2.4 (a), the field B_0 that makes transmission probability unity ($T(E) = 1$) at the position of the LUMO energy of its isolated configuration as a function of a number of carbon atoms for three different values of the coupling strength, $\Gamma = 5$ meV, 0.1 eV and 1 eV. We would like to stress here that the field B_0 is a measure of field required for effective control of current through the molecular junction and beyond which the field sensitivity is limited. In other words, it is a measure of the field beyond which field sensitivity is limited as the current saturates for $B > B_0$. Naturally, the value of B_0 decreases with an increase in the size of the graphene flakes due to the increase in the magnetic flux that they encompass. However, a closer examination of the variation reveals two important observations. First, for a given coupling strength, a decrease in the value of B_0 is relatively slow for larger structures, and second, the rapid increase of B_0 with Γ is more significant for larger structures. Both observations suggest that weak lead-molecule coupling is crucial for the magnetic field's ability to control current flow through smaller structures, but it plays a much smaller role in bigger structures that have more closely spaced energy levels. When calculated for a single benzene ring, $B_0 = 12.8$ and 25.4 T for $\Gamma = 5$ and 10 meV respectively. Since B_0 almost scales by a factor of 2 when Γ is doubled, we expect B_0 to vary linearly with Γ . This is exemplified in Fig. 2.4 (b) by plotting field B_0 as a function of Γ in the

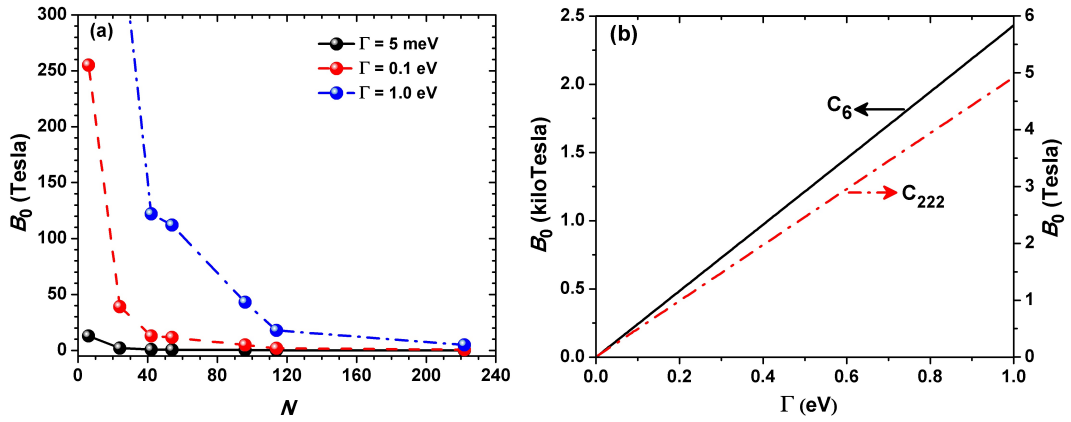


FIGURE 2.4: (a) Plot of magnetic field B_0 (a measure of the field required for effective control of current) as a function of the number of carbon atoms in the meta-connected model graphene nanosheets for coupling strength $\Gamma=5$ meV (solid line), 0.1 eV (dashed line) and 1 eV (dashed-dotted line). B_0 value for C_6 and C_{24} for $\Gamma = 1$ eV are 2.48 kT and 380 T, respectively. (b) Plot of B_0 as a function of Γ for C_6 (solid line) and C_{222} (dashed-dotted line) with slopes ~ 2.5 T/meV and 5 mT/meV, respectively.

range 1 meV - 1 eV for C_6 vis-à-vis C_{222} , however with seemingly different slopes, viz., ~ 2.5 T and 5 mT rise in the value of B_0 per meV increase in Γ , respectively.

A further study of the effect of the lead-molecule coupling strength on the magnetic field control of current conduction is presented in the transmission probability map in Fig. 2.5 for C_{42} and C_{222} . The map corresponds to transmission through the respective LUMO energy of the isolated configuration, where the dotted lines represent the locus of B_0 values. As is evident from the map Γ has comparatively less effect on C_{222} leading to a sharp transmission probability profile with a relatively slow increase of B_0 with Γ , while in C_{42} , significant level broadening smears out the transmission probability profile. In hindsight, this reveals a peculiar trade-off between the lead-molecule coupling strength and the relative energy level spacing in the molecule for effective control of the current

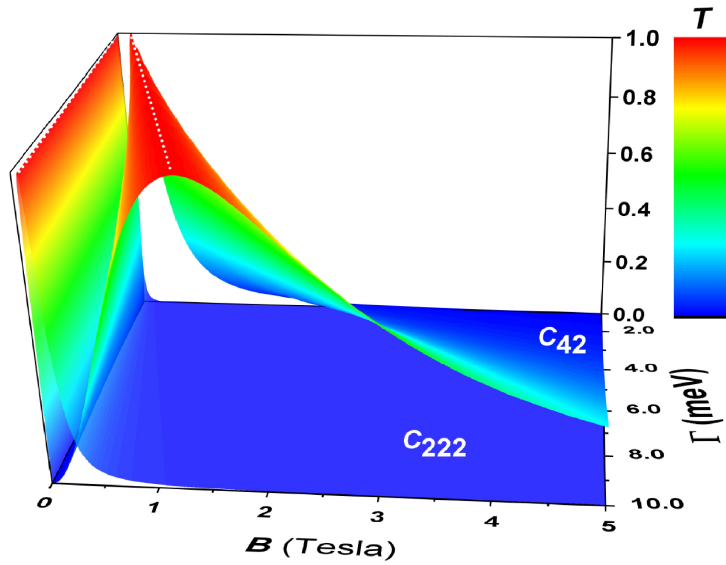


FIGURE 2.5: Transmission profile for C_{42} and C_{222} , for B and Γ in the range (0-5 T) and (1-10 meV), respectively. These profiles correspond to the transmission through the respective LUMO energies of the isolated configurations. The locus of transmission maxima $T(E) = 1$ is represented by the dotted line along the peaks, and the corresponding fields are B_0 values.

conduction. The more distinct the energy levels, which is often the case for smaller molecular structures at low contact coupling, the less magnetic field is required for the modulation of the energy levels and hence the transmission peaks. This allows for effective control of current only at weak coupling limits. Whereas, for larger structures, which have a relatively large number of closely-spaced energy levels that are insensitive to the lead-molecule coupling strength, the increased flux through them leads to modulation of energy levels with relative ease even in the case of strong contact coupling, leading to the possible control of current conduction at relatively small field strengths (\sim few Tesla). Several factors [62] affect the transport of electrons in molecular junction devices that include the electrode material,[63] anchoring groups,[55, 64–66] interface configuration,[67] molecular structure [68] and the environment [69–71], however, a suitable construction of

the graphene nanosheet junctions taking into consideration the above observations undoubtedly enhances the feasibility of current control under externally applied magnetic field.

2.4.3 Current-voltage characteristics

We here investigate the effect of inter-site Coulomb interaction on the magnetic field control of current through a weakly coupled molecular bridge. We perform a model calculation on the smallest and largest graphene nanosheet under consideration i.e., benzene (C_6) and PAH (C_{222}), wherein the Coulomb interaction between the electrons in the ring is effected through renormalised on-site energy and hopping integral, i.e., Eqs. (2.6 - 2.7). The renormalised on-site energy and hopping integral are calculated self-consistently within a predefined relative convergence tolerance of 10^{-5} . For definiteness, we use the Meir-Wingreen formula, Eq. 2.11, for calculating current through the molecular junction in the steady-state situation.

(a) PAH (C_{222}) molecular junction

As pointed out earlier in section 2.4.1, the current through the molecular junction is directly proportional to the area under the transmission probability curve, the applied magnetic field enhances the transmission to a maximum, resulting in an increase of current progressively to a constant value. This is shown

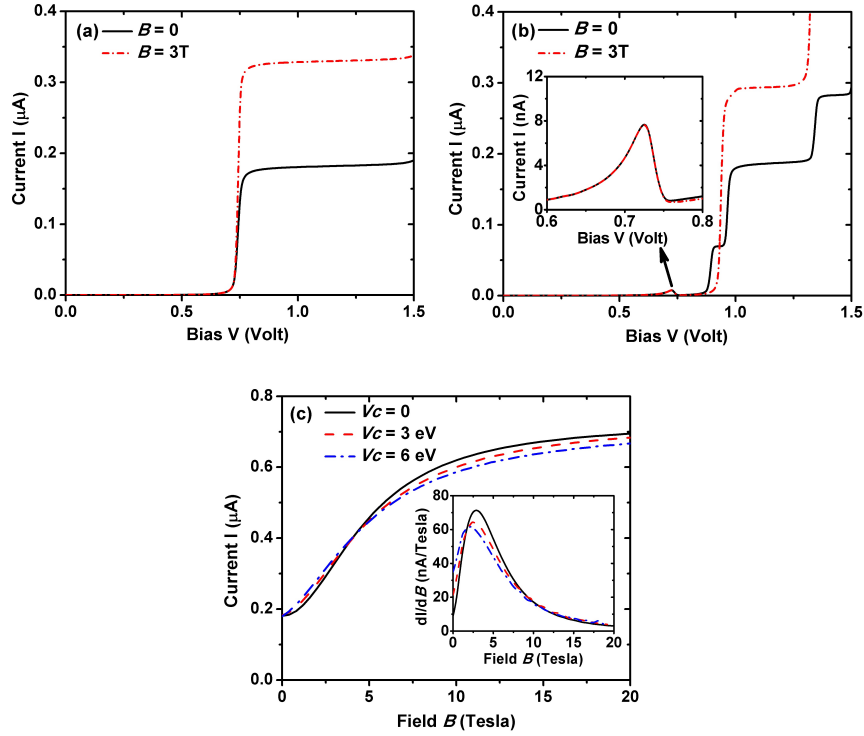


FIGURE 2.6: (a) I-V characteristics of a meta-connected C_{222} for fields, 0 T (solid line) and 3 T (dashed-dotted line) at 10 K with $\Gamma=1$ eV. (b) Respective I-V curves at the same scale are plotted in the presence of Coulomb interaction ($V_C=6$ eV) for comparison. Inset exhibits NDR at around 0.7 V. (c) Plot showing current as a function of applied magnetic field (B) for Coulomb interaction, $V_C=0$ (solid line), 3 eV (dashed line) and 6 eV (dashed-dotted line), at bias voltage $V=1.2$ V. Inset displays dI/dB as a function of B for respective interactions.

in Fig. 2.6(a) for a meta-connected C_{222} graphene nanosheet, demonstrating effective current control by a small field value, $B < 5$ T. The Fermi energy E_F of the metal lead is set at -1.50 eV, which for the choice of tight-binding parameters considered in this work, lies in the energy gap between the degenerate HOMO and LUMO located at -2.27 eV and -1.13 eV respectively. This makes it possible to analyse electron transport of the LUMO. As shown in Fig. 2.3, the degenerate energy levels of C_{222} remain unaffected when connected symmetrically to the contact leads. This leads to a single transmission maximum peak ($T(E) = 1$) at

the position of LUMO energy of the isolated structure. On the application of a magnetic field, this single transmission peak splits into two distinct peaks while the area under the transmission curve remains unchanged. Thus, a symmetrically connected molecular junction does not exhibit magnetic field-controlled features other than the step-like characteristic that results from the entry of new energy levels in the energy window at significantly large field values (~ 100 T or more).[21]

A comparison of the calculated I-V characteristics for a meta-connected (C_{222}) in the absence and presence of inter-site Coulomb interaction ($V_C = 6$ eV) is presented Fig. 2.6. It is clear that there is a significant current modulation with the emergence of multiple step-like features, but the field sensitivity persists along with the negative differential resistance (NDR) feature, which is discernible through a decrease in current with an increase in the bias voltage around 0.7 V. Although our main purpose is to investigate the possible magnetic field control of current, we shall discuss the physical mechanism triggering the observed NDR at the end of this section. At the moment, we plot in Fig. 2.6 (c), current as a function of the applied field away from the NDR region for two different values of inter-site Coulomb interaction V_c . It is important to note that current is suppressed, but that this suppression is relieved when the field strength is increased. In contrast, the current is significantly reduced for strong interactions with $V_c \gg \Gamma$. Looking at the inset reveals that there is sensitivity to magnetic fields in the lower field region, which in the event of weak coupling would be in the range of a few hundred milli-Tesla. Sensitivity diminishes at higher field values ($B > B_0$) due to

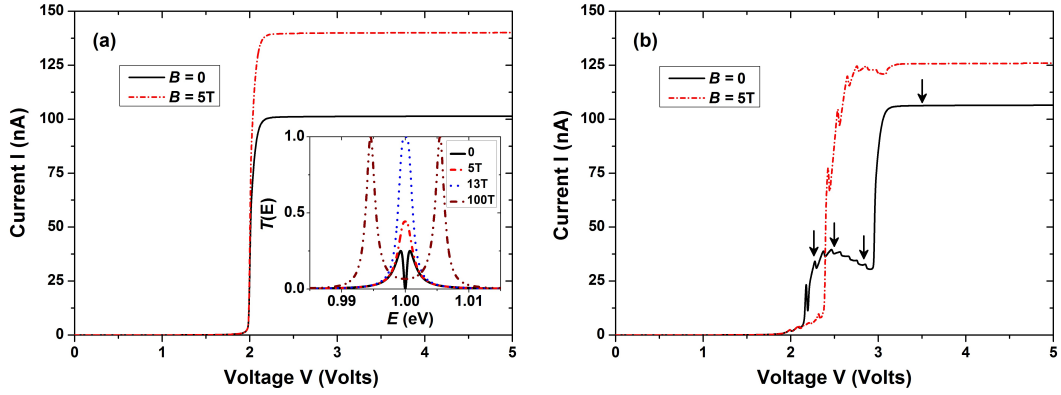


FIGURE 2.7: (a) I-V characteristics of a meta-connected benzene ring for the fields, 0 T (solid line) and 5 T (dashed-dotted line), at 10 K, $\Gamma=5$ meV. (b) Respective I-V curves in the presence of Coulomb interaction ($V_C=100$ meV).

saturation in the current conduction. This appealing aspect of magnetic field sensitivity in a suitably constructed setup demonstrates its technological applicability in magnetic sensor applications. This provides extra functionality to the magnetic field control of current in the proposed setup.

(b) Benzene single-molecule junction

As discussed in the preceding sections, we emphasize that a weak lead-molecule coupling strength is crucial for effective magnetic field-based control of current conduction in smaller ring structures. However, the Coulomb interaction between the electrons in a weakly coupled molecule in a junction can have a significant impact on the electron transport because the electrons entering the weakly coupled molecule spend a sufficiently long time in the molecule availing enough interaction before leaving it. Although not shown here, calculations using $E_F = 0$ for a meta-connected benzene ring revealed that for $V_c \gg \Gamma = 5$ (meV) current diminishes significantly, which is consistent with the closely related studies.[31] The

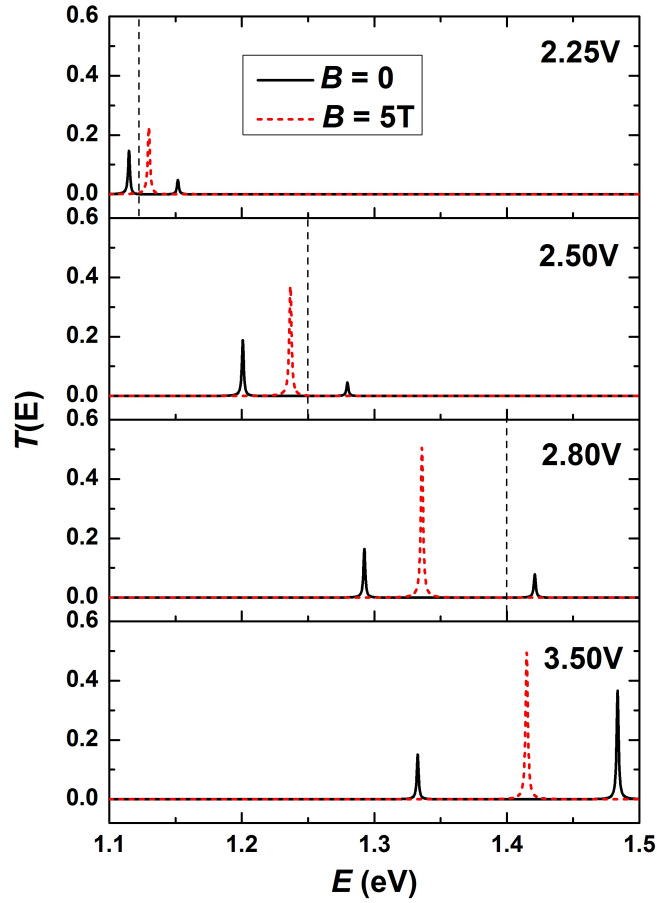


FIGURE 2.8: Transmission probability as a function of electron energy (corresponding to the arrows in the I-V characteristic, Fig. 2.5 (b)) for a meta-connected benzene ring at bias voltages; 2.25, 2.50, 2.80, 3.50 V, showing the evolution of transmission peaks in the respective energy windows $E_F \pm eV/2$ ($E_F = 0$) for the fields, zero (solid line) and 5T (dashed line), $\Gamma=5$ meV. The upper edge of the energy window is represented by the dashed vertical line in each picture; in the bottom panel (3.50 V), it is located at 1.75 eV. No transmission peaks are located in the energy windows except the ones shown above.

I-V characteristics for meta-connected benzene ring (C_6) in the absence and presence of inter-site Coulomb interaction shown in Fig. 2.7 (a) and (b), respectively, demonstrate effective current control by relatively small field strength, $B=5$ T. The observed NDR feature in absence of a magnetic field (Fig. 2.7 (b)) closely resembles the experimental results on nitro-phenylethynyl-benzenethiol molecules.[72] While the current is found to sustain for $V_C (= 0.1$ eV) $> \Gamma$ that appears with

the NDR feature for bias voltage in the range (2-3 V), however, the observed NDR feature is greatly suppressed when the external magnetic field is switched on. To get insights into the underlying effects, we plot in Fig. 2.8, the transmission probability as a function of the energy of incoming electrons at four different bias voltages (2.25, 2.50, 2.80, and 3.50 V) corresponding to the arrows as marked in the I-V characteristics shown in Fig. 2.7 (b). It is important to notice that when bias voltage increases, the relative positions of the transmission peaks shift, and a comparison of the transmission spectra at bias voltages of 2.50 and 2.80 V shows that the height of the transmission peak decreases, which results in a reduction in current. Also, we observe that the modification of transmission peak height is negligible at low bias but gradually becomes more pronounced with an increase in the bias voltage.

The NDR phenomena may have originated from a number of different physical mechanisms. However, relevant to us are the two widely accepted processes that can cause the NDR effect in metal-molecule-metal junctions are either modification of the transmission peaks along with a shift in the molecular energy level within the bias window, or a shift of the molecular energy levels away from the bias window, which results in fewer or no energy levels contributing to the current. The cause of the former situation is largely attributed to physical mechanisms, such as conformational changes in the molecule under increasing bias voltage, changes in lead-molecule coupling at different biases, etc., whereas the latter is attributed to an energy level shift caused by an electron-vibration

coupling that requires weak lead-molecule coupling so that the broadening of the energy level smaller than the polaron shift. This effect resembles the Coulomb blockade phenomenon, in which the energy necessary to charge the molecule with one elementary charge (the charging energy) moves energy levels away from the bias window, thereby preventing the current conduction through the molecule. When the thermal energy of the electron and the bias potential are both below the charging energy, which is normally a few meV or less, this effect completely inhibits current through the junction, which is not the case here. The Coulomb blocking of the energy levels responsible for the current conduction that causes the NDR in a para-connected benzene ring, but not in the meta-connected configuration, is another blockade mechanism that results in the NDR. In our case, the inter-site Coulomb interaction renormalizes the energy levels that depend on the occupation number of the electron and the bond charge, and consequently on the bias voltage. The transmission peaks are modulated and their locations are changed with an increase in bias, which causes the NDR features to appear in the I-V characteristics. This is due to the renormalization of the on-site energy and hopping integral. A similar system is found to exhibit NDR effects that persist even at room temperature.[73] In our setup, the peak-to-valley current ratio (PVR) consistently increases with temperature, albeit insignificantly. However, the use of a magnetic field creates the opportunity to tune the peak-to-valley ratio to a level acceptable for specialised applications, such as switching devices. [74] Further studies are required to validate the above observations of technological importance.

2.5 Summary and Concluding Remarks

The generic evolution of energy-resolved transmission peaks under the influence of an applied magnetic field leads to effective control of current conduction through ring structures such as graphene nanosheets. However, this requires geometrical asymmetry in the coupling of graphene nanosheets to the contact leads and weak coupling between them. Asymmetry in contact position is essential as this splits the otherwise degenerate energy levels of the graphene nanosheets leading to energy-resolved transmission peaks, which evolve with the applied magnetic field. The weak lead-molecule coupling is crucial for producing the energy-resolved transmission peaks corresponding to the relatively distinct energy levels, which are easily influenced by the applied magnetic field. We stress that weak coupling is essential for current control in smaller structures, while its role is significantly less in larger structures. However, the increased flux through larger structures enables the modulation of energy levels with relative ease, leading to current control at relatively small values (\sim few Tesla). Although a number of factors have a direct bearing on electron transport through the graphene nanosheet junctions, a suitably designed setup would significantly increase the prospects of current control under the applied magnetic field. Model calculations on C_6 and C_{222} junction with inter-site Coulomb interaction are found to sustain sensitivity to the magnetic fields in the lower field region ($B \leq 5\text{T}$), which in the case of weak coupling limit would lie in the range of a few hundred milli-Tesla. This property may be

explored in depth for the potential applications in magnetic sensors. Furthermore, the observed modulation of the NDR feature by an applied magnetic field might find useful applications in magnetic switching devices. We attribute the observed NDR to the renormalization of the molecular energy levels leading to the modulation of transmission peaks within the bias window. However, due to the underlying delicate requirements of weak coupling, asymmetric connection at appropriate sites, and conduction preferably at low temperature, the observations highlighted here present significant challenges for experimental realisation. Nevertheless, it is worthwhile to try because they are both intriguing and crucial for the implementation and advancement of molecular-scale device technologies.

References

- [1] M. Wimmer, J. L. Palma, P. Tarakeshwar, and V. Mujica, *J. Phys. Lett.* **7**, 2977 (2016).
- [2] J. P. Bergfield and M. A. Ratner, *Phys. Status Solidi B* **250**, 2249 (2013).
- [3] L. Sun, Y. A. Diaz-Fernandez, T. A. Gschneidner, F. Westerlund, S. Lara-Avila, and K. Moth-Pulsen, *Chem. Soc. Rev.* **43**, 7378 (2014).
- [4] D. Xiang, X. Wang, C. Jia, T. Lee, and X. Guo, *Chem. Rev.* **116**, 4318 (2016).
- [5] R. L. McCreery and A. J. Bergren, *Adv. Mater.* **21**, 1 (2009).
- [6] N. A. Zimbovskaya and M. R. Pederson, *Phys. Rep.* **509**, 1 (2011).
- [7] V. Fatemi, M. Kamenetska, J. B. Neaton, and L. Venkataraman, *Nano Lett.* **11**, 1988 (2011).
- [8] U. Peskin and M. Galperin, *J. Chem. Phys.* **136**, 044107 (2012).
- [9] S. Ballmann, R. Härtle, P. B. Coto, M. Elbing, M. Mayor, M. R. Bryce, M. Thoss, and H. B. Weber, *Phys. Rev. Lett.* **109**, 056801 (2012).
- [10] Le-Jia Wang, A. Yong, Kai-Ge Zhou, L. Tan, J. Ye, Guo-Ping Wu, Zhu-Guo Xu, and Hao-Li Zhang, *Chem. Asian J.* **8**, 1901 (2013).
- [11] A. Saffarzadeh, F. Demir, and G. Kirczenow, *Phys. Rev. B* **89**, 045431 (2014) .

- [12] M. Ridley, A. MacKinnon, and L. Kantorovich, *Phys. Rev. B* **93**, 205408 (2016).
- [13] I. Diez-Perez, Z. Li, J. Hihath, J. Li, C. Zhang, X. Yang, L. Zang, Yijun Dai, X. Feng, K. Muellen, and N. Tao, *Nature Comm.* **31**, 1 (2010).
- [14] F. Prins, A. Barreiro, J. W. Ruitenber, J. S. Seldenthuis, N. Aliaga-Alcalde, L. M. K. Vandersypen, and H. S. J. van der Zant, *Nano Lett.* **11**, 4607 (2011).
- [15] J. L. Speyer, I. V. Ovchinnikov, D. Neuhauser, and D. Baugh, *J. Chem. Phys.* **123**, 124704 (2005).
- [16] E. R. Hedin, R. M. Cosby, Y. S. Joe, and A. M. Satanin, *J. Appl. Phys.* **97**, 063712 (2005).
- [17] O. Hod, E. Rabani, and R. Baer, *Acc. Chem. Res.* **39**, 109 (2006).
- [18] J. Brüning, L. A. Chernozatonskii, V. V. Demidov, and V. A. Geyler, *Russ. J. Math. Phys.* **14**, 417 (2007).
- [19] O. Hod, R. Baer, and E. Rabani, *J. Phys.: Condens. Matter* **20**, 383201 (2008).
- [20] S. Compornolle, L. F. Chibotaru, and A. Ceulemans, *J. Phys. Chem. B* **110**, 19340 (2006).
- [21] S. Compornolle, L. F. Chibotaru, and A. Ceulemans, *Chem. Phys. Lett.* **428**, 119 (2006).

- [22] D. Rai, O. Hod, and A. Nitzan, *J. Phys. Chem. Lett.* **2**, 2118 (2011).
- [23] D. Rai, O. Hod, and A. Nitzan, *Phys. Rev. B* **85**, 155440 (2012).
- [24] T. Hansen, G. C. Solomon, D. Q. Andrews, and M. A. Ratner, *J. Chem. Phys.* **131**, 194704 (2009).
- [25] A. Fuhrer, S. Lüscher, T. Ihn, T. Heinzel, K. Ensslin, W. Wegscheider, and M. Bichler, *Nature* **413**, 822 (2001).
- [26] J. G. Analytis, S. J. Blundell, and A. Ardavan, *Am. J. Phys.* **72**, 613 (2004).
- [27] T. Zhang, D. Guérin, F. Alibart, D. Vuillaume, K. Lmimouni, S. Lenfant, A. Yassin, M. Oçafrain, P. Blanchard, and J. Roncali, *J. Phys. Chem. C* **121**, 10131(2017).
- [28] V. Ulansky, A. Raza, and H. Oun, *Electronics* **8**, 409 (2019).
- [29] F. Chen and N. J. Tao, *Accounts Chem. Res.* **42**, 429 (2009).
- [30] X. W. Sha, E. N. Economou, D. A. Papaconstantopoulos, M. R. Pederson, M. J. Mehl, and M. Kafesaki, *Phys. Rev. B* **86**, 115404 (2012).
- [31] M. Nuss, W. von der Linden, and E. Arrigoni, *Phys. Rev. B* **89**, 155139 (2014).
- [32] H. Haug and A. -P. Jauho, *Quantum Kinetics in Transport and Optics of Semiconductors*, Springer, Berlin, 2008.

- [33] D. Ryndyk D, R. Gutiérrez, B. Song, and G. Cuniberti, in: Energy Transfer Dynamics in Biomaterials Systems, Springer, Berlin, 2009, Vol. 93, p. 213.
- [34] A. G. Redfield, *IBM J. Res. Dev.* **1**, 19 (1957).
- [35] H. -P. Breuer and F. Petruccione. The Theory of Open Quantum Systems, Oxford University Press, Oxford, 2003, p. 132.
- [36] R. Härtle, C. Benesch, and M. Thoss, *Phys. Rev. Lett.* **102**, 146801 (2009).
- [37] R. Volkovich, R. Härtle, M. Thoss, and U. Peskin, *Phys. Chem. Chem. Phys.* **13**, 14333 (2011).
- [38] H. Li, L. Wang, Z. Lan, and Y. Zheng, *Phys. Rev. B* **79**, 155429 (2009).
- [39] S. V. Faleev and M. I. Stockman, *Phys. Rev. B* **66**, 085318 (2002).
- [40] M. Galperin, M. Ratner, and A. Nitzan, *Nano Lett.* **4**, 1605 (2004).
- [41] D. Darau, G. Begemann, A. Donarini, and M. Grifoni, *Phys. Rev. B* **79**, 235404 (2009).
- [42] R. E. Peierls, *Z. Phys.* **80**, 763 (1933).
- [43] D. R. Hofstadter, *Phys. Rev. B* **14**, 2239 (1976).
- [44] F. London, *J. Phys. Rad.* **8**, 397 (1937).
- [45] C. Weeks and M. Franz, *Phys. Rev. B* **81**, 085105 (2010).
- [46] M. Daghofer and M. Hohenadler, *Phys. Rev. B* **89**, 035103 (2014).

- [47] C. Barreateau, Marie-Catherine Desjonquères, A. M. Oleś, and D. Spanjaard, *Phys. Rev. B* **69**, 064432 (2004).
- [48] A. Freyn and J. -L. Pichard, *Eur. Phys. J. B* **58**, 279 (2007).
- [49] M. Amini, V. E. Kravtsov, and M. Müller, *New J. Phys.* **16**, 015022 (2014).
- [50] Y. Meir and S. N. Wingreen, *Phys. Rev. Lett.* **68**, 2512 (1992).
- [51] J. P. Lowe, K. Peterson, Quantum Chemistry, Elsevier Academic Press, 2011, Ed. 3, p. 278.
- [52] I. A. Popov and A. I. Boldyrev, *Eur. J. Org. Chem.* **2012**, 3485 (2012).
- [53] M. Galperin, M. A. Ratner, and A. Nitzan, *Nano* **4**, 1605 (2004).
- [54] K. Walczak, *Physica E* **33**, 110 (2006).
- [55] L. A. Zotti, T. Kirchner, J. -C. Cuevas, F. Palay, T. Huhn, E. Scheer, and A. Erbe, *Small* **6**, 1529 (2010).
- [56] T. Kirchner, B. Briechle, E. Scheer, J. Wolf, T. Huhn, and A. Erbe, *Acta Phys. Pol. A* **121**, 410 (2012).
- [57] N. Bennett, G. Xu, L. J. Esdaile, H. L. Anderson, J. Em. Macdonald, and M. Elliott, *Small* **6**, 2604 (2010).
- [58] R. J. Bursill, C. Castleton, and W. Barford, *Chem. Phys. Lett.* **294**, 305 (1998).

- [59] J. Rincón, K. Hallberg, A. A. Aligia, and V. Ramasesha, *Phys. Rev. Lett.* **103**, 266807 (2009).
- [60] J. A. Vergés, E. SanFabián, G. Chiappe, and E. Louis, *Phys. Rev. B* **81**, 085120 (2010).
- [61] J. D. Barr, C. A. Stafford, and J. P. Bergfield, *Phys. Rev. B* **86**, 115403 (2012).
- [62] T. A. Su, M. Neupane, M. L. Steigerwald, L. Venkataraman, and C. Nuckolls, *Nat. Res. Mater.* **1**, 1 (2016).
- [63] Y. Cho, W. Y. Kim, and K. S. Kim, *J. Chem. Phys. A* **113**, 4100 (2009).
- [64] F. Chen, X. Li, J. Hihath, Z. Huang, and N. Tao, *J. Am. Chem. Soc.* **128**, 15874 (2006).
- [65] V. Kaliginedi, A. V. Rudnev, P. Moreno-García, M. Baghernejad, C. Huang, W. Hong, and T. Wandlowski, *Phys. Chem. Chem. Phys.* **16**, 23529 (2014).
- [66] V. Obersteiner, D. A. Egger, and E. Zojer, *J. Phys. Chem. C* **119**, 21198 (2015).
- [67] G. Ji, D. Li, C. Fang, Y. Xu, Y. Zhai, B. Cui, and D. Liu, *Phys. Lett. A* **376**, 773 (2012).

- [68] F. Chen, Lin-Lu Peng, Ze-Wen Hong, Jin-Chuan Mao, Ju-Fang Zheng, Y. Shao, Zhen-Jiang Niu, and Xiao-Shun Zhou, *Nanoscale Res. Lett.* **11**, 380 (2016).
- [69] Y. Selzer, L. Cai, M. A. Cabassi, Y. Yao, J. M. Tour, T. S. Mayer, and D. L. Allara, *Nano Lett.* **5**, 61 (2005).
- [70] D. P. Long, J. L. Lazorcik, B. A. Mantooth, M. H. Moore, M. A. Ratner, A. Troisi, Y. Yao, J. W. Ciszek, J. M. Tour, and R. Shashidhar, *Nat. Mater.* **5**, 901 (2006).
- [71] B. Capozzi, J. Xia, O. Adak, E. J. Dell, Zhen-Fei Liu, J. C. Taylor, J. B. Neaton, L. M. Campos, and L. Venkataraman, *Nat. Nanotechnol.* **10**, 522 (2015).
- [72] I. Kratochvilova, M. Kocirik, A. Zambova, J. Mbindyo, T. E. Mallou, and T. S. Mayer, *J. Mater. Chem.* **12**, 2927 (2002).
- [73] J. Chen, W. Wang, M. A. Reed, A. M. Rawlett, D. W. Price, and J. M. Tour, *Appl. Phys. Lett.* **77**, 1224 (2000).
- [74] B. Warner, F. E. Hallak, H. Prüser, J. Sharp, M. Persson, A. J. Fisher, and C. F. Hirjibehedin, *Nat. Nanotechnol.* **10**, 259 (2015).

Chapter 3

Circular Current-Induced Force In Molecular Junctions[†]

Abstract

We revisit the bias-induced circular current in a molecular ring junction and calculate the circular current on the basis of the magnetic response of the ring junction to an external flux in the zero-flux limit. This allows circular current to be determined without calculating the bond currents in the molecular ring. We also investigate the possibility of circular current-induced force rupturing the covalent bonds in the ring leading to the eventual breakdown of the ring junction. Our results highlight the reliability issue concerning the current magnification effect in molecular ring structures.

[†]Work presented in this chapter is based on the following research article:
Circular current and induced force in a molecular ring junction.
Umesh Dhakal and Dhurba Rai, *J. Phys.: Condens. Matter* **31**, 125302 (2019).

3.1 Background

Significant progress has been made in understanding the electron transport features of the ring structure junctions.[1–7] The majority of the studies have focused on the conduction properties of the ring structure junctions concerning the lead-molecule interface geometry and the electronic structures, while only a few studies are related to the internal current distribution in the molecular rings structures.[5, 8, 9] In a molecular junction where the size of the molecule is comparable to the phase coherence length of the electron, the phase of the electron waves strongly influences the electron transport properties of the molecular junction.[10–14] The phase difference arises when an electron wave propagates through various pathways leading to quantum interference effects, thereby influencing the overall electron transport with either an increase in electron transmission probability associated with constructive interference or a decrease in the probability due to destructive interference. One of the important aspects of electron transport through a ring junction is the ability to tune the phase of the electrons waves by modulating the Aharonov-Bohm (AB)-like phase of the electron.[15, 16] This leads to the possibility of controlling the current conduction through the molecular ring structures by an externally applied magnetic field.[3, 4] When the bridging molecule is connected asymmetrically to the contact leads (either meta- or ortho-), quantum interference effects arise due to electrons competing for the multiple pathways, which result in unequal bond currents (direction as well as magnitude)

at a certain range of bias voltage, which sometimes exceeds the net current across the molecular junction.[5, 8] This results in a bias-induced circular current in the molecular ring structures that are seemingly identical to the persistent current induced in a mesoscopic ring, where the current is driven by an external magnetic field, however, persists even after the field is removed.

The circular current is defined as the component of current in the ring that acts as the sole source of induced-magnetic flux in the ring, while the associated component in the ring is identified as the transverse current, which does not contribute to the total flux. Such circular current has been studied in both mesoscopic ring and molecular ring junctions.[17–19] The existence of circular current in the molecular loop structures is considered to be a purely quantum interference effect associated with the electron waves propagating along different pathways. Calculations show that in a certain voltage range, the circular current can be considerably larger than the net current and reaches its maximum value at the resonant transmission through the frontier orbitals, for example, through the lowest unoccupied molecular orbital (LUMO). Studying circular current and the associated magnetic moment in the molecular ring structures is crucial for understanding the optimal performance and reliability of molecular ring-based devices. As an illustration, exposure to the external magnetic field may cause the ring structures to torsionally deform due to interaction between the magnetic moment of the rings and the applied magnetic field, thereby affecting their conductive properties that depend on the orientation between the rings.[20]

It must be mentioned here that the quest for designing single-molecule device components in molecular electronics has been primarily dominated by benzene-based molecular junctions.[21, 22] On a molecular scale, the benzene ring junction provides versatile test-beds for analysing bias-induced circular current and associated phenomena. Also, the quantum interference-based functionalities of a benzene ring can be suitably modified using different chemical substituents.[23, 24] Here we consider the benzene ring as a typical molecular ring for our model calculations of circular current and the associated induced force.

3.2 Scope of the Work

As discussed in the preceding section, one of the important characteristics of the molecular ring junctions is the possible control current conduction at relatively small magnetic field values. If such molecular ring junctions are to be used as basic components in molecular electronics, it is imperative to study the local currents (bond currents) and the related phenomena for better insights into the design, operation, and stability of the molecular electronics devices. For instance, junction breakdown has been seen to be taken place by the weakening of chemical bonds generated by current-induced force, both at the lead-molecule interface and within the molecule, even when the temperature increase due to current-induced heating is not very considerable.[25] The current-induced force is due to the momentum transfer by the scattered electrons to the lattice atoms. The present analysis aims at providing some deeper insights into the mechanical stability of the molecular

ring junctions particularly when they are operated at a bias voltage corresponding to which the circular current becomes maximum. However, before diving in, we provide a reliable method for computing circular current without calculating the local currents.

3.3 Computational Framework

We succinctly go over the computational strategy undertaken in this work. All the calculations were carried out within the framework of the tight-binding approximation. We have employed the non-equilibrium Green's function (NEGF) technique to calculate the current through the junction in steady-state situations. Throughout calculations, we consider zero temperature, however, the non-zero temperature can be considered through the Fermi distribution function in the leads. Also, in our calculations, the equilibrium chemical potential μ is set to zero in the energy scale. The metal leads are treated as free-electron reservoirs that transfer electrons to the bridging molecule at a rate Γ/\hbar . Unless otherwise stated, we consider metal-molecule coupling strength $\Gamma=0.5$ eV. The on-site energy $\epsilon = 1.7$ eV and the hopping integral, $t_{ij} = 2.7$ eV, are assumed to be uniform in the benzene ring that has equilibrium bond length $a_0 = 1.4$ Å. Although the calculations are model-based, they capture the essential physics of the circular current and the associated induced force. The realistic calculations involving many-body effects are beyond the scope of the present venture.

3.4 Model and Formulation

We now present various models employed in this work to determine the local currents (i.e., bond currents) and the current-induced force in the ring. The circular current calculated from the local currents is compared with that calculated from the magnetic response of the ring in the zero-flux limit.

3.4.1 Local current in the molecular bridge

We consider electron transport through a molecular junction consisting of a single benzene molecule bridging the two metal electrodes in an asymmetric configuration, i.e., in meta connection. The entire analysis is based on the consideration that the electrons are non-interacting. In such a case, the tight-binding (TB) model is suitable for capturing the basic electron transport properties. We begin with the tight-binding Hamiltonian of the ring connected to the metal electrodes that act as free-electron reservoirs. It is customary to write the total Hamiltonian of the molecular junction as the sum of the sub-Hamiltonians, i.e.,

$$\hat{H} = \hat{H}_K + \hat{H}_M + \hat{H}_{KM}; \quad K = L, R \quad (3.1)$$

where the symbols have usual meanings and the explicit details of each Hamiltonian are covered in the preceding chapter. Since a driven system with particles getting in and out of the system is a non-equilibrium system, we employ the

non-equilibrium Green's function (NEGF) technique [26, 27] to estimate the local currents in a biased molecular ring junction under the steady-state conditions.

There exist several methods to estimate the local current I_{ij} and the total current I in steady-state situations.[28] In particular, in the NEGF formulation, their closed-form expressions are available. The basic components of the NEGF technique are presented in the preceding chapter that include the retarded (advanced) Green's function $G^r(G^a)$, the Keldysh equation for the Green's lesser function $G^<$ and the lesser self-energy function $\Sigma_{K=L/R}^< = if_K(E)\Gamma_K(E)$, where $f_K = 1/[1 + \exp((E - \mu_K)/k_B T)]$ is the Fermi-distribution function for the contact lead at temperature T and chemical potential, μ_K . Here we directly present the expression for the local current between the sites (i, j) , or the current through k^{th} segment containing (i, j) bond of the molecular ring as [29, 30]

$$I_k \equiv I_{ij} = \frac{|e|}{\pi\hbar} \int [t_{ij}G_{ij}^<(E) - t_{ji}G_{ji}^<(E)] dE, \quad (3.2)$$

where the trace is taken in the finite-Hilbert space of the molecule spanned by its relevant atomic orbitals, and t_{ij} is the hopping integral between the sites (i, j) . The integration limits are defined by the energy window $(\mu_L - \mu_R)$, with a lower limit $\mu_L = \mu + |e|V/2$ and upper limit $\mu_R = \mu - |e|V/2$ for the applied bias voltage V . The total current under the steady-state condition is calculated using Meir-Wingreen formula,[31, 32]

$$I = \frac{|e|}{\pi\hbar} \int \frac{i}{2} Tr [(f_L\Gamma^L - f_R\Gamma^R) (G^r - G^a) + (\Gamma^L - \Gamma^R) G^<] dE. \quad (3.3)$$

It is important to note that both of the aforementioned equations contain a factor of 2 to account for the spin degeneracy. Also, it is imperative to ensure the current conservation at the connecting sites. We now quickly go over calculating the circular current in the ring junction from the bond currents.

3.4.2 Circular current in a ring junction

We consider a 1D planar ring of radius R connected to the metal contacts leads through the sites (a, b) that divide the ring into two segments ($k = 1, 2$) as shown in Fig. 3.1. A net current I flows through the ring, where I_1 and I_2 are the currents through the upper and lower segments of the ring having length segments l_1 and l_2 , respectively. Since the magnetic flux Φ enclosed by a ring is directly proportional to the current in the ring and the ring length, the total magnetic flux threading through the ring is the sum of the flux due to segmental currents I_1 and I_2 through the ring i.e. $\Phi = \frac{\mu_0}{4\pi} \lambda \sum_k I_k l_k$, where λ is a geometry dependent constant. As is customary, we assign a positive sign to the current flowing in the anti-clockwise direction. In addition to the current distribution shown in the figure, we consider the segment current I_k is composed of circular and transverse components i.e. $I_k = I_k^c + I_k^{tr}$. The circular components ($I_k^c \equiv I_c$) lead to net magnetic flux Φ threading the ring, while the net contribution to the flux due to transverse components I_1^{tr} and I_2^{tr} is zero. The Kirchhoff's law at the coupling

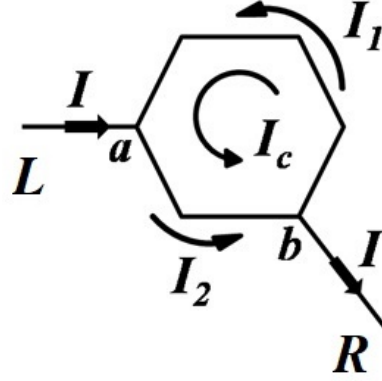


FIGURE 3.1: Schematic showing current distribution in a two-terminal junction with a benzene ring coupled to an external bias circuit through sites (a, b) . Current configuration shown in the ring corresponds to $V > 2.6$ V, wherein current I_1 in the upper arm is in opposite direction to the total current I .

sites (a, b) dictates that

$$I = I_2 - I_1 = (I_2 - I_c) - (I_1 - I_c) = I_2^{tr} - I_1^{tr}, \quad (3.4)$$

where the third equality arises due to the decomposition scheme as discussed above. For the ring under consideration, where the contact leads divide the ring into two segments $k = 1, 2$ of length l_k , the circular current in the ring is

$$I_c = \frac{I_1 l_1 + I_2 l_2}{l_1 + l_2} = \sum_k \frac{I_k l_k}{\mathcal{L}}, \quad (3.5)$$

where $\mathcal{L} = l_1 + l_2 = 2\pi R$ is the circumference of the ring. Thus, one needs bond/local currents to calculate I_c using Eq. 3.5. It must be noted that the bond currents in the ring are, however, not accessible in the experimental setup.

3.4.3 An alternative formulation of the circular current

As discussed above the bias-induced circular current in a molecular ring junction can be calculated using Eq. 3.5, however, this requires the calculation of the bond currents. Alternatively, in analogy to the persistent current induced in an isolated mesoscopic ring due to externally applied magnetic flux threading the ring, the bias-induced circular current can be calculated in a molecular ring junction from the flux-derivative of the thermodynamic potential (Ω) of the ring in the zero-flux limit.[33] This can be understood as the response of the molecular ring to the external magnetic flux introduced perturbatively and then reduced to zero, i.e.,

$$I_c = - \lim_{\phi \rightarrow 0} \frac{\partial \Omega}{\partial \phi}. \quad (3.6)$$

As, $\Omega = \mathbf{Tr}[\hat{\rho}^{neq} \hat{\Omega}]$, the circular current can be expressed as

$$I_c = - \lim_{\phi \rightarrow 0} \mathbf{Tr} \left(\hat{\rho}^{neq} \frac{\partial \hat{\Omega}}{\partial \phi} \right) = - \lim_{\phi \rightarrow 0} \mathbf{Tr} \left(\hat{\rho}^{neq} \frac{\partial \hat{H}_M}{\partial \phi} \right), \quad (3.7)$$

where $\hat{\rho}^{neq}$ is the single-particle density matrix operator which describes the charge redistribution due to the flow of current, while as mentioned before, the trace is taken in the finite-Hilbert space of the molecule spanned by the relevant atomic orbitals of the molecule. It must be mentioned here that in writing Eq. 3.7, we have not considered the electronic contribution to the entropy, while the chemical potential of both the electrodes is considered constant. Also, any additional terms

in Eq. 3.7 can be considered as paramagnetic (that emerges in a symmetrized way) or flux-dependent diamagnetic response of the molecular ring.[33] A deeper analysis of these additional terms is beyond the scope of the present work. Instead, we focus on the alternative method for calculating circular current from the magnetic response of the molecular ring without calculating the bond/local currents.

In the tight-binding approximation, the magnetic field ($\vec{B} = \vec{\nabla} \times \vec{A}$) is effected through Peierl's substitution.[4] In presence of a magnetic field, the nearest-neighbor hopping integrals get modified by a phase factor, i.e. $t_{ij} \rightarrow t_{ij} \exp(i2\pi\delta\phi_B/\phi_0)$, where $\delta\phi_B = \int_{\vec{r}_i}^{\vec{r}_j} \vec{A} \cdot d\vec{l}$ is the magnetic flux through the triangle spanned by position vectors (\vec{r}_i, \vec{r}_j) of the sites (i, j) and $\phi_0 = h/|e|$ is the flux quantum. In the NEGF approach, the non-equilibrium single-particle density matrix is given by

$$\rho_{ij}^{neq} = -i \int \frac{dE}{2\pi} G_{ij}^<(E). \quad (3.8)$$

Thus, using Eq. 3.8 in Eq. 3.7, the circular current induced in the molecular ring junction can be expressed as

$$I_c = \lim_{\phi \rightarrow 0} 2i \int \frac{dE}{2\pi} \mathbf{Tr} \left(G^< \frac{\partial H_M}{\partial \phi} \right), \quad (3.9)$$

where factor 2 accounts for spin degeneracy of electrons. The equilibrium electrochemical potential μ of both electrodes (source and drain) is set to zero in the energy scale. In all the calculations presented below, unless otherwise stated, we have considered electron transport at zero temperature.

3.4.4 Circular current-induced force

We consider a tight-binding Barišić-Labbé-Friedel (BLF) model Hamiltonian [34] to calculate the current-induced force in a molecular ring junction. In this model, the interaction between the electron and ion is described by the displacement-dependent hopping integral,[35]

$$\hat{H}_M = \sum_{i \in M} \epsilon_i \hat{d}_i^\dagger \hat{d}_i - \sum_{\langle ij \rangle \in M} (t_{ij} \{1 + \zeta \frac{(\vec{R}_j - \vec{R}_i)}{|\vec{R}_j - \vec{R}_i|} \times \cdot (\vec{u}_i - \vec{u}_j)\} \hat{d}_i^\dagger \hat{d}_j + H.c.), \quad (3.10)$$

where $\vec{u}_{i,j}$ are the displacements of the lattice ions from their equilibrium positions $\vec{R}_{i,j}$, and ζ is an atomic orbital exponent characterizing the exponential decay of the atomic orbitals positioned at the lattice site. Throughout the calculation, we use $\zeta=1.56$ corresponding to 2p slater-type orbitals (STO) of the ground state carbon atom.[36] The calculation of current-induced force is considered to be challenging because it involves the estimation of the atomic force in a non-equilibrium situation, where the total number of particles and energy is not defined. For a closed system at equilibrium, the atomic forces are well defined and can be obtained from the well-known Hellmann-Feynman (HF) theorem. In contrast, the situation is more complex for an open and non-equilibrium case, where the HF theorem does not apply. However, it is shown recently [37, 38] that the current-induced force in a non-equilibrium steady-state situation is equivalent to the equilibrium case with equilibrium quantities replaced by non-equilibrium ones.[39, 40] To this end,

the steady-state force exerted on the i^{th} ion along the x-direction by the current-carrying electrons can be expressed in terms of a single-particle non-equilibrium density matrix as,[41–45]

$$F_{iX} = -2\mathbf{Tr} \left(\hat{\rho}^{neq} \frac{\partial \hat{H}_M}{\partial R_{iX}} \right) = 2i \int \frac{dE}{2\pi} \mathbf{Tr} \left(G^< \frac{\partial H_M}{\partial R_{iX}} \right), \quad (3.11)$$

where, as before, the factor of 2 accounts for spin degeneracy. We now present numerical results based on model calculations.

3.5 Numerical Results and Discussion

As stated earlier, the metal electrodes are considered free-electron reservoirs that exchange electrons with the benzene molecule at a rate Γ/\hbar . We consider symmetric coupling strength, $\Gamma_L = \Gamma_R = 0.50$ eV. The nearest-neighbor hopping integral $t_{\langle ij \rangle} = 2.70$ eV is considered uniform in the molecular ring with equilibrium bond length $a_0 = 1.40$ Å and on-site energies, $\epsilon_i = -1.70$ eV.

3.5.1 Circular current

The calculation of circular current in a benzene ring is presented in Fig. 3.2. Interestingly, the calculation reveals that the circular current obtained from Eq. 3.5 and Eq. 3.9 are identical, although the methods for determination are based on completely different approaches. However, the equivalence between these two

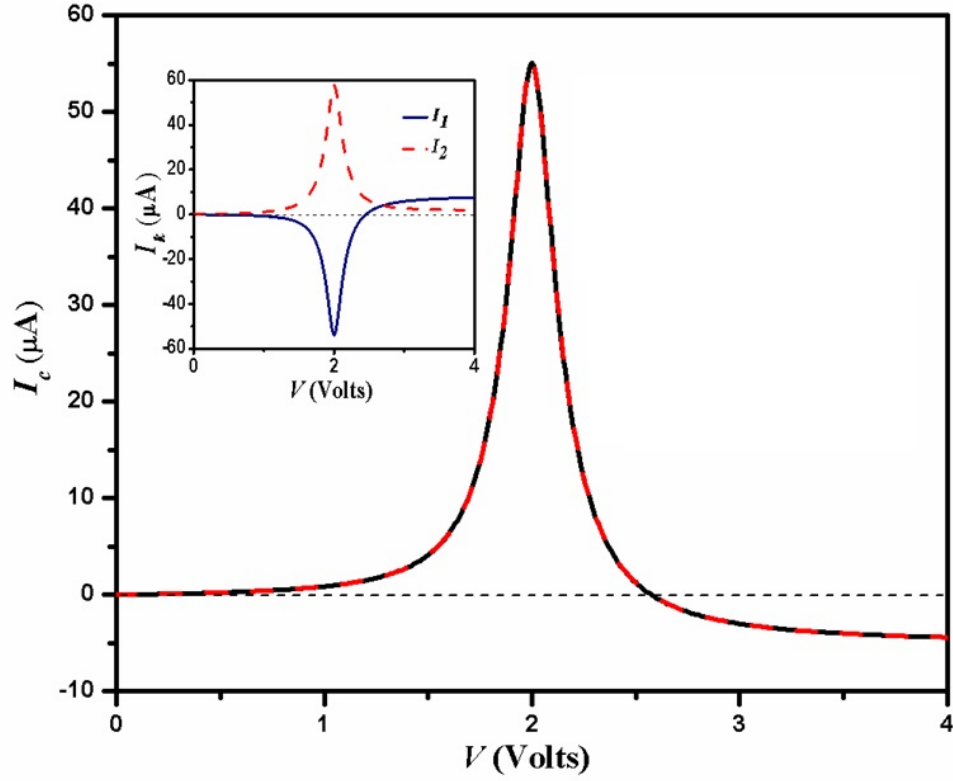


FIGURE 3.2: Bias-induced circular current I_c in a benzene ring junction computed using Eqs. 3.5 and 3.9 for an asymmetric (meta-) connection of the metal lead. They overlap as depicted and are identically similar. Inset shows the bond current ($I_k, k = 1, 2$) in the upper and lower segments of the benzene ring.

equations arises due to the fact that when magnetic flux ϕ equivalent to the flux Φ produced by the bias-induced circular current I_c is applied externally, an equivalent circular current will be induced in the molecular ring. This can be understood by identifying the current in the k th segment of the molecular ring as

$$I_k = - \left(\frac{\partial H^{Ring}}{\partial \Phi} \right)_k = - \frac{\partial H_k^{Ring}}{\partial \Phi_k}. \quad (3.12)$$

Since the circular current is equal in each of the k segments, the associated flux is

$$\Phi_k = \frac{l_k}{\mathcal{L}} \Phi = \frac{l_k}{\mathcal{L}} \phi. \quad (3.13)$$

and thus,

$$I_k = -\frac{\mathcal{L}}{l_k} \frac{\partial H_k^{Ring}}{\partial \phi}.$$

Therefore, the circular current is

$$I_c = \sum_k \frac{l_k I_k}{\mathcal{L}} = -\sum_k \frac{\partial H_k^{Ring}}{\partial \phi} = -\frac{\partial H^{Ring}}{\partial \phi}. \quad (3.14)$$

Although not shown here for brevity, the results for ortho-connection are qualitatively similar, whereas the para-connected ring leads to zero circular current for all energies due to geometrical symmetry reasons. The sharp resonance feature and sign reversal of the circular current in Fig. 3.2 is associated with the entry of split energy levels within the energy window $\mu_L - \mu_R$, with energy states favoring clockwise circular current (negative) at higher bias voltage. At resonance near $V=2$ Volt, for contact coupling $\Gamma=0.50$ eV, significant current magnification as large as $I_c \approx 15I$ is observed. However, smaller value of Γ , the current magnification ratio I_c/I increases furthermore. This may lead to considerable momentum transfer to the carbon atoms in the ring as discussed in the section below.

3.5.2 Current-induced force

In order to calculate the current-induced force, we consider each carbon atom of the benzene molecule under a breathing mode oscillation (A_{1g} symmetry) with a radial displacement of 0.01 \AA . For simplicity, the temperature is set to zero. Although current-induced force calculated using Eq. 3.11 on each carbon atom in

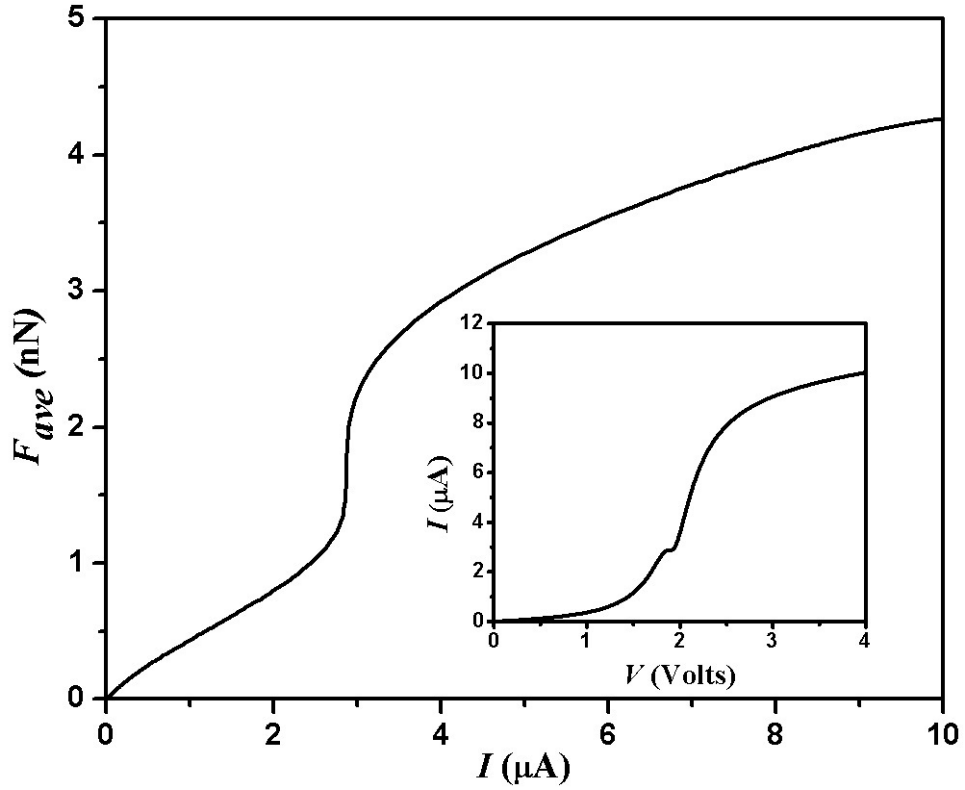


FIGURE 3.3: Plot of average current-induced force (F_{ave}) on a carbon atom in an asymmetrically (meta-) linked benzene ring as a function of transport current (I) through the molecular ring junction. $I - V$ curve of the junction, exhibiting a ledge at $2V$ is due to the split of otherwise degenerate energy levels of the benzene ring owing to the asymmetric connection of the metal leads, is presented in the inset.

the benzene ring was found to satisfy the zero-force sum rule, i.e., $\sum_i F_{iX}=0$,^[46] the calculated force, however, did not reflect the peculiar nature of the local current (cf. Fig. 3.2, inset) that reaches its maximum at resonance bias $V \sim 2$ Volt and reverses its direction when the bias voltage is increased. Thus, the calculated force seems to us rather inconsistent and not discussed here furthermore. Similar results (not shown) are obtained for other in-plane vibrational modes that include B_{1u} and B_{2u} . Instead, the calculated current-induced force is found to vary with bias voltage the way the net current varies. Thus, in Fig. 3.3 we show the functional relationship between the calculated average force F_{ave} on each carbon atom in the

benzene ring and the net current I through the molecular ring junction, while the inset shows the I-V curve.

As of now, we consider the current-induced force in benzene as a function of the net current through it. However, in the tight-binding model, the electronic current may be considered as flowing along the bonds between the nearest atoms. Hence, it is desirable to calculate the current-induced local force directly in terms of circular current. In the following, we calculate the circular-current induced force (F_c) in the benzene molecule resulting from scattering transport accompanying the net momentum transfer to the target carbon atoms from the electrons in the current flow. In literature, this current-induced force is generally referred to as electron-wind force.[47, 48] This can be determined in terms of net momentum transferred due to the electrons with energies within the bias window, i.e.,

$$F_c = \frac{1}{|e|} \int \gamma I_c(E) p(E) dE. \quad (3.15)$$

Here γ is the aspect ratio for electron scattering, expressed as the ratio of momentum transfer cross-section σ_{tr} to the bond cross-section σ_b . Although, the scattering cross-section σ_{tr} for momentum transfer by an electron is energy-dependent, however, in the present study we consider this an energy independent in the range $(10 - 20) \text{ \AA}^2$ [49] and set $\sigma_b = 1 \text{ \AA}^2$ for the C-C covalent bonds.[50] This sets the aspect ratio γ in the range of $(10 - 20)$, while we consider $\gamma = 10$.

In the above Eq. 3.15, $I_c(E)$ is the bias-induced circular current in the

molecular ring as a function of incident electron energy E , and $p(E)$ is the corresponding momentum of the incoming electron that gets transferred to the target atom in the scattering events. For our conservative estimates, we consider $p(E) = \sqrt{2m_e(E + |e|V)}$ for electrons crossing the biased molecular junction at energy E in the range $\mu_R \leq E \leq \mu_L$. This can be understood considering the incoming electrons from the free-electron reservoir, which can be viewed as plane waves $e^{i\vec{k}\cdot\vec{x}}$ with the associated momentum $\vec{p} = \hbar\vec{k}$, incident on the bridging molecule from left alone and zero molecular electrostatic potential so that the bias voltage V shifts μ_L by the amount $|e|V$ with respect to the molecular energy levels, while μ_R is held fixed. The latter is often considered in the studies of molecular rectifiers.[51] It is worth mentioning here that only the electron flux ($\frac{1}{|e|} \frac{I_c}{\sigma_b}$) is calculated within the tight-binding approximation while the incident electron momentum is calculated from the energy conservation condition, viz., $\frac{\hbar^2 k^2}{2m_e} = E - v_{eff}$, where v_{eff} is the effective potential energy term. In principle, v_{eff} also includes the exchange-correlation energy (many-body effects) other than the usual electrostatic potential energy term ($-|e|V$).

We here consider three different values of coupling strength, $\Gamma = 0.05$ eV, 0.50 eV, and 1.50 eV and calculated the circular current-induced force F_c . The variation of induced force F_c on a carbon atom in an asymmetrically (meta-) connected benzene ring as a function of circular current I_c is shown in Fig. 3.4. Positive circular current for voltage in the range (0-2 V) indicates current flow in

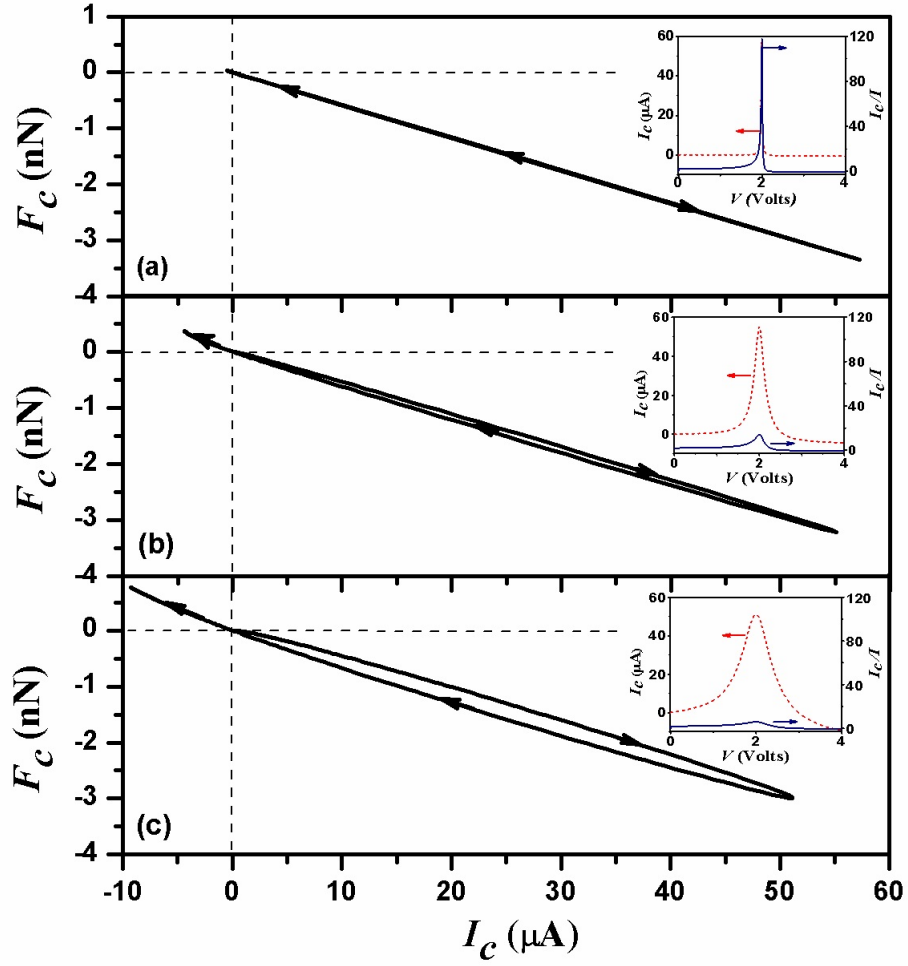


FIGURE 3.4: Circular current-induced force on a carbon atom is depicted as a function of circular current in a meta-connected benzene ring for three different coupling strengths (a) $\Gamma = 0.05$ eV, (b) 0.50 eV, and (c) 1.50 eV for $\gamma = 10$. The downward and upward arrows represent force corresponding to an increase in bias voltage in the range $(0 - 2\text{V})$ and $(2 - 4\text{V})$ respectively. Inset depicts the variation of circular current with the bias voltage at respective coupling strengths. The current magnification ratio (I_c/I) achieving its maximum value ~ 118 , 15 , and 6 at the resonant bias of 2V is also presented.

a counter-clockwise direction and thus the induced force acts in a clockwise direction, tangentially, which is shown by a downward arrow. However, beyond 2 Volt, both circular current and induced force decrease and reverse their direction. This is shown by the upward arrow. In a hindsight, it must be noted that F_c varies the way the local current varies with external bias, while the average force F_{ave}

mimics the net transport current. It is evident from Fig. 3.4 (a) that for a weak lead-molecule coupling ($\Gamma = 0.05$ eV), the circular current in the benzene ring at the resonant bias ($V \sim 2$ Volt) could become significantly large, $I_c \sim 118I$, and the corresponding force could reach a value ~ 3 nN. It must be noted, however, that a weak lead-molecule coupling does not necessarily mean a weak lead-molecule bonding. Instead, we stress that the electronic coupling between the energy levels associated with multiple pathways through the molecule is weakly coupled to the energy states of the metal lead. As a result, the weak lead-molecule coupling may not actually result in the bond-breaking at the lead-molecule interface. Instead, due to a significant current magnification ($I_c/I \sim 118$) at the resonant bias voltage, the current-induced force becomes comparable to the mechanical strength of the C-C covalent bond (2.6 - 13.4 nN) [52] leading to a possible breakdown of the molecular junction due to rupture of the C-C bond at the resonant bias. However, it was found that though the current-induced forces can induce unusual dynamical changes in the structure of the benzene molecule, no current-induced breakdown was observed for bias as high as 5 Volt.[53] This is possibly due to the absence of a current magnification effect in a symmetrically connected ring junction. Interestingly, in a recent study it is shown that in a suitably designed benzene ring junction, current-induced force tends to rotate the benzene molecule leading to a possibility of electrically controllable motors at the single-molecule scale.[54]

While emphasising the circular current-induced force in molecular junctions, we would like to draw attention to two points in particular. First, the

circular current-induced instability underscores the reliability issue of the molecular junction devices due to the current magnification effect in the biased molecular rings.[33] Second, the circular current-induced instability is deterministic as it occurs at the resonant bias at which the circular current reaches a maximum value. Although the predictions in the present study are model-based tight-binding estimates at absolute zero, thermal fluctuations can play a significant impact on the mechanical instability caused by the current in molecular junction devices. It would be questionable in practice to develop molecular ring-based devices without taking the circular current and its effects into consideration.

3.6 Summary and Concluding Remarks

The study of local currents is as important as the net current through the molecular ring structures. The associated circular current in the ring under certain bias voltage is phenomenal and exceeds the net current by a factor of several hundred at low metal-molecule coupling strengths. However, the calculation of circular current would require the estimate of local/bond currents, whereby the circular current is essentially the weighted average bond current in the ring. In practice, the bond currents are not accessible in the experimental setup. We here provide an alternative method to estimate the circular current from the magnetic response of the ring to the external flux in the zero-flux limit, thereby allowing the determination of circular currents without calculating the bond currents. The estimation of induced-force on the carbon atoms in the ring indicates situations where a large

circular current could cause considerable momentum transfer to the carbon atoms creating the ring junction instability. Thus, in the context of momentum transfer to the atoms in the ring, the calculation of circular current opens up new avenues for electron scattering studies.

Our calculations reveal that for weak metal-molecule coupling, the circular current-induced force in the ring can reach a value ~ 3 nN, thereby weakening and eventually rupturing the covalent bonds in the ring. However, bonding at the metal-molecule interface remains largely unaffected due to the relatively small current through the junction in low coupling situations. It is worthwhile to note that the circular current-induced ring junction instability is deterministic because it generally occurs at the resonant bias voltage at which the circular current attains a maximum value. Although our calculations are only indicative of possible current-induced ring junction instability, a deeper study is needed for providing a quantitative analysis of the reliability issues posed by the current magnification effect in such ring junctions. It would be interesting to study if the circular current-induced force, like the Berry force, excites the runaway modes in the molecular ring junctions resulting in vibrational instability.[55] Any development in this direction will be covered elsewhere.

References

- [1] G. Mitra, V. Delmas, H. A. Sabea, L. Norel, O. Galangau, S. Rigaut, J. Cornil, K. Costuas, and Elke Scheer, *Nanoscale Adv.* **4**, 457 (2022).
- [2] F. Evers, R. Korytár, S. Tewari, and J. M. van Ruitenbeek, *Rev. Mod. Phys.* **92**, 035001 (2020).
- [3] D. Rai, O. Hod, and A. Nitzan, *J. Phys. Chem. C* **114**, 20583 (2010).
- [4] D. Rai, O. Hod, and A. Nitzan, *J. Phys. Chem. Lett.* **2**, 2118 (2011).
- [5] D. Rai, O. Hod, and A. Nitzan, *Phys. Rev. B* **85**, 155440 (2012).
- [6] S. Ganguly and S. K. Maiti, *J. Phys.: Condens. Matter* **33**, 045301 (2020).
- [7] M. Patra and S. K. Maiti, *Sci. Rep.* **7**, 43343 (2017).
- [8] S. Nakanishi and M. Tsukada, *Jpn. J. Appl. Phys.* **37**, 3805 (1998).
- [9] N. Tsuji, S. Takajo, and H. Aoki, *Phys. Rev. B* **75**, 153406 (2007).
- [10] D. Walter, D. Neuhauser, and R. Baer, *Chem. Phys.* **299**, 139 (2004).
- [11] T. Markussen, R. Stadler, and K. S. Thygesen, *Nano Lett.* **10**, 4260 (2010).
- [12] C. R. Arroyo, S. Tarkuc, R. Frisenda, J. S. Seldenthuis, C. H. M. Woerde, R. Eelkema, F. C. Grozema, and H. S. J. van der Zant, *Angew. Chem.* **125**, 3234 (2013).

References

- [13] T. A. Su , M. Neupane, M. L. Steigerwald, L. Venkataraman, and C. Nuckolls, *Nat. Rev. Mater.* **1**, 1 (2016).
- [14] M. Gantenbein, L. Wang, A. A. Al-jobory, A. K. Ismael, C. J. Lambert, W. Hong, and M. R. Bryce, *Sci. Rep.* **7**, 1794 (2017).
- [15] O. Hod, E. Rabani, and R. Baer, *Acc. Chem. Res.* **39**, 109 (2006).
- [16] O. Hod, R. Baer, and E. Rabani, *J. Phys.: Condens. Matter* **20**, 383201 (2008).
- [17] A. M. Jayannavar and P. S. Deo, *Phys. Rev. B* **51**, 10175 (1995).
- [18] S. Nakanishi and M. Tsukada, *Phys. Rev. Lett.* **87**, 126801 (2001).
- [19] K. Tagami and M. Tsukada, *e-J. Surf. Sci. Nanotech.* **2**, 205 (2004).
- [20] L. Venkataraman, J. E. Klare, C. Nuckolls, M. S. Hybertsen, and M. L. Steigerwald, *Nature* **442**, 904 (2006).
- [21] L. Venkataraman, *Physics* **1**, 5 (2008).
- [22] F. Chen and N. J. Tao, *Acc. Chem. Res.* **42**, 429 (2009).
- [23] L. Venkataraman, Y. S. Park, A. C. Whalley, C. Nuckolls, M. S. Hybertsen, and M. L. Steigerwald, *Nano Lett.* **7**, 502 (2007).
- [24] M. H. Garner, G. C. Solomon, and M. Strange, *J. Phys. Chem. C* **120**, 9097 (2016).

- [25] A. Erpenbeck, C. Schinabeck, U. Peskin, and M. Thoss, *Phys. Rev. B* **97**, 235452 (2018).
- [26] H. Haug, A.-P. Jauho, Quantum Kinetics in Transport and Optics of Semiconductors (Springer, Berlin, 2008), ch. 12.
- [27] D. Ryndyk, R. Gutiérrez, B. Song, and G. Cuniberti, in Energy Transfer Dynamics in Biomaterials Systems, edited by I. Burghardt, V. May, D. Micha, and E. Bittner (Springer, Berlin, 2009), Vol. 93, p. 213.
- [28] R. Härtle, C. Benesch, and M. Thoss, *Phys. Rev. Lett.* **102**, 146801 (2009).
- [29] A. Cresti, R. Farchioni, G. Grosso, and G. P. Parravicini, *Phys. Rev. B* **68**, 075306 (2003).
- [30] L. P. Zárbo and B. K. Nikolić, *Europhys. Lett.* **80**, 47001 (2007).
- [31] Y. Meir and N. S. Wingreen, *Phys. Rev. Lett.* **68**, 2512 (1992).
- [32] M. Di Ventra, Electrical Transport in Nanoscale Systems (Cambridge University Press, New York, 2008), p. 242.
- [33] M. Cini, E. Perfetto, and G. Stefanucci, *Phys. Rev. B* **81**, 165202 (2010).
- [34] S. Barišić, J. Labbé, and J. Friedel, *Phys. Rev. Lett.* **25**, 919 (1970).
- [35] A. L. Kuzemsky, A. Holas, and N. M. Plakida, *Physica* **122B**, 168 (1983).
- [36] J. P. Dahl, Introduction to the Quantum World of Atoms and Molecules (World Scientific Publishing Co. Pte. Ltd, 2001), p. 262.

- [37] M. Di Ventura and S. T. Pantelides, *Phys. Rev. B* **61**, 16207 (2000).
- [38] M. Di Ventura and N. D. Lang, *Phys. Rev. B* **65**, 045402 (2001).
- [39] R. Zhang, I. Rungger, S. Sanvito, and S. Hou, *Phys. Rev. B* **84**, 085445 (2011).
- [40] L. S. Pedroza, P. Brandimarte, A. R. Rocha, and M. -V. Fernández-Serra, *Chem. Sci.* **9**, 62 (2018).
- [41] M. Brandbyge, K. Stokbro, J. Taylor, J. -L. Mozos, and P. Ordejón, *Phys. Rev. B* **67**, 193104 (2003).
- [42] A. P. Horsfield, D. R. Bowler, A. J. Fisher, T. N. Todorov, and C. G. Sánchez, *J. Phys.: Condens. Matter* **16**, 8251 (2004).
- [43] D. Dundas, E. J. McEniry, and T. N. Todorov, *Nat. Nanotechnol.* **4**, 99 (2009).
- [44] T. N. Todorov, D. Dundas, and E. J. McEniry, *Phys. Rev. B* **81**, 075416 (2010).
- [45] N. Bode, S. V. Kusminkiy, R. Egger, and F. von Oppen, *Beilstein J. Nanotechnol.* **3**, 144 (2012).
- [46] T. N. Todorov, J. Hoeskstra, and A. P. Sutton, *Phil. Mag. B* **80**, 421 (2000).
- [47] T. N. Todorov, D. Dundas, A. T. Paxton, and A. P. Horsfield, *Beilstein J. Nanotechnol.* **2**, 727 (2011).

- [48] T. N. Todorov, D. Dundas, J. -T. Lü, M. Brandbyge, and P. Hedegård, *Eur. J. Phys.* **35**, 065004 (2014).
- [49] I. Kyriakou, D. Emfietzoglou, A. Nojeh, and M. Moscovitch, *J. Appl. Phys.* **113**, 084303 (2013).
- [50] R. Couto and N. Silvestre, *J. Nanomater.* **2016**, 7487049 (2016).
- [51] C. A. Nijhuis, W. F. Reus, and G. M. Whitesides, *J. Am. Chem. Soc.* **132**, 18386 (2010).
- [52] M. K. Beyer and H. Clausen-Schaumann, *Chem. Rev.* **105**, 2921 (2005).
- [53] M. Di Ventra, S. T. Pantelides, and N. D. Lang, *Phys. Rev. Lett.* **88**, 046801 (2002).
- [54] B. C. Hsu, I. Amanatidis, W. -L. Liu, A. Tseng, and Y. -C. Chen, *J. Phys. Chem. C* **118**, 2245 (2014).
- [55] J. -T. Lü, M. Brandbyge, and P. Hedegård, *Nano Lett.* **10**, 1657 (2010).

Chapter 4

Thermoelectric Properties of Molecular Junctions in Externally Applied Magnetic Field[†]

Abstract

Thermoelectric property measurements provide crucial details about the underlying characteristics of molecules that would otherwise be outside the scope of electronic transport measurements. We examine thermopower (Seebeck coefficient S) and figure of merit (ZT) in two molecules, viz., benzene and fullerene. The fullerene has a negative thermopower, while benzene has a positive value. In order to assess how successful molecular junctions are as a thermoelectric device, we also examine how an external magnetic field impacts thermopower.

[†]This chapter is based on a research article under preparation:
Umesh Dhakal, Yam P. Rai, and Dhurba Rai, “*Magnetic field effects on thermoelectric properties of ring structure molecular junctions*”.

4.1 Background

The innovative idea [1] of using single-molecule as active electronic device components has inspired extensive theoretical and experimental research on electronic transport through the molecular junction.[2-9] In recent years, the field of single-molecule electronics has seen an upsurge in interest due to their interesting transport properties and potential applications in the future nanosensor and nanoelectronic devices.[10-16] In the spirit of this, various electronic transport properties have been experimentally studied in single or few molecules using the scanning tunneling microscopy-based break junction (STMBJ) and mechanically controllable break junction (MCBJ) methods.[17, 18] Greater understanding of the electron transport across a single-molecule junction has been made possible by the current-voltage (I-V) properties of the individual molecules. However, a molecular junction's electrical structure cannot be fully understood by focusing solely on the I-V characteristics. For instance, the location of the Fermi energy level E_F of the metal electrodes determines whether they are closer to the lowest unoccupied molecular orbital (LUMO) or the highest occupied molecular orbital (HOMO), which is generally unknown due to the lack of intricate microscopic details of the electrodes.[19-21] The relative position of HOMO/LUMO with respect to E_F is important and this electronic information can be obtained from thermopower measurements.[22-25] The sign of thermopower is positive for hole-dominated transport and negative for electron-dominated conduction. The measurements

also reveal where the Fermi level of the contact electrodes is located relative to the LUMO or HOMO energy levels of the bridging molecule.[20] This has been the subject of numerous experimental studies. For example, in benzenedithiol (BDT) and fullerene (C_{60}), the current conduction is reported to be dominated by the holes and electrons, consequent to S values positive and negative, respectively. A great deal of work has been carried out to study the low-bias conductance of molecular junctions using different anchor groups which, in principle, can change the nature of charge carriers through the molecular junctions.[26–29]

The prospective use of molecular junctions in thermoelectricity is quite intriguing as the molecular thermoelectric devices may serve as a key component in finding a solution to the world's energy issue.[30, 31] Due to significant progress and advancement in the theory and computation in the last decade, the study of thermal transport and energy conversion capabilities of molecular junctions have received a lot of attention.[10–15] The obvious benefit of thermoelectric energy conversion is its applicability in harvesting waste heat and potential energy-efficient devices.[32] Though conceptually a wonderful idea, this is not technically feasible given the state-of-the-art technology available today, therefore it is still a long way from the energy market. The primary reason is the inefficiency of the present-day polymer-based organic thermoelectric devices, which makes it nearly difficult to compete with conventional silicon-based energy-conversion devices.[33, 34] Single-molecule junction devices provide a potential route for improving thermoelectric performance due to their low dimensionality, special flexibility, structural stability,

and low thermal conductivity.[35] In fact, a number of theoretical studies suggest that specifically created molecular junctions may serve as highly efficient thermoelectric devices.[36–44]

As discussed in the introductory chapter, the thermopower S measures the voltage generated per unit of the temperature difference across the device. The efficiency of heat-to-electrical energy conversion of a thermoelectric device is quantified by the figure of merit $ZT = GS^2\mathcal{T}/k$,[45] where G represents the electrical conductance of the junction, $k = k_{el} + k_{ph}$ is the net thermal conductance which includes both electronic and thermal (phonon) contributions, and \mathcal{T} represents the average temperature of the device. The most important factor that requires utmost attention for enhancing the performance of a thermoelectric device is to increase the value of ZT . This can be accomplished by simultaneously lowering the thermal conductance and raising the electrical conductance and power factor GS^2 in the numerator of the expression for ZT . However, the Wiedemann-Franz law forbids this. It is due to this reason, a bulk sample will not be a very good option for designing thermoelectric devices. It must be noted, however, that the traditional Wiedemann-Franz law does not apply to molecular systems.[46] As a result, in principle, the condition in question may be satisfied in molecular junction devices.[47] It is widely considered that for $ZT > 1$, organic thermoelectric devices could emerge as perspective participants providing commercially viable green energy solutions.

4.2 Scope of the Work

The reasons highlighted in the preceding section have led to an increase in research activities for possible exploitation of single-molecule junctions in increasing the ZT value. Due to the fact that electron transport in molecular junctions occur through distinct molecular energy levels, the transport properties of the molecules can be manipulated by exploiting the quantum interference effects, for which ring molecules and fullerene (C_{60}) are suitable, and thus these molecular systems could be promising candidates for achieving the desired thermoelectric performance. While the quantum interference is found to influence the thermoelectric properties [48, 49] and the magnetic field affects the quantum interference, it is highly desirable to study the effect of magnetic field on the thermoelectric properties of ring structure molecular junctions. Viewed in terms of electron transmission, if the magnetic field modulates the transmission probability function in the neighborhood of Fermi energy E_F of the electrodes, the thermoelectric properties can be suitably altered by the applied magnetic field. The investigations into the thermoelectric properties of molecular junctions are especially important because, in addition to their potential uses, they provide an in-depth understanding of the nature and characteristics of the electron and heat transport mechanisms in these systems, making them particularly relevant for device applications.

In this chapter, we investigate how magnetic fields affect the thermoelectric characteristics of molecules with ring structures. The possible modulation

of thermopower as a function of the magnetic field will be explored.

4.3 Model and Theoretical Framework

We now present our tight-binding model and the theoretical framework for the calculation of relevant quantities necessary for the determination of thermoelectric properties that include Seebeck coefficient S and figure of merit ZT . Although the expressions for S and ZT are presented in the introduction chapter, we provide them here once more in a form practical for calculations.

4.3.1 Tight-binding Hamiltonian

Although the theoretical background was covered in the preceding chapters, we still succinctly present it here for the purpose of completeness. In order to characterise the model, we use a tight-binding theory, which is particularly well suited in exploring both heat and electron transport through a molecular junction, particularly in the case where the spin degrees of freedom and electron-electron interactions are not considered. The effective tight-binding Hamiltonian for a molecular junction can be expressed as,

$$\hat{H} = \hat{H}_M + \hat{H}_K + \hat{H}_{KM}, \quad (4.1)$$

where, as usual, the different sub-Hamiltonians characterise the different regions of the molecular junction. The Hamiltonian \hat{H}_M accounts for the electronic degrees of freedom in the bridging molecule M , \hat{H}_K for the contacts ($K = L, R$), while \hat{H}_{KM} describe the electronic coupling between the molecule and the contact leads. In the present study, we do not consider electron spin and electron correlations (electron-electron interactions). The second quantization form of the Hamiltonian for molecule, which uses the creation and annihilation operators, can be written as

$$\hat{H}_M = \sum_{i \in M} \epsilon_i \hat{d}_i^\dagger \hat{d}_i - \sum_{\langle ij \rangle \in M} (t_{ij} \hat{d}_i^\dagger \hat{d}_j + H.c.), \quad (4.2)$$

where \hat{d}_i and \hat{d}_i^\dagger destroys and creates an electron at site i in the Hilbert space of the molecule, respectively. As is customary in the subject area, ϵ_i denotes the on-site energy and t_{ij} is the nearest-neighbor hopping integral in the molecule that connects the metal contacts. As discussed in Chapters 2 and 3, the applied magnetic field \vec{B} enters the calculation through the hopping integral t_{ij} . Similarly,

$$\hat{H}_K = \sum_{i \in K} \epsilon_i \hat{c}_i^\dagger \hat{c}_i, \quad K = L, R, \quad (4.3)$$

where ϵ_i is the on-site energy of the electrons in the metal contacts, which we consider as the reservoirs of free electrons, and \hat{c}_i^\dagger and \hat{c}_i are the creation and annihilation operators in the reservoirs. The second quantized form of the last term in Eq. 4.1 is

$$\hat{H}_{KM} = \sum_{i \in M; j \in K} (v_{ij} \hat{d}_i^\dagger \hat{c}_j + H.c.). \quad (4.4)$$

The coupling matrix element v_{ij} describes the strength of interaction between the metal leads and the electronic states of the bridging molecule. This is related to the level-width function $\Gamma_{K,ij}(E) = 2\pi \sum_{k \in K} v_{ki}^* v_{kj} \rho(E)$, where $\rho(E)$ is the density of states in the metal leads. Calculation of electron transmission function $T(E)$ is crucial in the determination of thermoelectric properties. We will now discuss this in the following section. This is discussed in the section below.

4.3.2 Thermopower and figure of merit

We use the non-equilibrium Green's function (NEGF) method to assess the transmission probability function $T(E)$ under the steady-state condition, which is a basic quantity necessary to determine the thermoelectric transport capabilities of the molecular junctions. Within the NEGF method, $T(E)$ can be expressed in terms of retarded (G^r) and advanced (G^a) Green's function through a relation $T(E) = Tr(\Gamma^L G^r \Gamma^R G^a)$, where Γ^L and Γ^R are the coupling or tunneling matrices, which describe the bonding between the bridging molecule with left and right contact leads, respectively. They are expressed in terms of the self-energies of the contact leads through a relation, $\Gamma^K = i[\Sigma_K - \Sigma_K^\dagger]$. The self-energies come into play to take into account how the discrete energy levels of the molecule are impacted by the continuum states in the metal contacts. As a result, the molecular energy levels are broadened, which affects the transport properties. The retarded and advanced Green's functions are calculated as $G^r = (E - H_M - \Sigma_L - \Sigma_R)^{-1}$, and $G^a = (G^r)^\dagger$.

As stated above, the calculation of transmission function $T(E)$ is crucial. All other physical parameters that characterize the thermoelectric properties of molecular junctions are estimated following the calculation of $T(E)$ with and without a magnetic field. The electrical conductance G , thermopower or Seebeck coefficient S , thermal conductance due to electrons k_{el} , and figure of merit ZT in the domain of linear-response and around room temperature, in which we are concerned, are given by [39, 50]

$$G = G_0 K_0, \quad (4.5)$$

$$S = - \frac{K_1}{|e| \mathcal{T} K_0}, \quad (4.6)$$

$$k_{el} = \frac{2}{h \mathcal{T}} \left(K_2 - \frac{K_1^2}{K_0} \right), \quad (4.7)$$

$$ZT = \frac{K_1^2}{K_0 K_2 - K_1^2}, \quad (4.8)$$

where, as usual, h is the Planck's constant, e is the electronic charge, k_B is Boltzmann's constant and $G_0 = \frac{2e^2}{h}$ is the quantum of conductance. One of the metal contacts is at an elevated temperature \mathcal{T}_H , while the other is at temperature \mathcal{T}_C , and thus $\mathcal{T} = (\mathcal{T}_H + \mathcal{T}_C)/2$ is the average temperature across the junction. The Landauer integrals K_n in Eqs. (4.5) - (4.8) are given by [39, 50]

$$K_n = \int T(E) \left(- \frac{\partial f(E)}{\partial E} \right) (E - E_F)^n dE, \quad (4.9)$$

where $f(E) = 1/[1 + \exp((E - \mu)/k_B \mathcal{T})]$ is the Fermi-Dirac distribution function for electrons in metal contacts. We consider the equilibrium chemical potential to

be approximately equal to the Fermi energy of the metal contacts, i.e., $\mu \sim E_F$ when analysing the thermoelectric properties of molecular junctions. The low temperature limit of the above expressions read

$$G = G_0 T(E_F), \quad (4.10)$$

$$S = - \frac{\pi^2 k_B^2 \mathcal{T}}{3|e|} \frac{1}{T(E_F)} \frac{\partial T(E_F)}{\partial E}, \quad (4.11)$$

$$k_{el} = K_0 G \mathcal{T}, \quad (4.12)$$

$$ZT = \frac{GS^2 \mathcal{T}}{k_{el}}. \quad (4.13)$$

These are the quantity of interest in the present study. The effect of the magnetic field on thermopower is investigated.

4.4 Numerical Results and Discussion

We now present our results obtained from the tight-binding model-based calculations of the thermoelectric properties of a benzene ring and a fullerene (C_{60}) molecule connected symmetrically to the metal electrodes. The results presented below focus on the response of these molecular junctions to an externally applied uniform magnetic field in terms of modification in their thermal properties. The molecular junction is described by the tight-binding Hamiltonian and the metal electrodes are considered as free-electron reservoirs, each at its own thermal equilibrium. The electron reservoir exchanges electrons with the bridging molecule

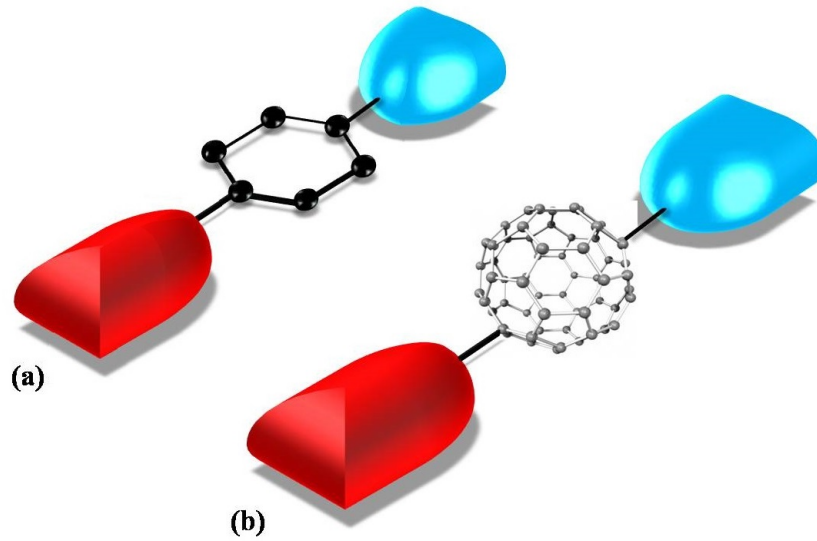


FIGURE 4.1: Schematic depiction of the (a) benzene and (b) fullerene molecular junction studied in this work. Transport of the electrons between the left and right leads ($K = L, R$) appears due to the difference $\Delta\mathcal{T}$ between the leads' temperatures, \mathcal{T}_L and \mathcal{T}_R . The hot left lead and cold right lead are kept at temperatures $\mathcal{T}_L = \mathcal{T} + \Delta\mathcal{T}/2$ and $\mathcal{T}_R = \mathcal{T} - \Delta\mathcal{T}/2$, respectively.

at the rate Γ/\hbar . For both models, the tight-binding parameters, viz., the on-site energies ϵ_i are set to zero for all atoms considered in the model, while the nearest-neighbor hopping integrals are considered uniform, $t_{ij}=2.5$ eV. Unless specified, we consider metal-molecule coupling $\Gamma=0.1$ eV and temperature $T=300$ K.

4.4.1 Seebeck coefficient

As shown in Fig. 4.1 (a), the benzene ring is connected symmetrically to the metal electrodes. For the chosen parameters, the two-fold degenerate HOMO and LUMO are positioned at 2.50 eV and -2.50 eV respectively, however, broadened due to coupling to the electrodes. The transmission probability function $T(E)$ as a function of energy is shown in Fig. 4.2 (a). Transmission resonance occurs for

$E \sim E_{HOMO}$ and E_{HOMO} and thus $T(E) \sim 1$ at the location of the frontier energy levels, i.e., the transmission peaks correspond to the position of HOMO and LUMO energy levels. Also plotted are the logarithmic transmission function and the negative differential transmission function (with appropriate factors in accordance with Eq. 4.11). The major challenge in the model-based calculations of the Seebeck coefficient is the location of the Fermi energy level E_F in the energy continuum of the metal electrodes. However, the zero-bias conductance measurement offers a solution as it corresponds to the transmission through a single channel at $E = E_F$, i.e., $G = G_0 T(E_F)$. The experimentally measured value for a benzene dithiol molecule bridging gold electrodes as reported in Refs. [22, 23] is $G \sim 0.012G_0$ and Seebeck coefficient, $S > 0$. For our setup, this corresponds to $E_F \sim 0.5$ eV above the HOMO energy level, represented by a dotted line in Fig. 4.2 and thus from Fig. 4.2 (c), $S = 1.02\mu\text{V}/\text{K}$. It must be made clear that this is not a new and significant result, however, this quantitative value at zero field helps understanding its evolution under the magnetic field applications as discussed in the next section. In contrast, owing to the enhanced structural symmetry, the LUMO and HOMO in C_{60} possess three- and five-fold level degeneracies, respectively. However, due to geometrically asymmetric connection to the contact leads, the degenerate energy levels remain nearly unsplit, and thus, the otherwise expected split features will not appear in the transmission spectrum. For the choice of our parameters, the LUMO and HOMO are positioned at 0.34 eV and -1.54 eV, respectively. Undoubtedly, the transport properties of the molecules depend on several factors but most

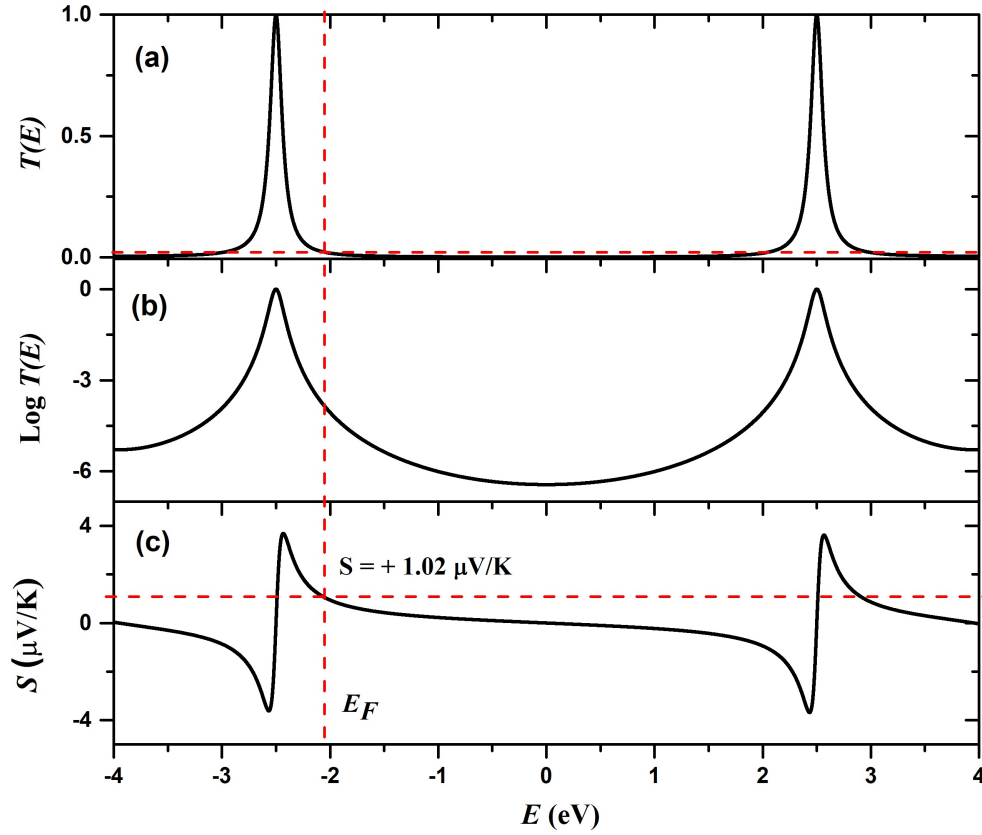


FIGURE 4.2: Variation of (a) transmission probability $T(E)$, (b) logarithmic transmission $\text{Log}T(E)$ and (c) Seebeck coefficient S , as a function of energy for a para-connected benzene ring junction. The vertical dotted line represents the position of Fermi energy at ~ 0.5 eV above the HOMO energy level, as estimated from the experimental zero-bias conductance value, $G \sim 0.012G_0$ with a positive thermopower, $S > 0$. [22, 23]

importantly on the molecule-lead coupling and the molecular energy level alignment relative to the Fermi energy E_F of the metal electrodes. The calculations presented in Fig.4.3 are only representative of the generic characteristics of a C_{60} molecule with the electrodes connected diametrically opposite. This includes the transmission probability, logarithmic transmission and the Seebeck coefficient as a function of energy. The experimentally measured value for a C_{60} molecule in contact with the gold electrodes is $G \sim 0.1G_0$ [24, 25] and Seebeck coefficient, $S < 0$. [51] This value corresponds to $E_F \sim 0.02$ eV below the LUMO energy

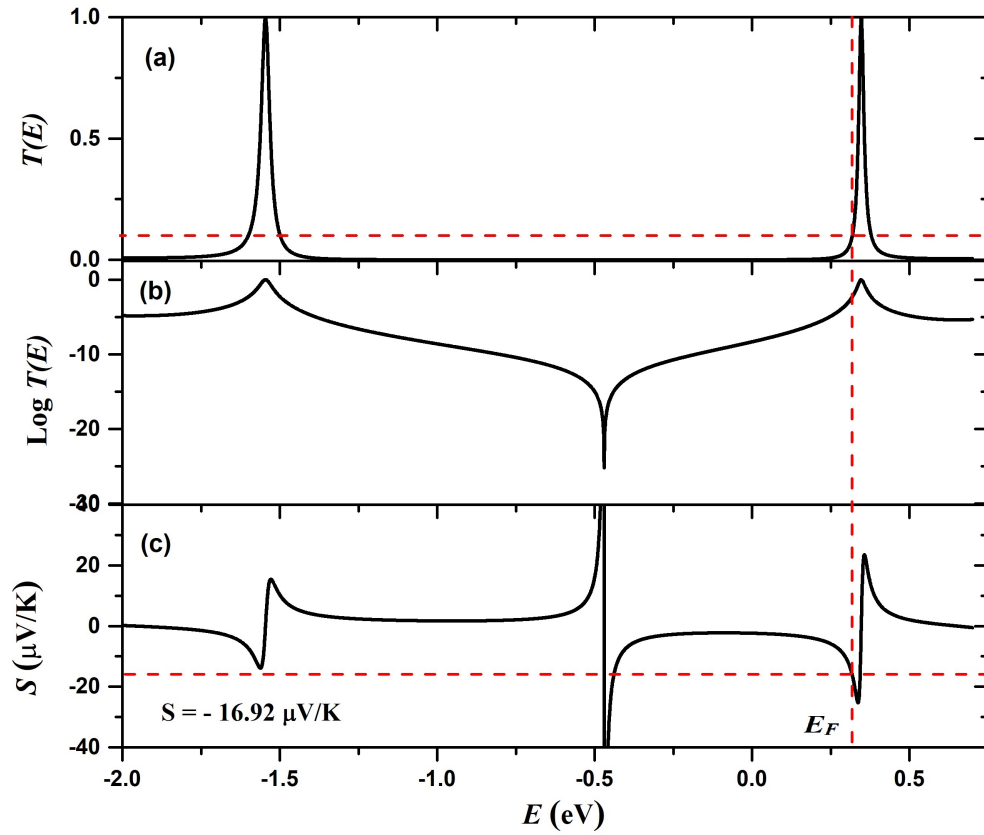


FIGURE 4.3: Same as in Fig. 4.2 for a C_{60} junction connected symmetrically to the contact leads. The Fermi level that is positioned at ~ 0.02 eV below the LUMO is estimated from the experimental zero-bias conductance value, $G \sim 0.12G_0$ with a negative thermopower, $S < 0$. [24, 25]

level, represented by a dotted line in Fig. 4.2 and thus $S = -16.92\mu\text{V/K}$. As stated before, this result is only qualitative. Realistic calculations that reflect the physical scenario require the incorporation of many-body effects, which is outside the purview of the current effort. Our attention is more on the magnetic field's influence on thermopower.

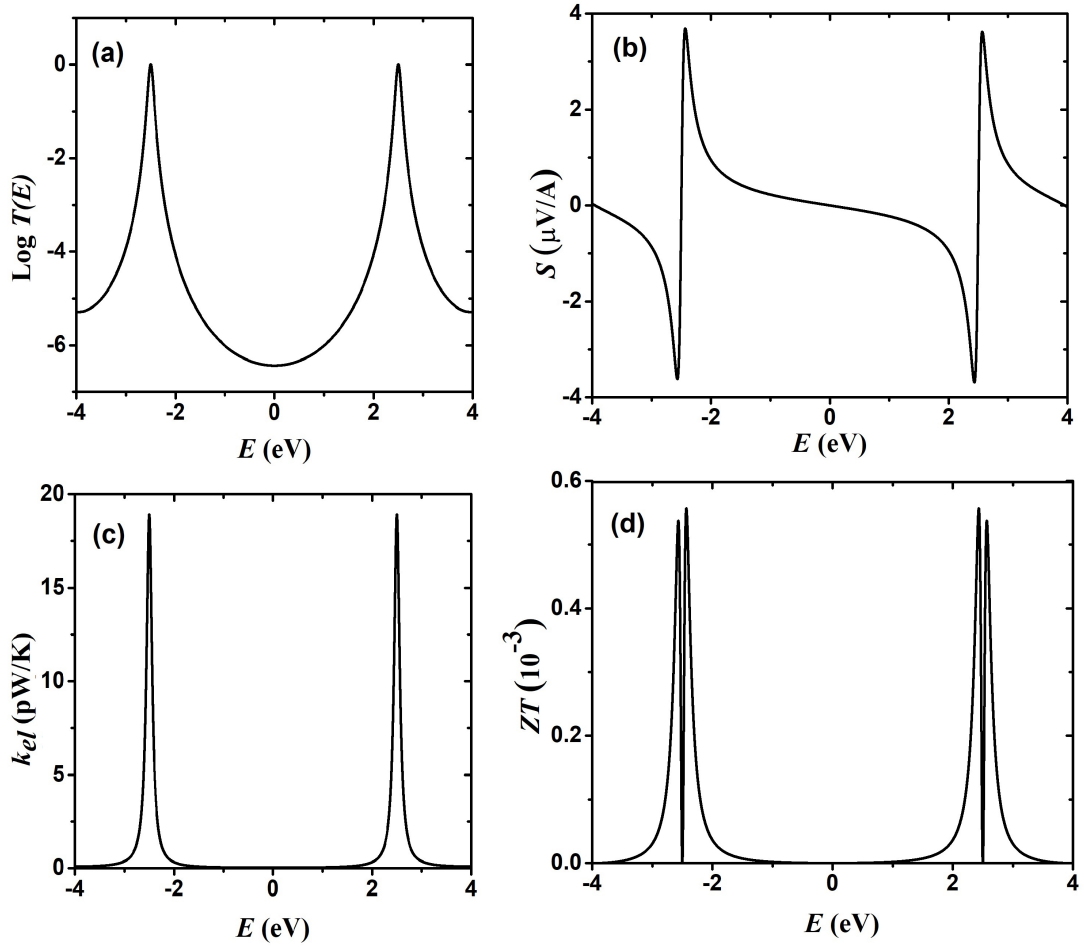


FIGURE 4.4: Thermoelectric properties of a symmetrically connected benzene ring junction:(a) Electrical conductance, (b) thermopower, (c) thermal conductance, and (d) figure of merit, as a function of incident energy E , calculated for metal-molecule coupling strength $\Gamma=0.1$ eV and temperature $T=300$ K.

4.4.2 Figure of merit

As discussed in the introductory section, the efficiency of a thermoelectric device is determined by the figure of merit (ZT). It is anticipated that an effective thermoelectric device will simultaneously increase the electrical conductance G to allow current to flow but with little Joule heating, reduce the thermal conductance k_{el} and increase the Seebeck coefficient S . However, the strong inter-dependence of

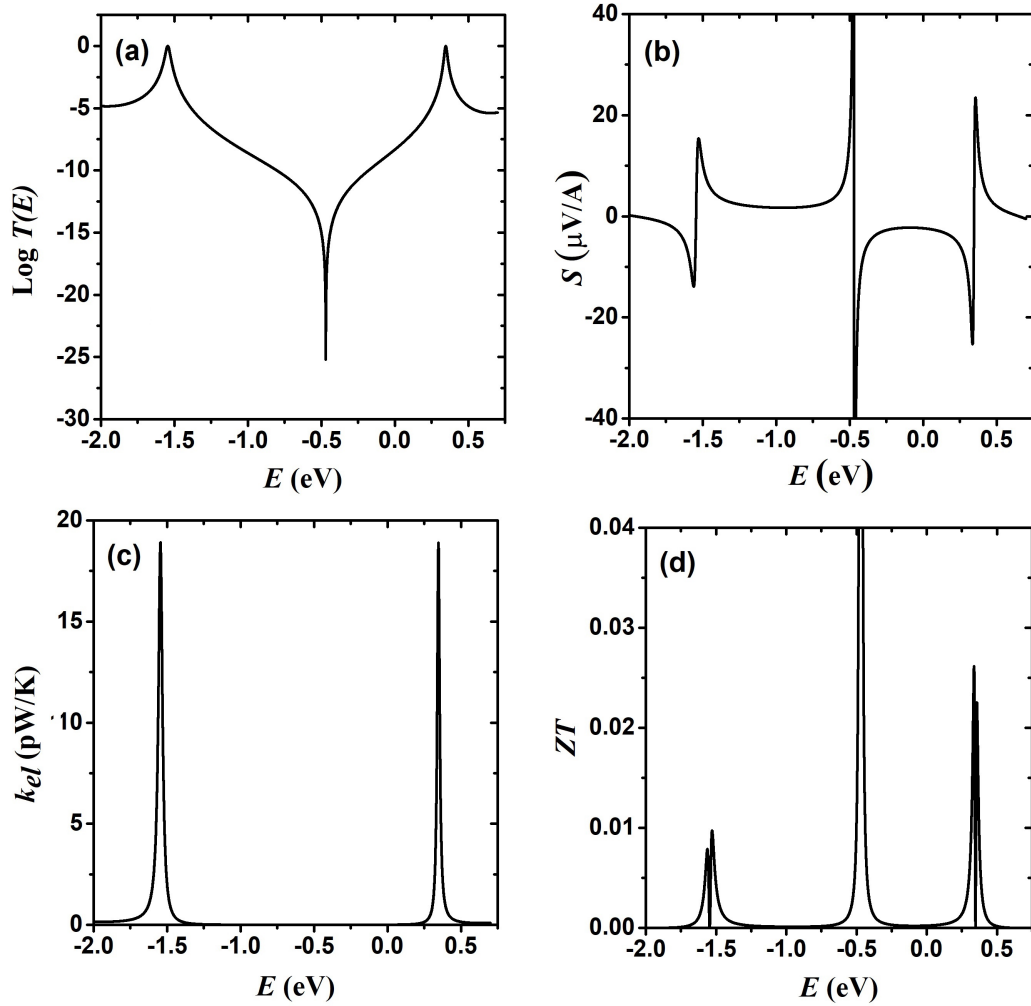


FIGURE 4.5: (a) Electrical conductance, (b) thermopower, (c) thermal conductance, and (d) ZT as a function of energy E , for a symmetrically connected C_{60} fullerene, calculated for metal-molecule coupling strength $\Gamma=0.1$ eV and temperature $T=300$ K.

heat and charge transfer, which is particularly prominent at the nanoscale level, makes ZT difficult to increase. Nevertheless, due to the incredibly narrow gap between the electrodes, transport across the molecule is predominantly ballistic. As a result, it is expected that the molecular junctions exhibit appreciable ZT values. Additionally, the molecules are expected to exhibit relatively strong amplification in ZT values near the interference features in the transport. Chemical substitutions are known to modify the interference effects in molecules, which could be

useful in designing efficient molecular thermoelectric devices.

The thermoelectric properties of a benzene ring junction is shown in Fig. 4.4 and that for C_{60} in Fig. 4.5. As is evident that the thermal conductance (k_{el}) closely follows the transmission peaks. This is due to the major electronic contribution to the thermal conductivity while the phonon contribution is not taken into account ($k_{ph} = 0$). In contrast to the bulk material, the molecular energy levels are relatively distinct while the level broadening due to metal electrodes depends on the metal-molecule coupling strength. In essence, the molecular energy can be modulated for a sharp resonance at low coupling strength. This increases the ZT value around the resonant transport due to enhanced conductance. For an optimum ZT , the molecular energy level must be on the order of $k_B T$ away from the Fermi energy level of the electrodes.[36] The ZT for benzene is $\sim 10^{-3}$, while it reaches ~ 0.03 for C_{60} , when both operated around the resonant transmission. Although the ZT values for the molecules under investigation are determined to be less than unity, a carefully designed setup may offer a good chance for $ZT \sim 1$ or more.[52, 53] Therefore, additional research in this area is required. We now move on to discuss the magnetic field modulation of the transport properties of C_{60} fullerene and study thermoelectric properties in relation to the magnetic field effect, if any.

4.4.3 Field effect on the transport properties of C_{60}

To study the magnetic field effects, we modify the hopping integrals suitably. As discussed in Chapter 2, the magnetic field enters the calculation through the phase factor in the hopping integrals. Furthermore, as explored in Chapter 2, the degeneracy of the molecular energy level is indispensable for the magnetic field control of current through the molecular ring structures. The frontier orbitals of the planar ring structures are usually 2-fold degenerate, however, it is appealing to explore the magnetic field effects in the n -fold ($n > 2$) degenerate energy level systems. C_{60} fullerene is a suitable molecule for the purpose which has 3-fold degenerate lowest unoccupied molecular orbital (LUMO) and 5-fold degenerate highest occupied molecular orbital (HOMO). One may view C_{60} as a non-planar multi-ring system that exhibits the current magnification effect at a certain bias voltage.[\[54–56\]](#)

We here focus on the evolution of the otherwise 3-fold degenerate LUMO energy states of C_{60} fullerene in a magnetic field, which could be useful in device applications. As discussed in Chapter 2, in order to see the magnetic field influence on the electron transport properties, we consider C_{60} connected asymmetrically to the metal electrodes. For a specific geometrical connection of C_{60} to the contact leads, we apply field along different symmetry axes, however, the results are essentially indifferent. The response to an externally applied magnetic field in terms of the modulation in the electron transmission probability is shown in Fig. [4.6](#)

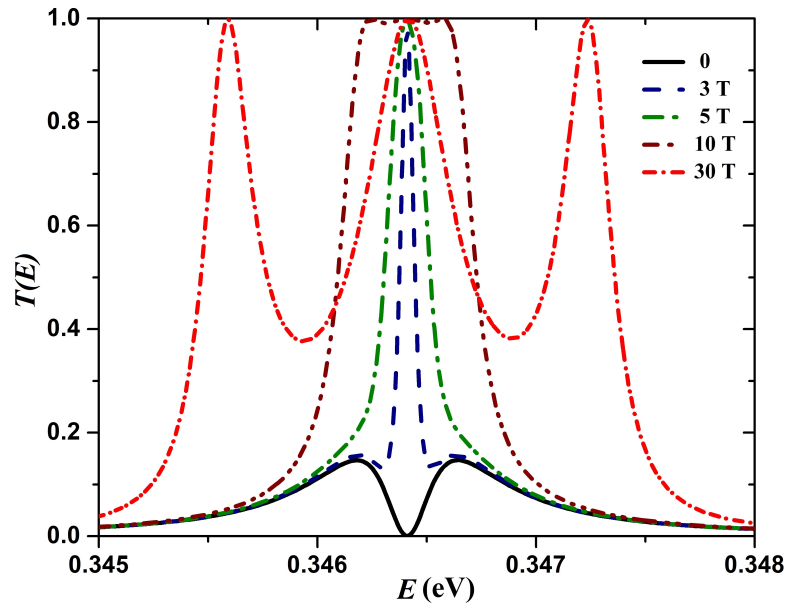


FIGURE 4.6: Evolution of transmission probability as a function of electron energy around the LUMO state of a C_{60} fullerene molecule connected asymmetrically to the metal electrodes at zero temperature for the metal-molecule coupling strength, $\Gamma = 0.01$ eV.

for a low coupling $\Gamma = 0.01$ eV so as observe the evolution of the well-resolved features of the transmission probability function, $T(E)$. As is evident from the figure that the contact leads do not lift the level degeneracy completely, leading to only two transmission peaks at zero field. However, the applied field makes the emergence of a third peak flanked by shoulder peaks on either side, which then grow and merge for transmission maximum at 5 T. Beyond this, the transmission maximum peak gets separated into three distinct peaks corresponding to 3-fold degeneracy of the LUMO and the area under the transmission probability curve continues to increase with the field until a high magnetic field is applied (50 T, not shown), beyond which the area gradually saturates. In contrast, in the symmetric connection of the contact leads, the level degeneracy remains unaffected until a high magnetic field is applied. This is considered in the next section in

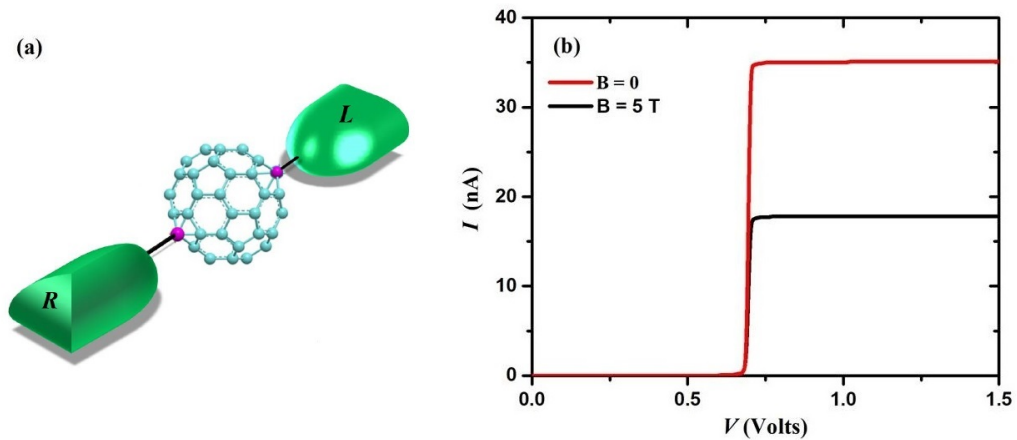


FIGURE 4.7: (a) C_{60} fullerene junction. (b) Field influence on the I-V characteristics of an asymmetrically-connected C_{60} for $\Gamma = 0.01$ eV at zero temperature and field is applied along the C_3 symmetric axis. Essentially indistinguishable I-V characteristics are obtained for the field applied along the C_2 axis (not shown).

relation to thermopower variation with the field. However, at the moment, we consider field-modulation of transmission probability for asymmetrical connection as reflected in the current-voltage characteristics shown in Fig. 4.7. Though not shown, the current increases furthermore with an increase in the magnetic field and eventually get saturated at high magnetic field values above 50 T.

Focusing more on the field modulation of current through C_{60} fullerene, we consider an atom added C_{60} in relation to the emergence of a discrete energy level in the energy spectrum of the resultant system. The added atom X occupying the atomic site on the C_{60} surface is known to significantly modify the energy levels leading to an enhanced conductance compared to a pristine C_{60} fullerene.[57] However, if the atom is in isolation within C_{60} , it interacts only weakly with the carbon atoms in the C_{60} cage resulting in a distinct energy level corresponding to the valence orbital of the added atom appearing close to frontier molecular orbitals

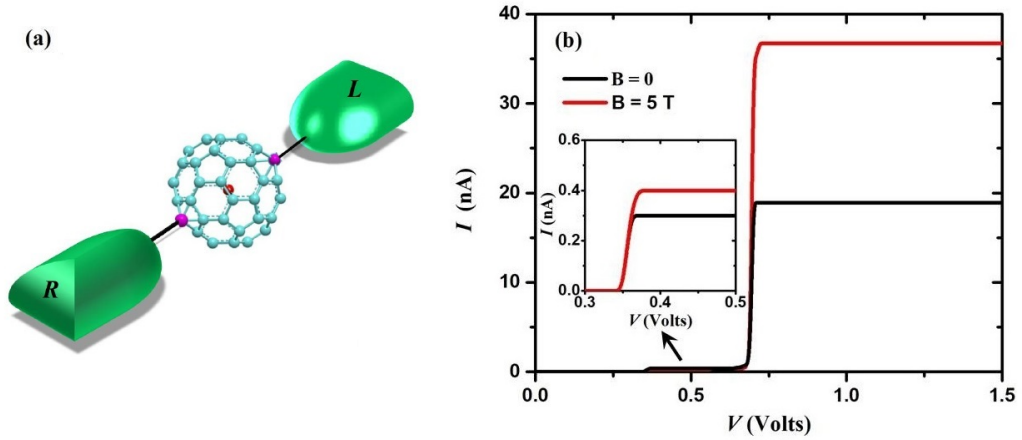


FIGURE 4.8: (a) Same as in Fig. 4.7, however, with an impurity atom placed at the center (red color). (b) I-V characteristics in presence of impurity energy level placed just below the LUMO. The inset shows a current around 0.4V bias voltage corresponding to current conduction through the impurity energy level.

of C_{60} or within its HOMO-LUMO gap.[58, 59] However, the discrete energy level of the added atom can be adjusted to lie within the HOMO-LUMO gap by suitably selecting specific atoms or confining the atom's location at a suitable position within the C_{60} cage.

Here, we consider an impurity energy level positioned below the LUMO and is susceptible to change depending on the tight-binding parameter values so chosen. We take the onsite energy of the impurity atom, which is considered to be located near the core of the C_{60} fullerene, to be 0.2 eV and the hopping integral, 0.1 eV. To be more precise, this is effected through the renormalized "two-site" tight-binding model.[60, 61] For the above chosen parameters, the impurity level is positioned at an energy 0.23 eV below the LUMO. The I-V characteristics of C_{60} with an atom X at the center in presence of a magnetic field are shown in Fig. 4.8. Unlike the doping that significantly changes the energy spectrum of C_{60} , the added atom at the center does not affect the energy spectrum other than the

emergence of discrete energy level in the vicinity of energy states corresponding to the frontier molecular orbitals (HOMO/LUMO). Thus, the I-V characteristics essentially remain unaltered, however, the conduction through impurity energy level gets modulated by the applied magnetic field. The electron transport characteristics of C_{60} fullerene may benefit from such alteration, and in particular, the field modulation of current conduction through impurity energy level, as illustrated in the inset, may be advantageous for device applications.

4.4.4 Magnetic field effect on thermopower

We now consider the magnetic field effects on thermopower. Since the transmission probability is more strongly modulated by the applied magnetic field around the resonance, which affects the slope of the transmission function, leading to a considerable chance of an increase of thermopower with the applied field. However, for a given field value, the degree of modulation, or the energy split of the molecular energy levels, depends on the metal-molecule coupling strength. Furthermore, if the increase in thermopower brought about by the increase in the slope of the transmission probability function resulting from the energy split is to have any practical importance, the energy split must be bigger than the thermal broadening or $k_B T$. This is demonstrated in a recent study that the dependence of thermoelectric properties on the applied magnetic field disappears at higher temperatures.[\[62\]](#)

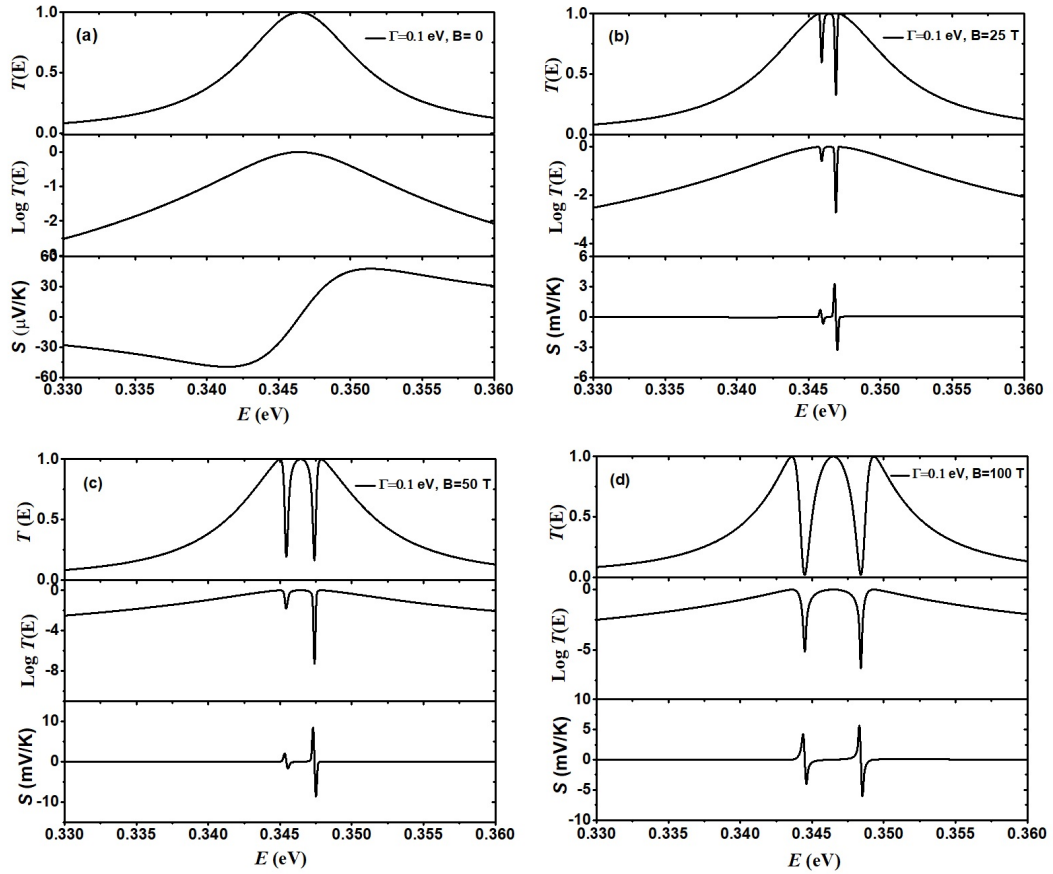


FIGURE 4.9: Magnetic field effects on the thermopower or Seebeck coefficient S around the LUMO energy of the symmetrically connected fullerene molecular junction for four different values of the magnetic field, $B = 0, 25 T, 50 T,$ and $100 T$.

The thermopower of a benzene molecule is small and an increase under field application is insignificant even for field values as high as 25 Tesla. We attribute this to a small magnetic flux the benzene molecule encloses. The demand for a strong magnetic field can be reduced by lowering the metal-molecule coupling, but the energy resolution needed to capture the sharp resonance at low coupling is exceedingly challenging to achieve. Furthermore, the thermal broadening removes such sharp and distinct features. We didn't pursue furthermore, though closely related works are available in the literature.[63, 64] For our model calculations, we

choose C_{60} instead. We apply fields along different symmetry axes, however, the results are essentially indifferent. The variation of thermopower with a field for energy around the otherwise 3-fold degenerate LUMO is shown in Fig. 4.9. The field employed for the purpose is extremely high so as to affect the energy split that results in a modulation of the slope of the transmission probability for an increase in thermopower. As is evident from the plot the thermopower is enhanced by a factor of 10^3 when the field strength is increased to 25 Tesla, beyond which the increase is insignificant. This clearly demonstrates that in a suitably designed molecular junction, the thermopower can be modulated by an externally applied magnetic field. On the usage of the large magnetic field, it must be made clear that the field required for the split of the energy levels can be lowered by reducing the metal-molecule coupling strength, however, the feasibility of the energy resolution required to capture the sharp resonance associated with the very distinct and precise energy levels at low coupling must be taken into consideration. Furthermore, exceedingly abrupt modulation of transmission function around resonance under field application at low coupling, which is more pronounced in asymmetric connection, resulting in the over-estimate of ZT (>10) has to be considered with some caution, as our calculation is valid only if the transmission function is smooth and slowly varying within $k_B T$ around Fermi energy E_F . A trade-off between the contact configuration (symmetric/asymmetric), coupling strength and magnetic flux must be investigated for optimum thermoelectric performance. Any advancement in this direction will be discussed elsewhere.

4.5 Summary and Concluding Remarks

The thermoelectric properties (S , ZT) of benzene and fullerene (C_{60}) are calculated within the tight-binding model. The study of their variation across the energy spectrum of the molecule help understand the possibility of enhancing the thermopower and the figure of merit. As they inherently depend on the transmission probability and on the slope of varying transmission probability function around the Fermi energy E_F , a finely tuned resonance conduction and modulation of transmission function can have a greater prospect of enhancing S and ZT values. Our study suggests that the magnetic field has a significant potential to increase thermopower. Although the results presented here are only indicative, the field dependence so pronounced in the analysis should have some significance that may be unveiled and discussed. Thus, an in-depth investigation is highly warranted to establish the magnetic field dependence of the thermoelectric properties.

References

- [1] A. Aviram and M. A. Ratner, *Chem. Phys. Lett.* **29**, 277 (1974).
- [2] A. Nitzan and M. A. Ratner, *Science* **300**, 1384 (2003).
- [3] N. J. Tao, *Nat. Nanotechnol.* **1**, 173 (2006).
- [4] S. V. Aradhya and L. Venkataraman, *Nat. Nanotechnol.* **8**, 399 (2013).
- [5] D. Xiang, X. Wang, C. Jia, T. Lee, and X. Guo, *Chem. Rev.* **116**, 4318 (2016).
- [6] F. Chen, J. Hihath, Z. Huang, X. Li, and N. J. Tao, *Annu. Rev. Phys. Chem.* **58**, 535 (2007).
- [7] L. Sun, Y. A. Diaz-Fernandez, T. A. Gschneidner, F. Westerlund, S. Lara-Avila, and K. Moth-Poulsen, *Chem. Soc. Rev.* **43**, 7378 (2014).
- [8] R. J. Nichols and S. J. Higgins, *Annu. Rev. Anal. Chem.* **8**, 389 (2015).
- [9] M. Galperin, M. A. Ratner, A. Nitzan, and A. Troisi, *Science* **319**, 1056 (2008).
- [10] M. Galperin, M. A. Ratner, and A. Nitzan, *J. Phys.: Condens. Matter* **19**, 103201 (2007).
- [11] Y. Dubi and M. Di Ventra, *Rev. Mod. Phys.* **83**, 131 (2011).
- [12] J. P. Bergfield and M. A. Ratner, *Phys. Status Solidi B* **250**, 2249 (2013).

- [13] W. Lee, B. Song, and P. Reddy, *Annu. Rev. Heat Transf.* **16**, 259 (2013).
- [14] L. Rincón-García, C. Evangeli, G. Rubio-Bollinger, and N. Agraït, *Chem. Soc. Rev.* **45**, 4285 (2016).
- [15] D. Segal and B. K. Agarwalla, *Annu. Rev. Phys. Chem.* **67**, 185 (2016).
- [16] J. A. Malen, S. K. Yee, A. Majumdar, and R. A. Segalman, *Chem. Phys. Lett.* **491**, 109 (2010).
- [17] W. Wang, T. Lee, and M. A. Reed, *Phys. Rev. B* **68**, 035416 (2003).
- [18] H. Song, M. A. Reed, and T. Lee, *Adv. Mater.* **23**, 1583 (2011).
- [19] P. Damle, A. W. Ghosh, and S. Datta, *Chem. Phys.* **281**, 171 (2002).
- [20] M. Paulsson and S. Datta, *Phys. Rev. B* **67**, 241403 (2003).
- [21] F. Zahid, A. W. Ghosh, M. Paulsson, E. Polizzi, and S. Datta, *Phys. Rev. B* **70**, 245317 (2004).
- [22] Y. Kim, A. Lenert, E. Meyhofer, and P. Reddy, *Appl. Phys. Lett.* **109**, 033102 (2016).
- [23] S. K. Lee, T. Ohto, R. Yamada, and H. Tada, *Nano Lett.* **14**, 5276 (2014).
- [24] C. Evangeli, K. Gillemot, E. Leary, M. T. González, G. Rubio-Bollinger, C. J. Lambert, and N. Agraït, *Nano Lett.* **13**, 2141 (2013).
- [25] T. Böhler, A. Edtbauer, and E. Scheer, *Phys. Rev. B* **76**, 125432 (2007).

- [26] Y. S. Park, A. C. Whalley, M. Kamenetska, M. L. Steigerwald, M. S. Hybertsen, C. Nuckolls, and L. Venkataraman, *J. Am. Chem. Soc.* **129**, 15768 (2007).
- [27] C. A. Martin, D. Ding, J. K. Sørensen, T. Bjørnholm, J. M. van Ruitenbeek, and H. S. J. van der Zant, *J. Am. Chem. Soc.* **130**, 13198 (2008).
- [28] S. T. Schneebeli, M. Kamenetska, Z. Cheng, R. Skouta, R. A. Friesner, L. Venkataraman, and R. Breslow, *J. Am. Chem. Soc.* **133**, 2136 (2011).
- [29] A. Mishchenko, L. A. Zotti, D. Vonlanthen, M. Bürkle, F. Pauly, J. C. Cuevas, M. Mayor, and T. Wandlowski, *J. Am. Chem. Soc.* **133**, 184 (2011).
- [30] L. E. Bell, *Science* **321**, 1457 (2008).
- [31] Nanoscale Thermoelectrics, edited by Xiaodong Wang and Zhiming M. Wang (Springer, New York, 2014).
- [32] M. Leclerc and A. Nazari, *Nat. Mater.* **10**, 409 (2011).
- [33] L. Tzounis in *Advanced Thermoelectric Materials for Energy Harvesting Applications*, edited by S. Memom (Intech Open, 2019).
- [34] Y. Zhang and S. -J. Park, *Polymers* **11**, 909 (2019).
- [35] G. D. Mahan and J. O. Sofo, *Proc. Natl. Acad. Sci. U.S.A.* **93**, 7436 (1996).
- [36] P. Murphy, S. Mukerjee, and J. Moore, *Phys. Rev. B* **78**, 161406(R) (2008).

- [37] J. P. Bergfield and C. A. Stafford, *Nano Lett.* **9**, 3072 (2009).
- [38] J. P. Bergfield, M. A. Solis, and C. A. Stafford, *ACS Nano* **4**, 5314 (2010).
- [39] C. M. Finch, V. M. Garcia-Suarez, and C. J. Lambert, *Phys. Rev. B* **79**, 033405 (2009).
- [40] O. Karlström, H. Linke, G. Karlström, and A. Wacker, *Phys. Rev. B* **84**, 113415 (2011).
- [41] D. Nozaki, H. Sevinçli, W. Li, R. Gutiérrez, and G. Cuniberti, *Phys. Rev. B* **81**, 235406 (2010).
- [42] R. Stadler and T. Markussen, *J. Chem. Phys.* **135**, 154109 (2011).
- [43] H. Nakamura, T. Ohto, T. Ishida, and Y. Asai, *J. Am. Chem. Soc.* **135**, 16545 (2013).
- [44] J. Vacek, J. V. Chocholousova, I. G. Stara, I. Stary, and Y. Dubi, *Nanoscale* **7**, 8793 (2015).
- [45] E. Z. -Harush and Y. Dubi, *Phys. Rev. Appl.* **3**, 064017 (2015).
- [46] G. T. Craven and A. Nitzan, *Nano Lett.* **20** (2020).
- [47] G. J. Snyder and E. S. Toberer, *Nat. Mater.* **7**, 105 (2008).
- [48] R. Miao, H. Xu, M. Skipnik, L. Cui et al. *Nano Lett.* **18**, 5666 (2018).
- [49] K. Wang, E. Meyhofer, and P. Reddy, *Adv. Funct. Mater.* **30**, 1904534 (2020).

- [50] N. R. Claughton and C. J. Lambert, *Phys. Rev. B* **53**, 6605 (1996).
- [51] L. Cui, R. Miao, C. Jiang, E. Meyhofer, and P. Reddy, *J. Chem. Phys.* **146**, 092201 (2017).
- [52] Y. Kim, W. Jeong, K. Kim, W. Lee, and P. Reddy, *Nature Nanotechnol.* **9**, 881 (2014).
- [53] R. Alughthawi, S. Hou, Q. Wu, Z. Liu, W. Hong, and C. Lambert, *ACS Sens.* **6**, 470 (2021).
- [54] L. G. Wang, D. W. Yu, Y. Li, and K. S. Wong, *IEEE Conf. Nano. El.*, 189 (2006).
- [55] S. Nakanishi and M. Tsukada, *Phys. Rev. Lett.* **87**, 126801 (2001).
- [56] C. Lei and W. Liguang, *Int. Conf. Adv. Comput. Appl.* **03**, 158 (2010).
- [57] X. Zhong, R. Pandey, A. R. Rocha, and S. P. Karna, *J. Phys. Chem. Lett.* **1**, 1584 (2010).
- [58] J. Lu, Y. Zhou, X. Zhang, and X. Zhao, *Chem. Phys. Lett.* **352**, 8 (2002).
- [59] E. V. Tkalya, A. V. Bibikov, and I. V. Bodrenko, *Phys. Rev. C* **81**, 024610 (2010).
- [60] S. Mishra, *Phys. Rev. B* **72**, 075421 (2005).
- [61] J. -J. Zheng, X. Zhao, S. B. Zhang, and X. Gao, *J. Chem. Phys.* **138**, 244708 (2013).

References

- [62] M. Crisan, I. Grosu, and I. Tifrea, *Physica E Low Dimens. Syst. Nanostruct.* **124**, 114361 (2020).
- [63] H. Li, Y. Wang, X. Kang, S. Liu, and R. Li, *J. Appl. Phys.* **121**, 065105 (2017).
- [64] S. K. Maiti and M. Dey, *Chem. Phys. Lett.* **731**, 136601 (2019).

Chapter 5

Future Prospects

In this thesis, the influence of magnetic field on electron transport through molecular quantum ring structure junctions and the associated effects are studied. It is found that weak coupling is essential for the magnetic field-based current control in smaller ring structures, while its role is significantly less in larger structures. This observation is based on the tight-binding calculations of electron transport through the polycyclic aromatic hydrocarbons (PAHs) of increasing size under the field application in the range, 0 to 10 Tesla. However, the increased magnetic flux through larger structures enables the modulation of energy levels with relative ease, leading to current control at relatively small field values (\sim few Tesla). The circular current-induced force in a ring junction is studied and the reliability issues concerning junction instability due to rupture of bonds in the ring owing to large induced force at resonant bias are explored. Towards the end of the thesis, the possibility of magnetic field modulation of thermoelectric properties of ring structure molecules, viz., benzene and C_{60} fullerene is investigated. The development of molecular devices with increased functionalities is likely to be facilitated by appropriately designed ring structure junctions that take into account the research

findings provided in this thesis.

Although the main objectives of the work undertaken have been accomplished, further research is required to validate the present findings based on the tight-binding model calculations. The ab initio-based calculations incorporating the many-body effects, inelastic processes and dephasing, are highly necessary to accurately reflect the physical situations. Future works in this area are expected to involve the physical demonstration of magnetic field effects studied in the present work. We feel that this thesis may provide crucial and necessary background information and a stimulating discussion for future studies. The following are some of the areas that have been identified as worthwhile problems for investigation.

- ☞ (1) Chapter 2: First-principles calculations of the magnetic field effects on current conduction through ring structure junctions.
- ☞ (2) Chapter 2: Experimental study of magnetic field control of current through graphene nano junctions.
- ☞ (3) Chapter 3: Determination of circular current in realistic situations.
- ☞ (4) Chapter 3: Quantitative analysis of circular current-induced force in ring junctions.
- ☞ (5) Chapter 4: Experimental study of magnetic field enhancement of thermopower of ring structure molecular junction.

The aforementioned key points highlight the future works which, however, require some justifications and thus the following brief overview is important.

(1) Our work is based on tight-binding calculations. Although it is the most widely used method for calculating the electron transport properties of the molecular junctions, the many-body interactions are, however, either neglected or treated on a mean-field level. The ab-initio approaches, on the other hand, are those that, in principle, rely only on the basic principle of physics and do not require inputs from the experimental results. The consideration of many-body interactions that include the electron-electron interaction, correlation effects, etc are important for capturing the electron transport features under realistic situations. However, the ab-initio calculations are computationally expensive and especially cumbersome to handle when the bulk metal electrodes with an infinite degree of freedom are considered. One of the most useful methods to calculate the transport properties is the density functional based tight-binding theory, which now has become an integral part in the study of molecular electronics. Calculations may take into account the external magnetic field, and the results reflecting the realistic situations with and without a magnetic field may be unveiled and discussed.[1]

(2) Notwithstanding the promising results of the calculations, the experimental studies are highly desirable for the detailed understanding of magnetic field-based characteristics of the nano-graphene molecular junction. Owing to the very small size of the molecular rings like benzene, the experimental test of the magnetic field

influence on the electron transport properties becomes extremely challenging and the test results are rare,[2] however, nano-graphene molecular junctions could be used as a testbed for investigating the field effects. Furthermore, it is possible to investigate the magnetic field sensitivity of current control by changing the anchoring groups that bind the nano-graphene sheet to the metal electrodes. The results are expected to be useful for the design of nano-graphene based molecular junction devices with magnetic field control features.

(3) Much of the basic physics of circular current is already been captured in the tight-binding calculations, however, it is imperative to go beyond the limitations of the tight-binding theory and investigate the impact of the many-body interactions. Equally crucial is the experimental determination of circular current, which can be accomplished by measuring the induced-dipole moment in a cantilever magnetometry setup. As the induced circular current in a suitably designed ring junction become significant at the resonance transmission, the setup can be considered as a molecular magnet possessing a tunable magnetic field. Careful consideration in this direction is invited adding thereby an extra functionality to the ring junction setup with a possible magnetic field modulation of the optoelectronic properties of the ring molecules.[3]

(4) One major concern in the molecular electronic devices is the Joule heating leading to a possible thermal runaway of the devices. Considering a narrow gap between the electrodes, the electrons traversing the gap through a bridging molecule

dissipate the majority of the heat in the molecule-electrode interface or in the metal electrodes. This leads to reliability issues of the molecular devices. Additionally, as studied in this work, the circular current-induced force may become significant at the resonant conduction leading to a possible bond rupture in the ring junction devices. Detailed theoretical and experimental studies are indispensable for quantifying the circular current-induced force in the ring junctions. This greatly helps in addressing the performance and reliability issues in the ring junction devices.

(5) Calculations have demonstrated the influence of magnetic field on the thermoelectric properties of monolayer graphene at low temperatures.[4] Our results suggest that the applied magnetic field may modulate the thermopower of the ring structure junctions that are of relevance to practical applications and further development of molecular thermoelectric devices. To corroborate the findings of the present work, however, much more precise calculations are absolutely required. Additionally, the experimental demonstration would provide new impetus for the development of efficient molecule-based thermoelectric devices.

We believe that the hitherto unexplored areas studied over the years culminating in the form of a thesis represent the actual physical conditions of the ring structure junctions, however, to validate our findings a careful and thorough assessment through the available state-of-the-art experimental techniques is indispensable. Undoubtedly, further study is needed and with the race for rapid development of sophisticated experimental techniques, we express a great hope that the results

of the systematic research work covered in the present venture will be realized in near future, or at the very least put to the test. Until then some of our predictions made and the trends observed in the present endeavor may remain elusive.

References

- [1] K. Luo and W. Sheng, *J. Appl. Phys.* **115**, 053705 (2014).
- [2] K. Horiguchi, T. Sagisaka, S. Kurokawa, and A. Sakai, *J. Appl. Phys.* **113**, 144313 (2013).
- [3] B. Kudisch, M. Maiuri, L. Moretti, et al, *Proc. Natl. Acad. Sci.* **117**, 11289 (2020).
- [4] M. Crisan, I. Grosu, and I. Tifrea, *Physica E Low Dimens. Syst. Nanostruct.* **124**, 114361 (2020).

Index

- A**
- Advanced Green's function, 12, 54, 112
 - Aharonov-Bohm, 79
 - Anchoring group, 17, 107
- B**
- BLF model, 89
 - Bond-charge, 52, 54
 - Break junction technique, 6
 - Broadening function, 12, 16, 48
- C**
- Chemical potential, 10, 54
 - Circular current, 23, 80, 86, 88
 - Contact coupling, 59, 115
 - Coulomb interaction, 46, 51, 62
 - Coupling strength, 48, 59
 - Current-induced force, 25, 81, 89, 92
 - Current-induced local force, 94, 97
- E**
- Electrical Conductance, 9, 19, 108
 - Electron flux, 95
 - Electron reservoirs, 8, 82, 90
 - Electron transport, 8, 42, 63, 109
 - Electron-phonon interaction, 20
 - Electron-wind force, 94
- F**
- Fermi distribution, 8, 54, 84
 - Fermi energy, 28, 55, 63, 106
 - Figure of merit, 29, 108, 112
- G**
- Graphene nanosheets, 45, 48, 62
- Green's function technique, 11
- H**
- Hamiltonian, 11, 50, 83, 89, 110
 - HOMO-LUMO gap, 28, 125
 - Hopping integral, 55, 82, 88, 115
- I**
- I-V characteristics, 64, 106, 125
 - Interface geometry, 18
- K**
- Keldysh formalism, 13, 54, 84
- L**
- Landauer formulation, 8, 12, 28
 - Lesser Green's function, 13, 53
 - Local current, 79, 84, 91
 - Local heating effects, 22
- M**
- Magnetic field, 43, 49, 58, 68, 122
 - Magnetic flux, 43, 49, 80, 85, 91
 - MCBJs, 6, 7, 106
 - Meir-Wingreen formula, 13, 54, 84
 - Metal-Molecule coupling, 15
 - Molecular junctions, 3, 62, 79, 106
 - Momentum transfer, 92, 99
- N**
- NDR, 44, 67, 70
 - NEGF, 13, 46, 53, 84
- O**
- Occupation number, 52, 54, 68

On-site energy, 55, 82, 115

Onsager symmetry, 56

P

Peierls substitution, 49, 88

Peltier effect, 26

Q

Quantum interference, 20, 23, 79, 109

Quantum loop current, 23

Quantum master equation, 14

R

Renormalized hopping integral, 52, 62

Renormalized on-site energy, 52, 62

Retarded Green's function, 12, 53, 112

S

Scattering cross-section, 94

Seebeck coefficient, 27, 115

Seebeck effect, 26

Self-energy, 16, 53, 112

Single-molecule junctions, 3, 5, 42

STMBJs, 6, 7, 106

T

t-V model, 51

Thermodynamic potential, 87

Thermoelectric power, 27, 106, 112, 126

Thermoelectric properties, 27, 109, 121

Thermoelectricity, 5, 26, 107

Tight-binding, 83, 110

Transmission probability, 8, 10, 56, 115

W

Wide band limit, 17, 48